INVESTIGATIONS ON PHOTOCONDUCTIVITY AND ELECTRICAL SWITCHING IN SELECTED CHALCOGENIDE GLASSES

THESIS SUBMITTED TO

COCHIN UNIVERSITY OF SCIENCE AND TECHNOLOGY

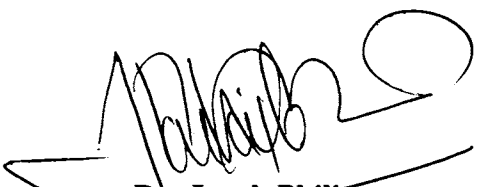FOR THE AWARD OF THE DEGREE OF

DOCTOR OF PHILOSOPHY

GREGORIOS MATHEW

DEPARTMENT OF INSTRUMENTATION

COCHIN UNIVERSITY OF SCIENCE AND TECHNOLOGY
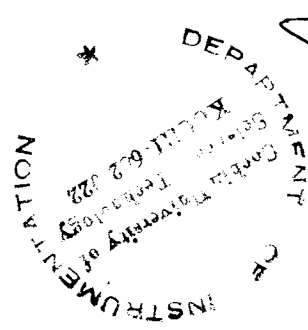
COCHIN- 682 022 INDIA

DECEMBER 1998

CERTIFICATE

Certified that the work presented in this thesis is based on the bona fide work done by Mr. Gregorios Mathew under my guidance in the Department of Instrumentation, Cochin University of Science and Technology, and has not been included in any other thesis submitted previously for the award of any degree.

Cochin - 682 022
22 December 1998

Dr. Jacob Philip
Supervising Philip
Dr. Jacobs
Professor & Head
Department of Instrumentation
COCHIN UNIVERSITY OF TECHNOLOGY
KOCHI 682 022

DECLARATION

Certified that the work presented in this thesis is based on the original work done by me under the guidance of Dr. Jacob Philip, Professor and Head, Department of Instrumentation, Cochin University of Science and Technology, and has not been included in any other thesis submitted previously for the award of any degree.

Cochin - 682 022
22 December 1998

Gregorios Mathew

Contents

Preface

Amorphous semiconductors form an important class of materials from the points of view of fundamental condensed matter research as well as technological applications. Although they have been investigated extensively, many of their electronic, optical and thermal properties have posed and still do pose an enigma for any kind of complete description. They do not exhibit long range order as in crystalline materials having a well defined periodicity. The wave vector **k**, which has critical importance in describing electronic behaviour of crystalline semiconductors, no longer has any significance for a disordered material.

Amorphous semiconductors can be divided into two groups as tetrahedrally coordinated silicon like materials and two-fold coordinated chalcogenide glasses. Chalcogenide glasses contain one or more of the chalcogens of the sixth column of the periodic table; sulphur, selenium or tellurium. The four-fold coordination in Si leads to symmetrical bonding and the formation of rigid structures. On the other hand, two-fold coordination in chalcogens is highly asymmetrical and the structure gives rise to greater degree of flexibility.

Chalcogenide glasses can be prepared in bulk as well as in thin film forms while Si type materials can only be prepared in the thin film form. The chalcogenides cover a wide range of compositions. Their physical properties vary appreciably from sample to sample and in some cases among samples of the same material. The greatest advantage of these glasses is the composition dependent tunability of their properties which enables one to design materials for specific requirements. The interest in chalcogenide glasses among scientists and engineers is mainly due to their potential technological applications arising out of their optical, electrical and photosensitivity properties. These glasses generally do not absorb IR radiations and so they are suitable for IR optical elements such as prisms, lenses, windows and other accessories. Though a large number of investigations have already been carried out on these materials by various research workers, still there are many chalcogenide glass systems which are not yet investigated in detail, particularly with regard to some of their properties.

In this thesis, we present the results of our investigations on the photoconducting and electrical switching properties of selected chalcogenide glass systems. We have used XRD and X-ray photoelectron spectroscopy (XPS) analysis for confirming the amorphous nature of these materials and for confirming their constituents respectively.

Photoconductivity is the enhancement in electrical conductivity of materials brought about by the motion of charge carriers excited by absorbed radiation. The phenomenon involves absorption, photogeneration, recombination and transport processes and it gives good insight into the density of states in the energy gap of solids due to the presence of impurities and lattice defects. Photoconductivity measurements lead to the determination of such important parameters as quantum efficiency, photosensitivity, spectral sensitivity and carrier lifetime. Extensive research work on photoconducting properties of amorphous semiconductors has resulted in the development of a variety of very sensitive photodetectors. Photoconductors are finding newer and newer uses every day. CdS, CdSe, Sb_2S_3, Se, ZnO etc. are typical photoconducting materials which are used in devices like vidicons, light amplifiers, xerography equipment etc.

Electrical switching is another interesting and important property possessed by several Te based chalcogenides. Switching is the rapid and reversible transition between a highly resistive OFF state, driven by an external electric field and characterized by a threshold voltage, and a low resistivity ON state. Switching can be either threshold type or memory type. The phenomenon of switching could find applications in areas like information storage, electrical power control etc. Investigations on electrical switching in chalcogenide glasses help in understanding the mechanism of switching which is necessary to select and modify materials for specific switching applications.

Analysis of XRD pattern gives no further information about amorphous materials than revealing their disordered structure whereas x-ray photoelectron spectroscopy(XPS) provides information about the different constituents present in the material. Also it gives

binding energies (b.e.) of an element in different compounds and hence b.e. shift from the elemental form.

Our investigations have been concentrated on the bulk glasses, Ge-In-Se, Ge-Bi-Se and As-Sb-Se for photoconductivity measurements and In-Te for electrical switching. The photoconducting properties of Ge-Sb-Se thin films prepared by sputtering technique have also been studied. The bulk glasses for the present investigations are prepared by the melt quenching technique and are annealed for half an hour at temperatures just below their respective glass transition temperatures. The dependence of photoconducting properties on composition and temperature are investigated in each system. The electrical switching characteristics of In-Te system are also studied with different compositions and by varying the temperature. A chapter wise description of the work presented in the thesis are given below.

Chapter 1 is devoted to an introduction to the work done in the thesis. It outlines the properties of amorphous semiconductors, especially those of amorphous chalcogenides and various theoretical models that have been proposed to explain the characteristics of these materials and their applications. In addition, this chapter gives an idea about the phenomena of photoconductivity and electrical switching and their important applications. The popular models explaining these phenomena are also discussed.

The details of sample preparation and analysis as well as the instrumentation for the experiments done in the thesis are discussed in chapter 2. The experimental setup for studying photoconductivity and electrical switching are explained with the help of block diagrams. The design and fabrication details of a photoconductivity cell used in the present work are also discussed. Relevant technical details of x-ray photoelectron spectrum analysis are also outlined in this chapter.

Results of photoconductivity measurements on $Ge_xIn_5Se_{95-x}$ glasses are presented discussed in chapter 3. The average coordination numbers(Z) of the compositions studied in this system varies from 2.39 to 2.79. The speciality of this system is that the two

topological thresholds and the chemical threshold occur at different Z values. It is an ideal system which enables one to isolate the effects of chemical ordering from those of topological origin. The temperature and composition dependence of photoconductivity have been studied by both d.c and a.c methods. Carrier life times of different compositions are obtained from frequency resolved photocurrent (FRPC) measurements. The spectral dependence of photoconductivity is also investigated and spectral sensitivity and quantum efficiency are calculated. The structural features are explained on the basis of the Chemically Ordered Covalent Network Model (COCNM) and topological models. ABFH (Arnoldussen-Bube-Fagen-and Holmberg) model is used for explaining the photoconductivity behaviour. Results of XPS studies of three compositions are presented along with the results on photoconductivity.

The Bi doped Ge-Se glasses exhibit a carrier type reversal (p→ n transition) at 7 atomic percent of Bi. In chapter 4, we focus our attention on the photoconducting properties of the $Ge_{20}Bi_xSe_{80-x}$ (x = 2- 12) system. The composition dependent variation of photoconductivity has a sharp change corresponding to the composition with x = 7. Carrier lifetimes of different compositions are calculated from FRPC measurements. The XPS analysis of two compositions are also presented in this chapter.

Chapter 5 deals with the photoconductivity characteristics of $As_xSb_{15}Se_{85-x}$ and $As_xSb_{10}Se_{90-x}$ systems. The dependence of photoconductivity on composition and temperature has been analysed. Carrier lifetime has been measured by FRPC method. Two compositions are analysed by XPS.

The characteristics of photoconductivity of amorphous $Ge_xSb_{10}Se_{90-x}$ thin films are presented in chapter 6. The steady state photoconductivity of this system is analysed in detail on the basis of ABFH model. The Ge-Sb-Se system shows a behaviour very close to that of a Type I photoconductor, as classified by the ABFH model. At the same time it shows some characteristics of a Type II photoconductor. The results on composition dependence are explained with the help of the COCN model.

The work done on the electrical switching properties of In_xTe_{100-x} glasses are outlined in chapter 7. This system exhibits memory type electrical switching under the action of an external electric field. The dependence of switching characteristics on temperature, composition and thickness are analysed. The results are explained on the basis of the electrothermal model. The OFF state behaviour of the material is also analysed.

The last chapter summarises the overall conclusions drawn from the work presented in earlier chapters. The scope for doing further work in this area is also outlined.

The following papers have been published/communicated for publication based on the work presented in this thesis.

1. Instrumentation to probe photoinduced effects in bulk samples.

>   Gregorios Mathew and J. Philip
>   *J. Instrum. Soc India 27 (1) (1997) 60*

2. Characteristics of photoconductivity in amorphous $Ge_xSb_{10}Se_{90-x}$ thin films

>   G. Mathew, K.N. Madhusoodanan and J. Philip
>   *Physica Status Solidi (a) (Germany) 168 (1998) 239*

3. Characteristics of electrical switching in indium telluride semiconducting glasses.

>   G. Mathew and J. Philip
>   *Ind. J. Pure & Appl.Phys. 36 (1998) 463*

4. Photoconductivity and carrier lifetime in In / Bi doped Ge-Se glasses.

>   G. Mathew and J. Philip
>   *J. Phys.: Condens. Matter (UK) (accepted)*

5. Photoconducting properties of As-Sb-Se glasses

>   G. Mathew and J.Philip
>   *J.Mat.Science. Letters. (submitted)*

The following papers have been presented in different symposia during the course of this work

1. Design of a photoconductivity cell for bulk samples.

> Gregorios Mathew and J. Philip
> *National Symposium on Instrumentation (NSI-20) Sept 25-28 (1995)*
> *Osmania University, Hyderabad.*

2. Thermally induced photoconduction in $Ge_xSb_{10}Se_{90-x}$ thin films

> G. Mathew and J. Philip
> *Solid State Physics Symposium (DAE) Dec 27-31 (1996), BARC, Mumbai*

3. Memory type electrical switching in In-Te semiconducting glasses

> G. Mathew and J. Philip
> *Solid State Physics Symposium (DAE) Dec 27-31 (1997) Cochin*

4. XPS studies on bulk $In_{40}Te_{60}$ and $In_{30}Te_{70}$ glasses

> G. Mathew and J. Philip
> *Solid State Physics Symposium (DAE) Dec 27-31 (1997) Cochin*

5. P→n transition in Bi doped Ge-Se glasses reflected in photoconductivity measurements

> G. Mathew and J. Philip
> *5th IUMRS International Conference, Oct 13-16 (1998) Bangalore*

6. Effect of In / Bi doping on the photoconducting properties of Ge-Se glasses

> G. Mathew and J. Philip
> *Solid State Physics Symposium (DAE) Dec.27-31 (1998) Kurukshetra (accepted)*

7. XPS analysis of Indium modified Ge-Se glasses

> G. Mathew and J. Philip
> *Solid State Physics Symposium (DAE) Dec.27-31 (1998) Kurukshetra (accepted)*

Acknowledgements

The work presented in this thesis has been carried out under the able guidance and supervision of Dr. Jacob Philip, Professor and Head, Dept. of Instrumentation, Cochin University of Science and Technology. I express my deep sense of gratitude to him for his constructive suggestions, patience and constant encouragement during the course of the work. Also, I am indebted to him for introducing me to the problem and for his sincere interest in academic as well as personal matters.

I am thankful to Dr. K. N. Madhusoodanan, Reader, Dept. of Instrumentation, for his cooperation in my work and for the discussions, I had with him.

I am grateful to Prof. M. Sabir, Head of the Dept. of Physics and the faculty of the department for their help and cooperation.

I am obliged to Prof. (Retd.) George Sebastian Vempani, Dept. of Physics, S. B. College, Changanacherry for directing me to higher studies in physics. I express my heartfelt thanks to him for the encouragement and endorsement I received from him during the post graduate days.

It is indeed my great pleasure to thank my colleagues, A. V. Alex, R. Rajesh, Alex Mathew, E. G. Vasanthakumar, Sheenu Thomas, C. Preethy Menon, H. Nagavally, Dr. M. S. Kala, Dr. R. Sreekumar, Dr. Nelson Rodrigues, Dr. A. A. Sudhakaran, Dr. Johney Isaac, Dr. L. Godfrey and Dr. K. Nandakumar for their helping hands at the time of need. I am also thankful to all the research scholars and friends in the campus with special regards to V. G. Reju, S. Ramkumar, Riju C. Isaac, Cyriac M. Odakal, Shelley John, Taji, Shaji, Aldrin, Joseph, and Saji. I would also like to thank Mr. V. M. Peter for his unreserved help at various stages.

Thanks are also due to the staff of the Departments of Instrumentation and Physics for their sincere cooperation.

I would like to thank RSIC, IIT, Chennai and IUC, (DAE) Indore for providing me an opportunity for doing x-ray photoelectron studies.

I gratefully acknowledge UGC and CSIR (Govt. of India) for financial support and fellowship.

I fondly recall the encouragement and support given by my parents, sister and brothers.

Finally I convey my sincere thanks to all my well wishers and friends who have directly or indirectly helped me.

Gregorios Mathew

Chapter 1

Introduction

Part A: Review of Amorphous Semiconductors

1.1 Introductory remarks

The general characteristics of semiconductors are the following, : (i) Resistivity less than that of an insulator, but more than that of a conductor (ii) Temperature coefficient of resistance is negative, ie, their resistivity decreases with increase of temperature. Many of the semiconductors become conductors at high temperatures. (iii) Properties may be changed by adding suitable impurities. On the basis of energy bands, a much more comprehensive definition can be given to semiconductors. They are materials which have almost filled valence band and nearly empty conduction band with energy gap generally in the range of 1 to 2 eV.

Semiconductors which are characterised by the absence of long range order in the arrangement of atoms, compared to their crystalline counterparts, are called amorphous semiconductors. Amorphous semiconductors include chalcogenide glasses and tetrahedrally coordinated materials like Si and Ge.

The study of physical properties of amorphous semiconductors is an active field of research in solid state physics. In particular, the nature of electronic transport in these materials has attracted much attention of research workers. The interest arose from the point of view of technological applications and fundamental research. Their properties like electrical switching, IR transmission, photoconductivity and photovoltaic effect have raised a great deal of interest in the areas of electronics and optoelectronics.

From the fundamental point of view amorphous materials are of considerable intrinsic interest. For many years crystalline solids have been studied well which has led to

a good understanding of their physical properties. Crystalline state is characterised by a regular periodicity in the atom or ion position over long distances. The salient features of crystalline semiconductors, like the existence of sharp edges in the valence and conduction bands leading to a well defined forbidden energy gap, are direct consequences of short and long range order. In the case of amorphous semiconductors it is more convenient to define them by stating what it is not than by precisely specifying what they are[1]. Amorphous semiconductors are non-crystalline. They lack long range periodic ordering of their constituent atoms. Although they have been known and investigated to some extent even longer than well known crystalline semiconductors such as Ge, GaAs etc., many of their electronic and structural properties have posed and still do pose an enigma for any kind of complete description. Since they do not exhibit the long range order typical of crystalline materials, their properties differ significantly from their crystalline counterparts. The wave vector **k** so important in describing electronic behaviour in crystalline semiconductors, no longer has any significance. There is no well defined density of states or sharp forbidden gap, but rather a continuous range of states throughout what was the forbidden gap in the corresponding crystalline material. Their conductivity cannot generally be increased appreciably by the incorporation of impurities, because the random network of atoms can accommodate an impurity without leading to an extra electron or hole [2-3]. This concept is based on the fact that the impurity atom can satisfy its valence requirements by adjusting its nearest neighbour environment and thus exerting little effect on the electrical properties. Another argument is that the high density of localized states in the forbidden gap effectively pin the Fermi level so that the properties of the material remain little affected.

1.2 Features of the amorphous state

In general, the structure of an amorphous solid can never be determined unambiguously and the uncertainty in the determination is compounded by the fact that the structure of a

non-crystalline material is both at microscopic and macroscopic levels, often depending on the method of preparation. Amorphous materials are not completely disordered on the atomic scale[1]. Short range order, similar to that present in crystalline materials, are present at very short distances in disordered materials. It is thus useful to do structural modeling which develops the structure by the repetetion of one or more basic molecular units in a way that cannot be identified topologically with any known crystalline structure. The atomic order within a molecular unit might be similar within small bond angle distortions in both crystalline and amorphous phases. This reveals the importance of short range in describing the structural behaviour of non-periodic networks. The important aspects of short range order are the number and type of immediate neighbours and their spatial arrangement about a given reference atom. Given the short range order (in the range of 2-5A°) with three parameters, the number of bonds, the bond length, and the bond angle having well defined values in a narrow range, it is possible to construct a model for amorphous structure.

The structural analysis of a material involves the determination of relative positions of each of the atoms. The absence of periodicity in a glass makes the concept of unit cell invalid or one can consider unit cell as infinite which implies that the coordinate of each and every atom should be known. The best information one can get from the diffraction methods for a glass is the radial distribution function (RDF) which expresses the probability of finding another atom at a given distance from an arbitrary point.

In both amorphous and crystalline materials the chemical forces holding the atoms together are the same. Therefore the amorphous state is always defined with reference to the crystalline state[4,5]. From a comparison of the radial distribution functions of amorphous and crystalline films of silicon, it has been revealed that covalent glasses exhibit some ordering in their atomic structure. The structural ordering in covalent glasses can be classified into two types depending upon their length scale[6,7]. They are of short range order in the range 2-5A° and of medium range order in the range 5-20 A°.

Structural models play an important role in the determination of structure of amorphous materials. In the RDF plot of amorphous silicon higher order peaks are not present in contrast to the crystalline one. This makes structure determination difficult. The continuous random network (CRN) model, the first model of an ideal glass or amorphous solid proposed by Zachariasen way back in 1932, is the basis[8] for all structural models. Various structural models are used to explain the structure related properties of covalent glasses. Electronic properties of amorphous semiconductors are explained on the basis of band models. The various band models suggested are mainly concerned with the existence of localized states in the tails of the valence and conduction bands and of a mobility edge separating the extended states from localized states. The various models for amorphous semiconductors are discussed in the following sections.

1.3 Structural models

1.3.1 Network models (CRN and COCN)

CRN (Covalent Random Network) model assumes a definite short range order as each of its atoms fulfill its chemical valence requirements according to Mott's 8-n rule [9] where n is the number of valence electrons of the particular atom. The underlying principle of this model is that a closed outer shell of eight electrons is the most stable structure. Small variations introduced in bond lengths and bond angles lead to disorder in the glassy matrix. The major source of randomness is the variations in bond angles. Variation in bond length is much less and are within 1% to those found in crystals. For two fold coordinated chalcogens the flexibility of covalent bond angles is largest compared to tetrahedrally coordinated Si type materials. CRN model generates the amorphous structure without taking into account structural defects such as dangling bonds and voids. It is not adequate to account for features observed in medium range order. However, this model is found to be suitable for glasses such as a -Si, SiO_2 and As_2Se_3.

The random covalent network (RCN) [1,10-11] and chemically ordered covalent network (COCN) models describe the structure of chalcogenide glass more appreciably The RCN and COCN models differ only in their approach to to the distribution of bonds.

Chalcogenide glasses can be prepared over a wide range of compositions. This allows glasses from non-stoichiometric compositions which contain wrong bonds or bonds between like atoms. Consider the case of a simple binary system A_xBi_{1-x}, where A and B atoms belong to say column 'a' and column 'b' of the periodic table respectively. It is essential to estimate the fraction of A-A, A-B, and B-B bonds as they determine a number of physical properties. A statistical estimation of these fractions is given by the RCN model. In RCN model different types of bonds are considered to be equally probable and neglects the relative bond energies. The bond distribution is determined by the local coordinates of A and B and their concentration x. So A-A, A-B and B-B bonds are equally preferred at all compositions except at x = 0 and x = 1. On the other hand, COCN model counts heteropolar bonds by considering the bond energies. Thermodynamically A-B bonds are preferred over A-A bonds and B-B bonds. So at all compositions A-B bonds are maximised first and then A-A and B-B bonds are favoured depending upon the concentrations of A and B. There exists a critical composition at which only A-B bonds are present. A completely chemically ordered phase occurs at this critical composition X_c = Z_B/Z_A+Z_B, where Z_A and Z_B are the coordination of A and B atoms respectively. $GeSe_2$ and As_2Se_3 are the critical compositions in Ge_xSe_{1-x} and As_xSe_{1-x} systems respectively [11]. At critical compositions of many systems, anomalous variations are observed in their physical properties[12-15].

1.3.2 Mechanical threshold model

Phillips and Thorpe [11] as well as Tanaka[16-18] interpreted the dynamical properties of chalcogenide glasses, which form an important class in amorphous semiconductors in terms of the average coordination number Z. They equated the total number of interatomic force field constraints per atom (N_c) to the number of degrees of freedom per atom (N_d).

The model attempts to relate the glass forming tendency with the number of constraints acting on the network. The glass structure is maximally optimised when the number of degrees of freedom (N_d) available for the atoms equals the number of constraints (N_c) in the network ($N_d = N_c$).

The number of constraints (N_c) can be written according to Phillips-Thorpe model as

$$N_c = Z/2 + (2Z-3) \qquad\qquad (1.1)$$

where $Z/2$ is the bond stretching constraints and $(2Z-3)$ is the bond bending constraints for the system with Z bonds. For a 3D system a structural phase transition at the critical value $Z = 2.41$ is predicted at which the network changes from a floppy to rigid type, thereby possessing mechanically optimized structures. Tanaka modified the concepts of Phillips and Thorpe model, by arguing that medium range order also should be considered in the constraint balancing conditions as evidenced by characteristic features in the composition dependence of certain physical properties at $Z = 2.67$, which can be connected to the formation of stable layer structures in the network[16]. As per this modification, the bond bending term $2Z-3$ in eqn.(1) reduces to $Z-1$, because for a planar cluster in the x-y plane an atom bonded to another at the origin has a freedom over the angle θ alone. Hence eqn.(1) gets modified to $N_d = Z/2 + Z-1$, predicting another composition driven structural phase transition at $Z = 2.67$. 2D layered structures are fully evolved at this critical value and for higher values of Z, due to the increase in the number of cross-linked sites, there is a transition to a 3D network.

Transition from an underconstrained to an overconstrained network has been interpreted by Thorpe [18-19] in terms of percolation of rigidity in an inhomogeneous medium containing both rigid and floppy regions. In his concept , there are glassy regions or islands which are rigid and spread out in a soft or floppy region, as shown in Fig.1.1. These regions increase in size as the average coordination number is increased. In other words, the rigid regions start percolating (grow in size and get interconnected) and at Zav

I Polymeric Glass   II Amorphous Solid
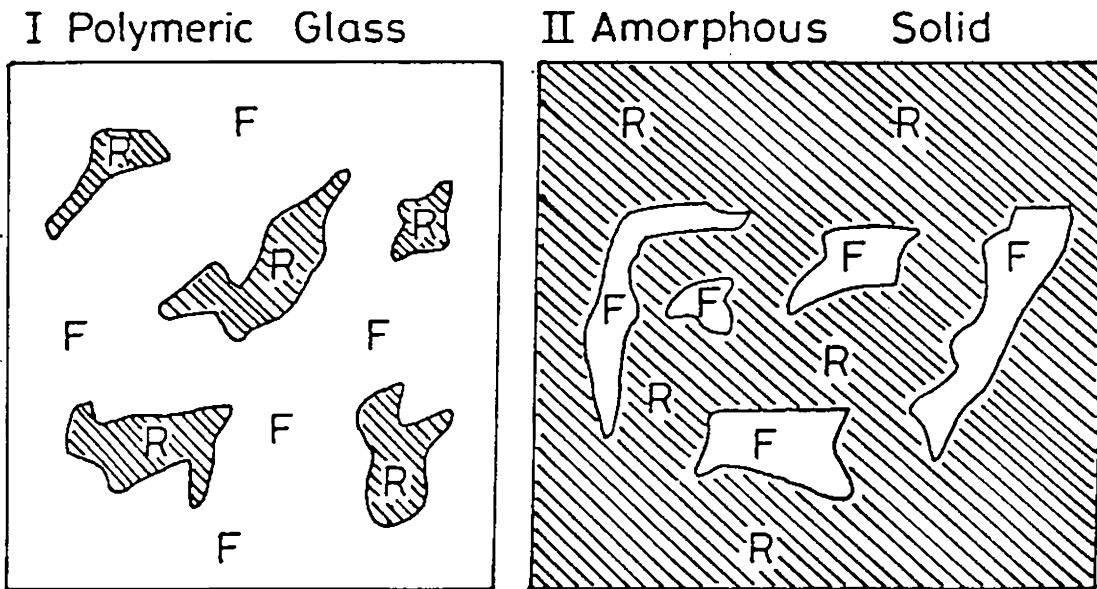
Fig.1.1 Rigid and floppy regions in the network of polymeric glass and amorphous solid

= 2.41 the system transforms into a mechanically rigid amorphous solid. This point at which the threshold occurs is termed the mechanical or rigidity percolation threshold.

Anomalous features in many physical properties have been reported around Z = 2.41 and Z = 2.67 as well as at the chemical threshold in several systems, which have helped in verifying the validity of the above mentioned model in different systems of glasses.

The CRN, COCN and mechanical threshold models discussed above are generally applicable to chalcogenide glasses which obey Mott's 8-n rule[9]. Liu and Taylor proposed a phenomenological model [20] which correlated the glass transition in metal chalcogenide glasses with short range order. This model, called the formal valence shell model, generalises the Mott's rule to include metal atoms. Based on the average coordination number, a classification of non-crystalline solids is shown in Fig 1.2 [21]. The average coordination number Z_{av} decreases from left to right. Towards the left hand

```
┌─────────────────────────────────────────────────────────────┐
│  ←——Metals ——→ ¦ ←——    Semiconductors    ——→               │
│                ¦        or insulators                         │
│                ¦       ¦         ¦                            │
│                ¦       ¦         ¦                            │
│                ¦Overcon¦         ¦underconstrained            │
│                ¦strained         ¦amorphous                   │
│                ¦amor-  ¦ glass   ¦                            │
│                ¦phous  ¦         ¦                            │
│                ¦       ¦         ¦                            │
│                ¦       ¦         ¦                            │
└─────────────────────────────────────────────────────────────┘
   6      5      4       3        2         1
```

Average coordination number
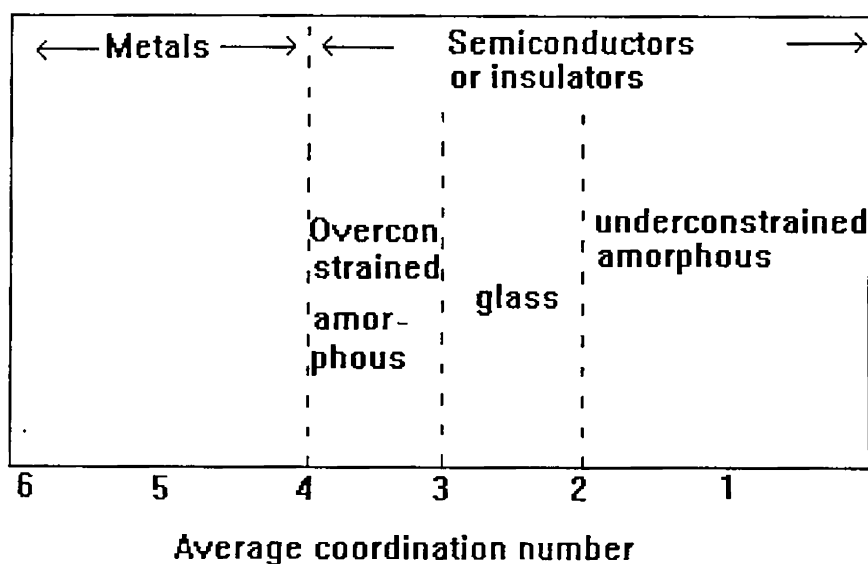
Fig.1.2 Classification of non-crystalline solids based on the average cooordination number.

side the internal strain increases with Z_{av}. Towrads the right, the entropy increases with decreasing Z_{av}, because the material becomes sufficiently cross linked. Glasses are normally restricted to $3 > Z_{av} > 2$. Materials with higher connectivity $4 > Z_{av} > 3$ are overconstrained amorphous whereas those having lower connectivity $Z_{av} < 2$ are under crosslinked amorphous. The mean coordination number $Z_{av} = 4$ separates non-crystalline metals that have close packed structures from covalently bonded semiconductors or insulators.

1.4 Band structure of amorphous semiconductors

1.4.1 General characteristics.

The band structure and hence the electrical properties of amorphous semiconductors are influenced by the long range disorder in their structure. The various models suggested for the energy distribution or the density of states is mainly concerned with the important

question of the existence of localized states in the tails of valence band and conduction band and of a mobility edge separating the extended states from the localized states. A type of conduction unique to amorphous semiconductors is variable range hopping in localized states close to the Fermi level.

If short range order is the same in amorphous state as in the crystalline one, some basic features of the electronic structure can be preserved. In order to account for the translational disorder accompanied by a possible compositional disorder in multicomponent systems, modifications have been proposed for the band structure of amorphous solids. These are the well known Cohen-Fritzsche-Ovshinsky (CFO) and Davis -Mott models. They introduced the basic idea of the presence of localized states in the band extremities. These models have been widely used to interpret experimental data on electrical and optical properties.

Experimental data on electrical transport properties can only be properly interpreted if a model for electronic structure is available. For semiconductors the main features of energy distribution of the density of electronic states $N(E)$ of crystalline solids are the sharp structure of the valence band and conduction band and the abrupt terminations at the valence band maximum and conduction band minimum. This sharp edges in the density of states produce a well defined forbidden energy gap. Within the band the states are extended, which means that the wave function occupies the entire volume. Specific features of the band structure are the consequences of the perfect short range and long range order of the crystal. In an amorphous solid the long range order is lacking whereas the short range order is only slightly modified. The concept of density of states is also applicable to non-crystalline solids. According to Mott, the spatial fluctuation in the potential caused by configurational disorder in amorphous materials may lead to the formation of localized states, which do not occupy all the different energies in the band, but form a tail above and below the normal band. Mott postulated further that there should be sharp boundary between the energy ranges of extended and localized states. These

states are said to be localized in the sense that an electron placed in a region will not diffuse at zero temperature to other regions with corresponding potential fluctuation.

Several models have been proposed for the electronic band structure of amorphous semiconductors. These models are almost similar as they use the concept of localized states in the band tails.

1.4.2 Cohen-Fritzsche-Ovshinsky (CFO) model

The energy states as described by CFO model [22] are shown in Fig.1.3. In this model it is assumed that the extensive tailing of band edges occurs due to the compositional and topological disorders. The extensive tailing makes the conduction and valence band tails overlap in the midgap, leaving an appreciable density of states. As a consequence, there are filled states in the valence band which have higher energies than the unfilled states in the conduction band as shown in the figure.

CFO model was specifically proposed for multicomponent chalcogenide glasses exhibiting switching properties. A redistribution of charges takes place, forming negatively charged filled states in the conduction band and postively charged empty states in the valence band. This ensures self compensation and pinning of the Fermi level near the midgap, as required by experimental observations on electrical properties[23-24].

One of the major objections against the CFO model has been the high transparency of amorphous chalcogenides below a well defined absorption edge. This leads to the conclusion that, the extent of tailing is only a few tenths of an electron volt in the gap[25]. Another is that, according to this model, the elemental semiconductors like a-Si, a-Ge. a-As etc. should not have the extensive band tailing as they are free from compositional disorder[26].
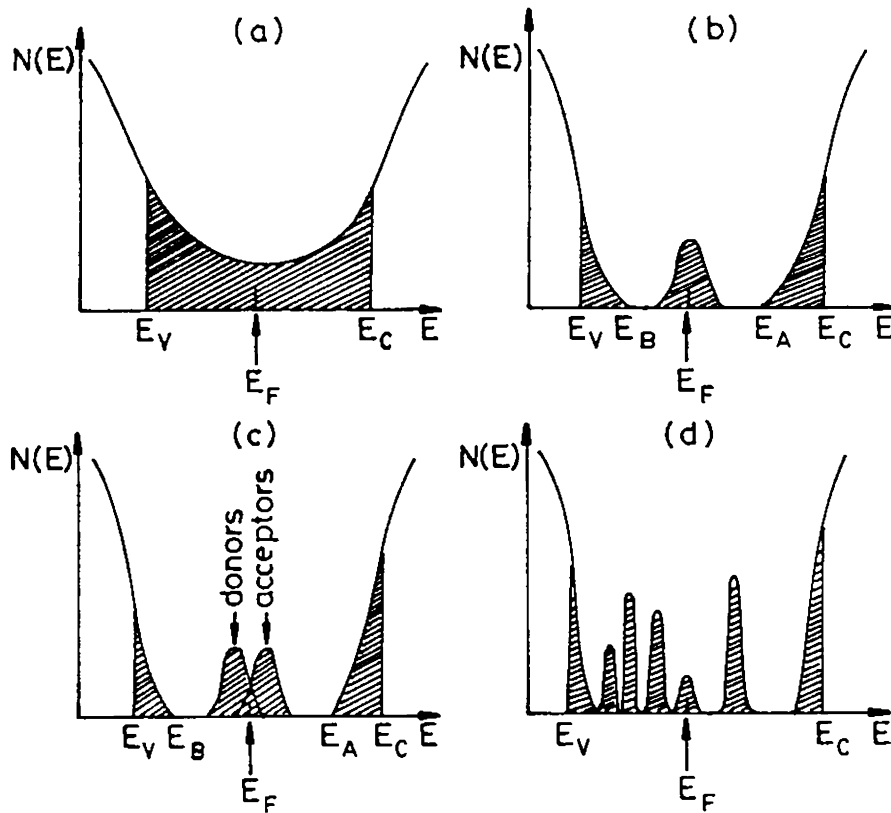
Fig.1.3 Schematic density of states for amorphous semiconductors (a) The CFO model (b) Davis - Mott model showing a band of compensated levels near the middle of the gap.(c) Modified Davis-Mott model (d) the "real" glass with defect states

1.4.3 Davis and Mott (DM) model

According to this model[26-28], the tails of localized states should be rather narrow and should extend a few tenths of an electron volt into the forbidden gap. Davis and Mott proposed further more the existence of a band of compensated levels near the middle of the gap originating from the defects in the random network, like dangling bonds, vacancies etc. Fig 1.3 also outlines the DM model, where E_v and E_b represent the energies

which separates the ranges where the states are localized and extended. The centre of the band may be split into a donor and an acceptor bands, which will also pin the Fermi level(Fig 1.3). Transition from extended to localized states drops the mobility by several orders of magnitude producing a mobility edge. The interval between the energies E_c and E_A act as pseudo gap and is defined as the mobility gap. Experimental evidences, mainly coming from photoconductivity, luminescence and drift mobility measurements, have been found for the existence of various localized gap states associated with defect centres, which are split off from the tail states and are located at well defined energies in the gap. The model explains three processes, which deal with electrical conduction in amorphous semiconductors. The details of these three processes are explained in section 1.6.2 of this chapter.

1.5 Models related to defects

1.5.1 Street and Mott model

Based on Anderson's idea[29] of negative correlation energy(U_{eff}) and experimental observations, Street and Mott [30-31] suggested that specific defects are the origin of important localized states. According to this model, chalcogenide glasses contain 10^{18}-10^{19} cm^{-3} dangling bonds. The bonds are point defects, where normal coordination is not satisfied due to the constraints of local topography. The energy (U_{eff}) formed by the removal of an electron from a dangling bond is sufficient to overcome the Coulomb repulsion resulting from the addition of an extra bond to a different dangling bond.

The major objection to this model is the assumption of high density of dangling bonds. Also the model does not explain why large negative U_{eff} characterises chalcogenide glasses and is absent in tetrahedrally bonded amorphous materials[32]

1.5.2 KAF model

This model has been suggested by Kastner, Adler and Fritzsche[33]. The attraction of this model is that it can identify the exact nature of specific defects believed to be present in the band gap. Thermodynamic arguments require that at finite temperatures all crystals contain defects[34]. If G_f is the free energy of creation of a defect and N_0 is the number of sites in the solid then the number of defects will be $N = N_0 \exp(-G_f/kT)$.

The defect density in crystals does not continue to decrease to zero with decreasing temperature, but freezes in near a temperature at which healing of such defects by diffusion and lattice concentration ceases. By the same argument , only those specific defects which are thermodynamically favored will be present in the glass. In glasses, the lowest temperature at which the defects anneal away is the glass transition temperature T_g. Thus the density of defects depends upon G_f and T_g.

In KAF model ,the lowest energy bonding configuration (the ideal network) is determined. The various possible deviations from ideal network are then identified and ordered according to increasing energy of formations.

1.6 Properties of amorphous semiconductors

1.6.1 Structural properties

In amorphous solids, the structure is developed by the repetetion of one or more basic molecular units that cannot be identified topologically with any known crystalline structure or with any infinite array. There are many discussions on the type of structural models that can be used to explain amorphous solids[30]. Eventhough three dimensional periodicity is absent, one can not say that the structure is completely random like that in liquid or a gas. Moreover, the binding forces between atoms are similar in crystals and amorphous materials. Generally in amorphous materials short range order of a few lattice spacings can be expected. Even within the restraints imposed by individual atoms and

short range order, there is an infinite number of allowed structures for an amorphous material. XRD, IR absorption , electron diffraction and Raman spectroscopy can be used for the detailed investigation of the structure of these materials. Based on the results of such investigations several random network models have been suggested for their structure[8, 36-38]. Structure of stoichiometric melt quenched network glasses show that they are not that random. The diffraction patterns suggest medium range order of the scale 15-30A° as observed in $GeSe_2$ and As_2Se_3[39].

The experimental methods used to determine the structure fall under four major categories; viz diffraction methods, vibrational spectroscopy, photoemission spectroscopy and hyperfine interactions[40-43]. The RDF of amorphous semiconductors give evidence for short range and medium range orders. EXAFs help to determine the local arrangement of each type of atom separately. IR absorption, Raman Scattering, x-ray and uv photoemission techniques are very useful in structural studies. Hyperfine interaction techniques include NMR, quadrupole resonance, Mossbauer effect etc. Differential thermal analysis provides information about changes in structure with variation of temperature[44].

1.6.2 Electrical properties

At room temperature the activation energy for electrical conduction in most of the amorphous semiconductors is approximately equal to 50% of the optical band gap energy. There is a band of localized states which exists near the centre of the band gap of amorphous semiconductors. These localized states arise from specific defect characteristics of the material like dangling bonds, interstitials etc., the number of which depends on the conditions of sample preparation and subsequent annealing treatments.

The d.c conductivity of amorphous semiconductors can be well understood within the frame work of Davis and Mott model[26-28]. The model predicts three regions of conductivity as follows (i) conduction in extended states (ii) conduction in band tails and (iii) conduction in localized states at Fermi energy E_F.

Conductivity in extended states is characterised by large mobility which decreases sharply at the mobility edge. Assuming a constant density of states and constant mobility, the conductivity is shown to vary as [45]

$$\sigma = \sigma_0 . \exp[(-E_c - E_F)/kT)] \tag{1.2}$$

where the pre-exponential factor σ_0 is given by

$$\sigma_0 = eN(E_c)k.T.\mu_c \tag{1.3}$$

$N(E_c)$ is the density of states at the mobility edge E_c and μ_c is the mobility. Electrons at and above E_c can move freely, while those below it can not except through activated hopping.[40]. The mobility in this region is of the order of $10 \ cm^2 V^{-1} s^{-1}$.

Conduction via band tails takes place by exchange of energy with a phonon. If the current is carried mainly by holes and conduction is by hopping, then

$$\sigma = \sigma_i \exp\{(-E_F - E_B + \Delta W_1)/kT\} \tag{1.4}$$

where ΔW_1 is the activation energy for hopping and E_B is the energy at the band edge. σ_i is expected to be less than σ_0 by a factor of 10^2 to 10^4.

In the third region (conduction in localized states), carriers move between states located at E_F via phonon assisted tunneling process which is analogous to impurity conduction observed in a heavily doped and highly compensated semiconductor at low temperatures. Conductivity in this region is given by

$$\sigma_1 = \sigma_2 \exp\{-\Delta\omega_2 / kT\} \tag{1.5}$$

where $\sigma_2 < \sigma_1$ and $\Delta\omega_2$ is the hopping energy of the order of half the width of the defect band shown in Fig 1.4. As temperature is lowered and the carriers tunnel to more distant cites, conductivity behaves as

$$\ln \sigma = A - B \ T^{-1/4} \tag{1.6}$$

This variable range hopping at low temperatures is one of the interesting properties of amorphous semiconductors. As one goes from extended to localized states, mobility decreases by a factor of 10^3 .This drop in mobility is called mobility shoulder[2].

The three mechanisms of charge transport that contribute to d.c current can also contribute to a.c conductivity. The first is due to transport by carriers excited to the extended states near E_c or E_v . Conductivity could be given by a formula of the Drude type,

$$\sigma_{(\omega)} = \sigma_{(0)}/(1+\omega^2\tau^2) \qquad\qquad (1.7)$$
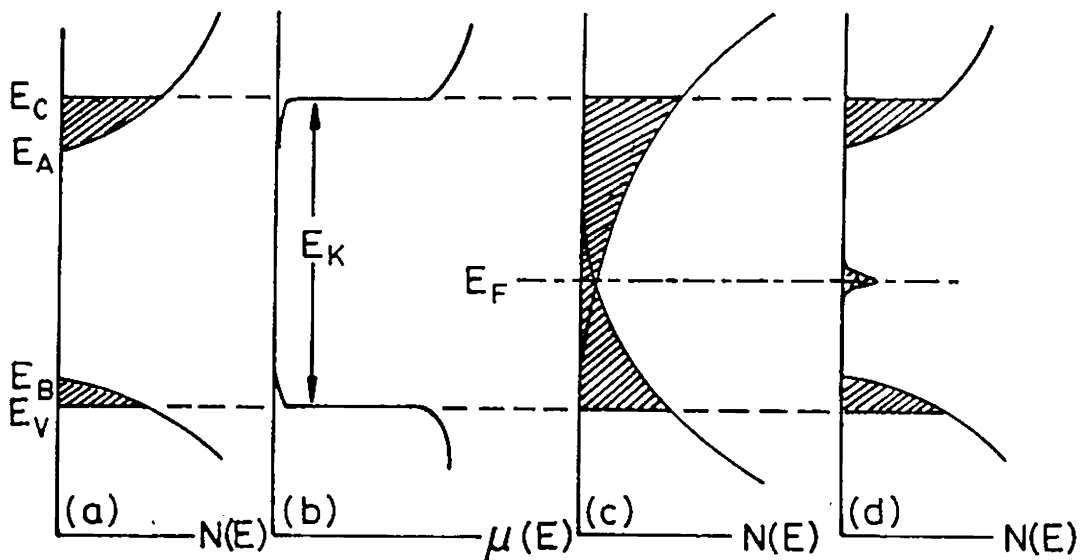
Fig.1.4 Density of states and mobility as a function of energy in amorphous semiconductors

where τ is the relaxation time. The second is due to transport by carriers excited to localized states at the edges of valence or conduction bands. Since transport here is by hopping, conductivity increases with frequency as $\omega^{0.8}$ The third is the transport by carriers with energies near the Fermi level. This again increases with frequency in the same manner as in the second case. Measurement of thermoelectric power as a function of

16

temperature provides the most direct way of determining the temperature coefficient of activation energy for conduction. Measurement of thermoelectric power in amorphous chalcogenides have shown them to be p type in majority of cases. Hall coefficient yields a sign for carriers that is frequently in contradiction with thermoelectric power measurements which are explained by the theory of Friedman[40]. Magnetoresistance [2], which is the fractional change of resistivity in a magnectic field, can also be used, like Hall effect, to determine the carrier mobilities. Magnetoresistance of several amorphous semiconductors are found to be negative over a wide range of temperature. Only at very low magnetic fields and low temperatures it is found to be positive. Studies of transient photoconductivity in several amorphous semiconductors indicate that the response is fast with rise times measured in microseconds at low temperatures and fractions of micro seconds at higher temperatures[46-47].

1.6.3 Thermal properties

For amorphous materials, the phonon mean free path is shorter than that in crystals and correspondingly thermal conductivity is low[48-52]. At low temperatures amorphous materials exhibit a markedly different behaviour from their crystalline counterparts in phonon related properties such as specific heat capacity, thermal conductivity and acoustic absorption.[52-53]. At low temperatures the thermal conductivity decreases slowly with decreasing temperature. Thermal conductivity is weakly temperature dependent near 10 K showing a plateau region and a T^2 dependence at temperatures below 10 K. The magnitude of the temperature dependence appear to depend on the amorphous structure of the material rather than the chemical composition. Hence the thermal transport below 10K is provided by phonons[54]. Acoustic and dielectric absorption in amorphous solids is strongly enhanced at low temperatures and in many glasses large absorption peak is found around liquid nitrogen temperature. The anomalous features observed in specific heat, thermal conductivity, acoustic and dielectric absorption below 4K etc. are interpreted using the two level system (TLS) model proposed by Phillips [48] et.al and Anderson et.al

17

[49]. At high temperatures the atoms forming the TLS change the configuration by means of thermally activated process by hopping over barriers while at low temperatures tunneling through the barriers dominates. The process of glass transition is another aspect that has been receiving continued attention all the time. Glass transitions are usually characterised by a phenomenological value T_g of the critical temperature and by a width ΔT_g of the so called glass transition region around T_g. In this region the diffusive motion of the melt begins to freeze in, before a glassy structure is achieved , with viscosity values typical of solids. Both T_g and ΔT_g depend smoothly on the cooling rate[45]. $\Delta T_g/T_g$ provides a rough estimate of the nonequilibrium effects occurring at glass transition: $\Delta T_g/T_g < < 1$ is a necessary condition for any thermodynamical approach. In good glass forming systems, the above mentioned condition is usually fulfilled at relatively low cooling rates. Nonisothermal heating studies such as differential scanning calorimetry (DSC) could provide great deal of information about thermal properties of glasses like the kinetics of crystallisation and thermal stability of glasses against crystallisation apart from being an indispensable characterisation tool to investigate glass transition.

1.6.4 Optical properties

Amorphous materials are optically isotropic. The sharp feature present in the spectra of crystals are absent in them even at low temperatures. The spectral fine structure is a consequence of k conservation in the crystallisation state. In amorphous solids the vibrational modes are no longer plane waves while in crystals they are plane. Though k is not a valid concept in glasses, the concept of vibrational density of states retains its validity.

Optical absorption in amorphous semiconductors can be separated into three regions with absorption coefficients as noted below: $\beta > 10^4 \text{cm}^{-1}$; $1 \text{cm}^{-1} < \beta < 10^4 \text{cm}^{-1}$ and $\beta < 1 \text{cm}^{-1}$ as shown in Fig 1.5. Regions B and C are due to transitions within the fully coordinated system, perturbed to some extent by defects while region A arises from

transitions involving the defect states directly. The absorption edge has a defect induced tail at lower energies, an exponential region at intermediate energies and a power law region at higher energies. The defects occur in numerous ways like voids arising from preparation techniques, occurence of like bonds , or occasional occurence of coordination variations.
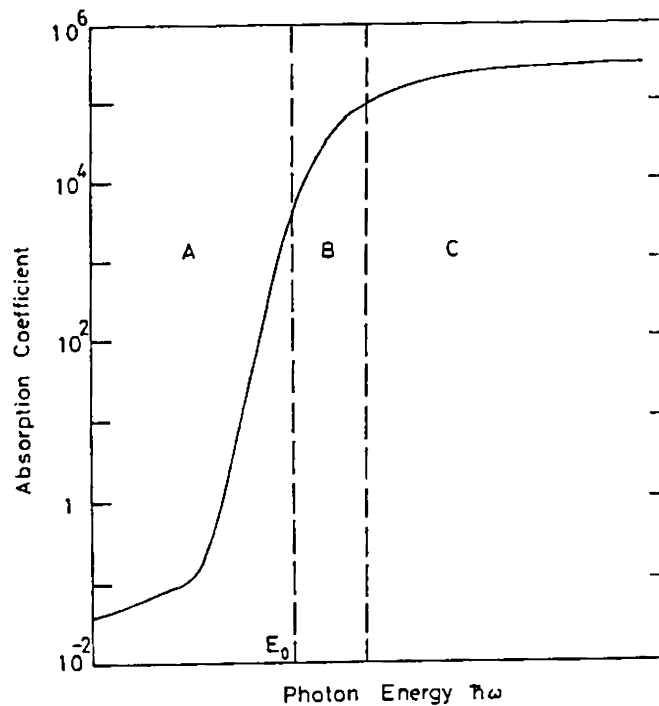
Fig.1.5 Schematic representation of the absorption spectrum of amorphous semiconductors showing three different regions A, B and C.

In the high absorption region, the absorption is governed by a power law of the type $\beta = const.(hv-E_g)^p$ where p=2 for amorphous semiconductors under the assumption of parabolic bands. Amorphous semiconductors continue to absorb strongly beyond the fundamental absorption edge also. Since the k conservation rule is relaxed, all pairs of extended states with energy difference hv can contribute to optical absorption. A plot of

$\beta^{1/2}$ versus hv yields a straight line and the extrapolated hv at which $\beta^{1/2}$ tends to zero gives the value of E_g, which can be used to define the optical gap. The exponential tail in β is associated with intrinsic disorder in amorphous semiconductors in the intermediate range of absorption coefficient. It has been suggested that it is due to disorder induced potential fluctuations [55-56] and strong electron-phonon interaction [57]. In chalcogenide glasses defects due to coordination variation explains several of the optical properties. In the weak absorption region, the shape of the absorption tail is found to depend on the preparation, purity and thermal behaviour of the material[53]. It has been found that the mobility gap in many amorphous semiconductors correspond to a photon energy at which the optical absorption coefficient has a value of approximately 10^4 cm^{-1}

1.7 Preparation and classification of amorphous semi conductors

1.7.1 Methods of preparation

There are at least a dozen techniques that can be used to prepare materials in the amorphous state. Thermal evaporation, sputtering, glow discharge decomposition, chemical vapour deposition and melt quenching are the commonly used techniques to produce most non-crystalline materials of commercial and academic interest[4]. Also there exist techniques like Gel desiccation, electrolytic deposition, reaction amorphisation, irradiation, pressure induced amorphisation solid state diffusion amorphisation etc. Thin films are usually prepared by vapour deposition or sputtering. Bulk glasses having a well defined Tg are usually prepared by the melt quenching technique.

The terms glassy or vitreous are often used synonymously for the amorphous or non-crystalline state. However, in some fields of study, glassy or vitreous connotes the technical preciseness of a definable thermodynamic phase. The existence of a glass state with its glass transition temperature has been documented for some chalcogenides but not for the tetrahedrally bonded amorphous semiconductors. For chalcogenide glasses this is

reflected in the ability to prepare them from a semiconductor melt by rapid cooling or quenching to temperatures below the glass transition temperature[46]. For silicon and the like, quenching from melt is difficult to freeze the melt rapidly to a disordered atomic arrangement. Polycrystallinity is the more common result in these cases. Amorphous semiconductors that can not be prepared directly from the melt are usually fabricated in the form of thin films by an atomic deposition procedure such as evaporation, sputtering, chemical vapour deposition, plasma decomposition of gases or electroplating.

The reason why some of the materials can be prepared in thin film as well as bulk forms whereas others can be prepared only in thin film form can be explained by the nature of the chemical bonds present in these materials. This difference has origin in the mismatch between constraints and the number of degrees of freedom in three dimensions and the flexibility required to accommodate the mismatch. The flexibility of covalent bond angles is largest for two fold coordinated chalcogens and the least for tetrahedrally coordinated Si type materials.

1.7.2 Glass formation

A glass can be considered as a liquid whose atoms have been frozen in place at the glass transition temperature. A glass or a substance in the glass or vitreous state is a material which has been formed by cooling from the normal liquid state and which has shown no discontinuous change in first order thermodynamic properties such as volume, heat content and entropy but had become rigid through a progressive increase in its derivative second order thermodynamic properties like specific heat capacity and thermal expansivity [58]. The temperature at which second order properties change from 'liquid like' to 'solid like' is known as the glass transition temperature(T_g).

Nearly all materials can, if cooled fast enough and far enough, be prepared as amorphous solids. The essential ingredient in the preparation of an amorphous solid is speed. A given material may solidify through either of the two routes indicated in Fig 1.6.

As soon as the temperature of the liquid is lowered to T_f, it may take route (1) to the solid state and crystallise. Crystallisation takes time. In the temperature interval between T_f and T_g, the liquid is referred to as the undercooled or supercooled. If its temperature can be taken below T_g before crystallisation has had time to occur, the undercooled liquid solidifies as glass and remains in this form essentially indefinitely. Therefore the formation of amorphous state is a process of bypassing crystallisation[59].

In order to bypass the crystallisation process, the liquid should be cooled very fast. It means that nearly all liquids can be driven to the amorphous state if sufficient cooling rate is achieved. Cooling rates of the order of 10^2 Ksec^{-1} to 10^6 Ksec^{-1} are required to freeze the disorder. For pure metals cooling rates of the order of 10^9 Ksec^{-1} are required.[59]. Details of glass formation and related processes are discussed in many review articles[60-64].
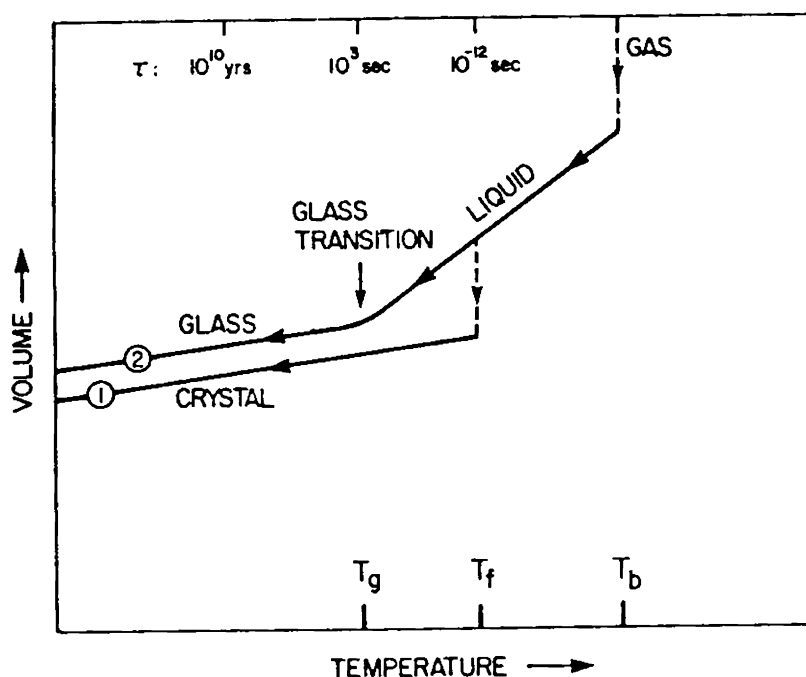

Fig.1.6 The two general cooling paths by which an assembly of atoms can condense into the solid state. Route(1) is the path to crystalline state. Route (2) is the rapid quench path to the amorphous solid state.

1.7.3 Classification of amorphous semiconductors

Amorphous semiconductors can, in general, be divided into two groups: tetrahedrally coordinated silicon like materials and two fold coordinated chalcogenide glasses. Chalcogenide glasses contain one or more of the chalcogens, sulphur, selenium or tellurium, of the sixth column of the periodic table. The distinction between these two classes can be well accounted for on the basis of chemical considerations. The four fold coordination in Si leads to symmetrical bonding and the formation of rigid structures. On the other hand two fold coordination in chalcogens is highly asymmetrical and the structure gives rise to greater degree of flexibility. In chalcogens, but not in 'Si,' the valence band is formed from the lone pair electrons. This is very important when we consider the defect chemistry and various properties that differentiate them from Si like materials. Chalcogenides can be prepared in bulk as well as thin film forms while Si type materials can be prepared only in thin film form.

1.7.4 Chalcogenide glasses

Chalcogenide glasses form an important class of materials. These glasses are a recognised group of materials which always contain one or more of the chalcogen elements, S, Se or Te but not O, in conjunction with more electropositve elements, most commonly As and Ge, but also Bi, Sb, P, Si, Sn, Pb, B, Al, Ga, In,Ti, Ag, lanthanides and Na. Chalcogenide glasses can also contain halogen elements, and include the TeX (X = halogen) glasses[65]. Chalcogenide glasses are generally less robust, more weakly bonded materials than oxide glasses. Both heteropolar (eg. Ge-Se) and homopolar (eg. Se-Se, Ge-Ge) bonds can form in them. Thus a glass contain a non-stoichiometric amount of chalcogens, and excess chalcogen atoms, if any can form chains. The chemical bonding of the matrix is usually directional and covalent. They are band gap semiconductors and are IR transmitting.

The two fold coordination present in the structure enables chalcogenides to cover a wide range of compositions. Their physical properties appreciably vary from sample to

sample and in some cases among samples of the same material. The greatest advantage of these glasses is the composition dependent tunability of their properties, which helps one to design materials for specific requirements. The interest in chalcogenide glasses among scientist and engineers is mainly due to their potential technological applications arising out of their optical, electrical and photosensing properties.

The field effect and doping experiments in chalcogenide glasses indicate that the Fermi level of a chalcogenide glass is nearly pinned. Within certain ranges of composition it is possible to form glasses by combination with one or more of the elements As, Ge, Si, Te, Pb, P, Bi etc. The problem of the classification of a large variety of ternary and quaternary systems becomes difficult due to the freedom to depart from stoichiometric proportions of the constituents. There have been several reports of the effect of impurities on the electrical conductivity of chalcogenide glasses[66-68]. Sometimes they are quite marked; for example, the addition of 1% of Ag to As_2S_3 has been reported to raise the room temperature conductivity by several decades. Eventhough they can not be doped, impurity concentrations in the range of 1% may play a role in modifying the structure by cross linking. The effect of this is to increase or decrease the range of localized states at the band edges and hence change the conductivity. In chalcogenide glasses conduction is predominantly by carriers hopping between localized states at the band edges. The d.c conductivity of most of these glasses at room temperature follows the relation $\sigma =$ $C \exp(-E/kT)$. The thermoelectric power of chalcogenide glasses are normally positive indicating that they are p-type conductors. The values are consistent with the idea of a Fermi energy near the centre of the gap, but nearer to the mobility edge in the valence band. Measurement of thermoelectric power as a function of temperature gives activation energies similar to those obtained in electrical conductivity measurements.

1.8 Applications of amorphous semiconductors

Amorphous or non-crystalline materials have many advantages over their crystalline counter parts when applications are concerned. Generally it is easy to prepare them. Large area homogeneous amorphous thin films can be prepared for solar cell applications. Bulk glasses can often be prepared easily by melt quenching technique.

Amorphous materials have widespread applications in electronic, electrochemical, optical and magnetic areas of modern technology. Many amorphous semiconductors are used as passive and active elements in electronic devices[69-70]. The different electronic applications are in the fabrication of solar cells, thin film transistors and in electrophotography. The ability of certain ions to diffuse readily in oxide or chalcogenide glasses in the presence of a concentration gradient or an electric field opens up a range of electrochemical applications such as solid-state batteries, electrochemical sensors and electrochromic optical devices [71-72]. The most widespread use of an electrochemical sensor is in the so called 'glass electrode' commonly used to monitor proton activity. amorphous materials find applications in communication systems. They are extensively used and being tested for the fabrication of optical fibres, prisms and optical windows. Also they are used as laser materials and light emitting diodes. Selected alloys of amorphous materials have found applications in the manufacture of transformer cores and related materials.

Amorphous chalcogenides have found many applications relating to their photoconducting property. Photoconductors are finding newer and newer applications every day. Two major applications are in xerography and photodetection[73]. Photoexcited charge generation on a metal-photoconductor interface is the basic technique employed in xerography. Regarding photodetection, amorphous materials are generally used in IR and visible detection. The sub band gaps in some amorphous materials are useful in the detection of far IR radiation. Photoconducting materials are finding applications in vidicons, image intensifiers, light operated relays, switches etc. Very good transmittance

of chalcogenide glasses reaching up to the far IR region and the possibility of a continuous shift of absorption edge make their utilisation possible as IR filters and other IR optical elements[74].

The application of tellurium rich glasses as computer memory elements exploit a phenomenon specific to amorphous materials. Electrical switching is actually field induced crystallisation of the material. When the glass to crystal transformation occurs, it results in a large increase in electrical conductivity. The interesting fact is that for materials with memory switching the OFF state may be restored by a short pulse of current, so that the glass to crystal transition is electrically reversible. Although not yet completely understood, the switching phenomena can be visualized in the following way. The OFF to ON and glass to crystal transition results from the Joule heating of the glass which produces conducting channels. By the application of short pulses, ON to OFF and crystal to glass transitions occur which ensure the reversibility of switching behaviour. Switching materials find applications in electrical power control also.

Part B : Photoconductivity, electrical switching and X-ray photoelectron spectral analysis.

1.9 Photoconductivty in amorphous semiconductors

1.9.1 The phenomenon of photoconductivity

Photoconductivity is the enhancement in the dark electrical conductivity of materials due to the absorption of electromagnetic radiation, especially in the visible region. It is different from conductivity induced by the bombardment of particles. The phenomenon of photoconductivity was observed by Willoughb Smith in 1873 with a selenium resistor. Thereafter extensive research had been carried out on different materials to understand this phenomenon and use it for various applications. As a result many of the photoconductors including Se, CdSe etc. found applications in various systems. Different models were suggested to account for the characteristics of photoconductivity in materials[3, 75-77].

The utility of photoconductors arises from the fact that they permit the simple conversion of radiation into electrical currents. Strictly speaking, any material is a photoconductor if the absorption of energy from photons increases its conductivity. On this basis every insulator and semiconductor is a photoconductor, but the number of materials for which the increase in conductivity is large enough to be useful is fairly limited. The reason for this is that many of the characteristics of a material which determine its sensitivity to radiation are associated with imperfections in the crystal structure. Only in certain materials these imperfections are of such a nature as to permit the long lifetimes of the excited charge carriers necessary to produce a large increase in conductivity.

As we have seen, photoconductivity is the improved electrical conductivity of matter produced by the motion of carriers created by absorbed radiation. In the dark under conditions of thermal equilibrium, the thermally generated carriers are distributed among the available energy states in accordance with Fermi-Dirac Statistics. These electrons and holes occupying conduction bands determine the dark electrical conductivity of the

material. Under illumination, a steady state is reached in which the rate of photogeneration is balanced by the various recombination processes, through which the carriers tend to relax to the normal equilibrium distribution. The phenomenon thus involves absorption, photogeneration, recombination and transport processes and an intimate relationship exist between them. This is one reason for the critical role played by photoconductivity in the development and understanding of the physics of semiconductors. Concurrent with the basic studies of photoconductivty there have been the emergence and successful exploitation of a wide range of technologies and devices utilizing this phenomenon. Both basic and applied science have been driven by the need for the development of better characterised materials with controlled properties.

While studying photoconductivity of amorphous solids, the profound effect of disorder on photoelectronic properties bring ample scope for investigations. Carrier mobilities in amorphous solids are typically much smaller than those in the crystalline state, reflecting significantly reduced mean free paths. The translational and, in the case of compounds, compositional disorder introduce large densities of states within the band gap. These can drastically curtail carrier lifetime and thus photosensitivity. In some materials considerable fluctuation in observed properties can occur depending on the preparation conditions, although in the case of certain materials like a-Se and a-Ge significant progress have been made in understanding and controlling such variations.

The following two simplifying assumptions are generally made during discussions of photoconductivity : (i) Conductivity is dominated by one of the carriers so that the contribution of the other can be neglected. (ii) The crystal remains electrically neutral during photoconductivity process without a build up of appreciable space charge so that Δn = Δp. The excess conductivity due to absorbed light is given by

$$\Delta\sigma = e(\Delta n\ \mu_n + \Delta p.\mu_p) \tag{1.8}$$

The increase in conductivity is due to the increase in the densities of n and p charge carriers compared to their values at thermal equilibrium. μ represents the mobility of corresponding carriers. At low temperatures the values of Δn and Δp may be considerably higher than the corresponding equilibrium densities n_0 and p_0. Under steady state conditions, the excess densities are equal to their rate of generation g which is the number of carriers generated per unit time in unit volume multiplied by their average lifetime τ.

$\Delta n = g\tau_n$ and $\Delta p = g\tau_p$

The generation rate is governed by the quantum yield η, which is the number of electron hole pairs generated by the absorption of a photon.

The non equilibrium charge carriers exist until they disappear by recombination of a free electron with a free hole, capture of an electron by a centre in which a hole is localized and capture of a hole by a centre in which there is a bound electron. In steady state the rates of generation and recombination of carriers are equal. In crystalline semiconductors steady state photoconductivity has been extremely successful in determining the recombination centre parameters, in particular, the location of the level in the forbidden gap

Generally, since only one type of recombination centre is present, the non-equilibrium life time is governed by the process of electron capture and subsequent hole capture by the local levels of the dominant centre. Hence the analysis is straight forward for crystalline semiconductors.

The band structure of a real amorphous semiconductor exhibits descrete energy levels associated with defect states. Due to this, analysis of experimental data becomes complex. Different approaches have been adopted regarding the band structure of photoconductors. One considers a slow varying trap distribution consistent with CFO model. When measured as a function of temperature, the photoconductivity of most amorphous semiconductors show a typical behaviour. In high temperature range (regime I) photoconductivity increases exponentially with 1/T, showing a well defined activation

energy. A linear variation of photoconductivity with light intensity is observed here. At lower temperatures (regime II) photoconductivity decreases with 1/T. At still lower temperatures , the curves seem to level off to a constant value. The maximum in temperature dependence generally occurs near the temperature where dark current exceeds the photocurrent. In order to explain these characteristics Weiser et.al [77] proposed a recombination model, which assumes that the electrical transport on either side of the maximum is of the same nature but that the recombination kinetics change in character. The temperature dependent variations are explained with the aid of monomolecular and bimolecular recombinations.

A variety of models exist that successfully explains different experimental findings satisfactorily[78-81] but no model does justice to all the phenomena associated with photoconductivity like the ABFH model[82-85].

1.9.2 Parameters related to photoconductivity

Photoconductivity measurements lead to the determination of certain important parameters like carrier life time, quantum efficiency, photoresponsivity, photodetectivity and spectral sensitivity. Knowledge of these quantities is essential to decide suitability of a photoconductor for any specific applications

1) Carrier lifetime:

Carrier lifetime has two different components as outlined below[75].

Excited lifetime: Excited lifetime is the total time that the carrier remains in the state of excitation. It is the time between the act of excitation and the act of recombination without replenishment. The excited lifetime includes any time that the carrier may spend in traps. It is usually longer than free lifetime and is difficult to determine accurately.

Free lifetime : Free lifetime is the time that a charge carrier remains free to contribute to the conductivity. It is the time that an excited electron spends in the conduction band or the time that an excited hole spends in the valence band.

If light falling on a photoconductor creates f electron-hole pairs per second per unit volume of the photoconductor, then

$$f\tau_n = \Delta n \quad \text{and}$$

$$f\tau_p = \Delta p \tag{1.9}$$

where τ_n is the free life time of an electron τ_p is the free lifetime of a hole and n and p are respectively the additional free electron and hole densities present as a result of the absorption of light. Photoconductivity is then given by

$$\Delta\sigma = f\,e\,(\mu_n\tau_n + \mu_p\tau_p) \tag{1.10}$$

where μ represents the corresponding mobility.

2) Quantum efficiency

It is the number of free electron-hole pairs created per absorbed photon. Quantum efficiency increases with electric field, temperature, and photon energy. It approaches unity for high values of these parameters . It saturates for very high values of these parameters. Quantum efficiency is given by [86]

$$\eta = (I_{ph}/q) / (P_{inc}/h\nu) \tag{1.11}$$

where I_{ph} is the photocurrent generated for an incident light power(P_{inc})

3) Photoresponsivity(R)

The responsivity (R) of a photoconductor is defined by

$$R = I_{ph}/P_{inc} = \eta q/h\nu \tag{1.12}$$

4) Photodetectivity (D)

If σ_{ph} is the excess conductivity due to incident radiation and σ_d is the conductivity under dark condition then photoconductivity is given by $D = \sigma_{ph}/\sigma_d$. Photodetectivity is also

referred as photosensitivity. In order that a photoconductor may behave as a sensitive photodetector the dark conductivity should be low.

5) Spectral Sensitivity (S)

It is the photocurrent generated due to unit change in wave length of incident radiation , assuming all the wave lengths to be of the same intensity.

$S = dI_{ph}/d\lambda$ (1.13)

1.9.3 Spectral variation of photoconductivity

Generally, in most crystalline semiconductors, photoconductivity peaks at wavelength corresponding to the onset of interband electronic transitions. In amorphous semiconductors the spectral response of photoconductivity rises to a maximum at approximately the same frequency corresponding to the optical absorption edge and remains relatively constant at higher energies. As the fall of on the high energy side of the edge in crystals is attributed to the increased rate of surface recombination for carriers generated by strongly absorbed light, this observation presumably implies very similar rates of recombination at the surface and in the bulk. The optical absorption edge of nearly all amorphous semiconductors is far from sharp and infact is normally characterised by an absorption constant that rises exponentially with photon energy. These two feature together make the determination of mobility gaps from photoconductivity data uncertain.

1.9.4 The ABFH model for photoconductivity

Photoconductivity in amorphous chalcogenides has proven to be a valuable tool in understanding the nature of localized levels and transport in these materials. Based on the photoconducting behaviour amorphous chalcogenides can be broadly be divided into two groups , namely Type I and Type II. Most amorphous chalcogenides show Type I photoconductivity which has the following characteristics: (i) Photoconductivity shows a

maximum at a temperature T_m, and it has defined activation energies above (E^+) and below (E^-) the maximum (ii) It shows a linear variation with light intensity and an exponential increase with $1/T$ at temperatures above T_m. (iii) It has a square root variation with light intensity at high intensities, a linear variation at low intensities and an exponential decrease with $1/T$ at low temperatures and (iv) Dark conductivity more than photoconductivity for $T > T_m$ and less for $T < T_m$. In the case of Type II photoconductors the maximum is not present and photoconductivity is much smaller than dark conductivity at all temperatures. Moreover, photoconductivity increases exponentially with temperature for them.

Although a variety of models exist that describe portions of this behaviour adequately[77-81], the entire phenomena is explained best with the model proposed by Arnoldussen, Bube, Fagen and Holmberg[83-85]. This model, which is referred to as the ABFH model, has been applied to analyse the behaviour of many IV-V-VI and V-VI compounds and found best fit with experimental results. The model is found to be consistent with photoconductivity as well as dark conductivity data[85, 87-88]

The striking conclusion that can be drawn from an extensive survey of photoconducting properties of amorphous systems is that many of the energy parameters scale directly with the optical band gap, virtually independently of the specific chemical composition. The ABFH model incorporates the standard carrier recombination statistics applicable to semiconductors and a generalised distribution of localized states within the mobility gap of amorphous semiconductors. Consistency with experimental observations have been established by including in to the model not only the traditional non localized to localized state recombination transitions but also localized to localized state recombination transitions including localized states near the band edges as well as those near the Fermi level

The basic energy parameters and transition processes are shown in Fig 1.7. The energy levels of the model are divided into four categories: (a) non localized states above an energy E_g(all energies are measured from the top of the valence band edge) (b)

localized states below E_g, decreasing rapidly in density or recombination probability below E_c^*, (c) a rapid increase in density or recombination probability for localized states
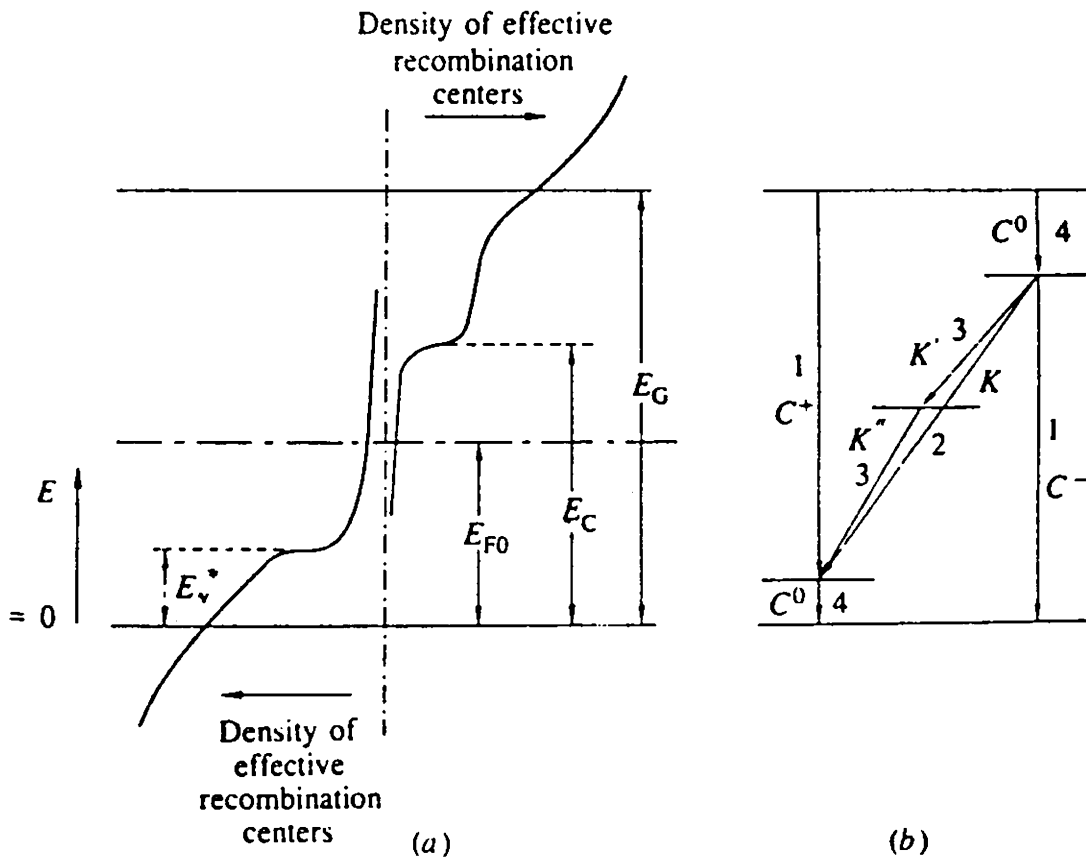

Fig.1.7 Proposed simple photoconductivity model for type I photoconductivity in chalcogenide amorphous semiconductors. (a) Schematic energy level diagram for the proposed model (b) Typical recombinationtransitions considered in the photoconductivity model.

below E_v^* and (d) non localized states below the top of the valence edge at E= 0. The localized states between E_c^* and E_g are called C states and are neutral when unoccupied by electrons; the localized states between E_v^* and 0 (E=0) are called V states and are neutral when occupied by electrons. The density distribution of states between E_g and E_c^* or between E_v^* and E = 0 is not critical to the results of the model. In the extreme case discrete levels at E_c^* and E_v^* would give equivalent results.

There are three types of electronic recombination transitions suggested by this model (i) non localized to localized state transitions such as transitions 1 and 4 (ii) localized near the conduction edge to localized near the valence edge with recombination coefficient K as transition 2 and (iii) localized near one of the edges and localized states near the equilibrium Fermi level as transitions of type 3 with recombination coefficients $K^{'}$ and $K^{''}$.

The various ingredients of this model have been tested for several chalcogenide systems like $AsSeTe_2$, Sb_2Te_3, As_2Te_3, As_2Se_3 etc.[89-90]. The study of temperature variation of photoconductivity presented in this thesis have been analysed on the basis of this model. The behaviour of Type I and Type II photoconductors mentioned above can be explained using this model. More detailed features of this model will be analysed later along with results presented in this thesis.

1.9.5 Analysis based on ABFH model

Type I photoconductivity : summary

Quantitatively photoconductivity of Type I materials can be summarised as follows:

(i) For $T > T_m$, $\Delta\sigma_{ph} < \sigma_d$, $\Delta\sigma_{ph} \propto G$, $\Delta\sigma_{ph} \propto \exp(E^+/kT)$ where G is the rate of generation of electron-hole pairs

(ii) For $T \geq T_m$ $\Delta\sigma_{ph} \propto G^{1/2}$ at high G

          $\Delta\sigma_{ph} \propto G$ at low   G

          $\Delta\sigma_{ph} \propto \exp(-E^-/kT)$

(iii) T_m shifts to lower T if $\Delta\sigma_{ph} \propto G^{1/2}$

    T_m is independent of T if $\Delta\sigma_{ph} \propto G$

(iv) For T<< T_m $\Delta\sigma_{ph}$ >> σ_d , $\Delta\sigma_{ph}$ $\propto$ G, $\Delta\sigma_{ph}$ approaches a constant value.

Photoconductivity model

In materials like amorphous chalcogenide semiconductors, the development of a model for photoconductivty must be a compromise between sufficient detail and necessary simplicity [3, 88]. Fig.1.7 outlines the characteristics of the ABFH model as applied to amorphous semiconductors. The formal procedure for calculating the steady state photoexcited carrier concentration is as follows. (i) Write the steady state occupancy function for a single localized level, in terms of all possible transitions to other localized and nonlocalized states. (2) Write the free carrier continuity equation in terms of these occupancy functions integrated over all localized states.

Consider the rate at which electrons enter and leave a conduction state. In steady state these two rates must be equal. The occupancy function $f_c(E)$, for a conduction state is given by [3]

$$\sum_i (R_{in})_i [1 - f_c(E)] g_c(E) = \sum_i (R_{out})_j f_c(E) g_c(E) \qquad (1.14)$$

where $(R_{in})_i$ is the product of the electron concentration in the initial state i and the rate constant for an electronic transition from state i to a $g_c(E)$ state and $(R_{out})_j$ is the product of the concentration of available final state j and the rate constant for an electronic transition from a $g_c(E)$ state to j. Then

$$f_c(E) = [\sum_i (R_{in} \downarrow)_i + \sum_i (R_{in} \uparrow)_i] \times$$

$$[\sum_i (R_{in} \downarrow)_i + \sum_i (R_{in} \uparrow)_i + \sum_j (R_{out} \downarrow)_j + \sum_j (R_{out} \uparrow)_j]^{-1} \qquad (1.15)$$

Here the terms are separated into upward($\uparrow$) and downward($\downarrow$) transitions of electrons into or out of the $g_c(E)$ state. A similar expression can be written for $F_v(E)$, the occupancy of valence states by holes. All of the terms in the above equation can be written out explicitly.

$$\sum_i (R_{in} \downarrow)_i = nC_e^0(E) \qquad (1.16)$$

$$\sum_i (R_{in}\uparrow)_i = N_v C_h^-(E)\exp(-E/kT) +$$

$$2\int_0^E K(E,E')\exp[(E'-E)/kT][1-f_v^*(E')]g_v(E')dE' \tag{1.17}$$

where $f_v^*(E')$ is the occupancy of valence states by holes.

$$\sum_i (R_{out}\downarrow)_j = \frac{1}{2}\rho C_h^-(E) + \frac{1}{2}\int_0^E K(E,E')f_v^* g_v(E')dE' \tag{1.18}$$

$$\sum_j (R_{out}\uparrow)_j = \frac{1}{2}N_c C_e^0(E)\exp[(E-E_G)/kT] \tag{1.19}$$

The factors 1/2 and 2 enter these equations as result of assuming that the localized states are s like with a spin degeneracy of 2, capable of being occupied by one electronic charge.

The recombination coefficients are explained as follows. $C_e^+(E)$ is the capture coefficient for a nonlocalized electron by a hole in a valence level at E, $C_h^-(E)$ is the capture coefficient for a nonlocalized hole by an electron in a conduction level at E. $C_e^0(E)$ is the capture coefficient for a nonlocalized electron by an empty conduction level at E, $C_h^0(E)$ is the capture coefficient for a nonlocalized hole by an electron occupied valence level at E, and $K(E, E')$ is the transition rate coefficient for an electron initially in a conduction state at E recombining with a hole in a valence state at E'

The continuity equation for nonlocalized electrons under steady state excitation is given in terms of G, the rate of generation of non localized electron hole pairs by incident light by

$$\frac{dn}{dt} = 0 = G - \int_0^{E_G} nC_e^0(E)[1-f_c(E)]g_c(E)dE$$

$$-\frac{1}{2}\int_0^{E_G} nC_e^+(E)f_v^*(E)g_v(E)dE$$

37

$$+\frac{1}{2}\int_0^{E_G} N_c C_e^0(E)\exp[(E-E_G)/kT]f_c(E)g_c(E)dE$$

$$+\int_0^{E_G} N_c C_e^+(E)\exp[(E-E_G)/kT][1-f_v^*(E)]g_v(E)dE \qquad (1.20)$$

A similar equation can be written for nonlocalized holes.

Expressions like those given in equations (1.15) and (1.20) can in principle be used to calculate the steady state photoexcited densities as a function of temperature and light intensity provided that certain assumptions are made about the energy dependence of the densities of localized states and of the rate coefficients. Certain simplifications are needed for careful evaluation of the significant features of the model.

The energy level diagram shown in Fig. 1.7 illustrates one of these simplifications . In order to obtain an exponential variation of photoconductivity with $1/T$ above and below the photoconductivity maximum, it is necessary to limit the distribution of effective localized states controlling recombination to regions of the mobility gap near the mobility edges.

The actual shape of the localized state distributions is not critical as long as there is a rapid change at E_c^* and E_v, compared to changes at higher or lower energies. In the extreme case, E_c^* and E_v^* could be approximated by discrete energy levels. We therefore consider a density of localized states G_c, at and above E_c^* and a density of localized states G_v at and below evacuate. We assume furthermore that mobility of nonlocalized carriers can be expressed as $\mu = \mu_0\exp(-E_\mu/kT)$, where $E_\mu = E_\sigma - E_{FO}$, where E_σ is the activation energy from $\ln\sigma$ vs $1/T$ plot. E_{FO} can be obtained from thermoelectric power measurements.

An analysis of all the possibilities provided by the model leads to the conclusion that, the above equations are consistent with experimental findings on materials possessing

Type I photoconductivity. We assume that in the high temperature range transitions 1 or 2 dominate, whereas in the intermediate temperature range, transition 2 dominates at high intensities and transition 3 at low intensities; and in the low temperature region, transition 4 dominates. Under these conditions fairly small expressions can be derived from the temperature dependence of $\Delta\sigma$ in the high temperature, intermediate temperatures and low temperature regimes assuming $\Delta p \gg \Delta n$, as is the case for these materials.

In the high temperature range $\Delta p \ll p_o$, and it is formally possible for either transitions 1 or 2 to dominate. In either case, charge neutrality is controlled by states at the Fermi level. If transitions 1 dominate, then

$$\Delta\sigma_1 = (Gq\mu_0 / 2kTC_h^- G_c)\exp[(E_c^* - E_{F0} - E_\mu) / kT] \tag{1.21}$$

If transitions 2 dominate, then

$$\Delta\sigma_2 = [Gq\mu_0 N_v / 4(kT)^2 KG_c G_v]\exp[(E_c^* - E_v^* - E_{F0} - E_\mu) / kT] \tag{1.22}$$

In general, transitions 2 dominate at high temperatures as well as at high intensities at intermediate temperatures , although major differences in the analysis of densities and recombination coefficients do not result from using either of the above equations (1.21) and (1.22) in place of the other.

For intermediate temperatures at high intensities $\Delta p \gg p_o$, transition 2 dominates and neutrality is determined by localized states near the mobility edges.

$$\Delta\sigma_{hi} = \left[\frac{G}{2k}\right]^{\frac{1}{2}}\left[\frac{N_v q\mu_0}{G_v kT}\right]\exp[-(E_v^* + E_\mu) / kT] \tag{1.23}$$

At low light intensities in the same temperature range, $\Delta p \ll p_o$, transitions 3 dominate and neutrality is determined by states at the Fermi level.

$$\Delta\sigma_{lo} = \left[\frac{Gq\mu_0 N_v}{N_{F0} K'' G_v kT}\right]\exp[-(E_v^* + E_\mu) / kT] \tag{1.24}$$

where N_{FO} is the density of states at the Fermi level.

Finally at low temperatures $\Delta p \gg p_0$, transitions 4 dominate, and neutrality is determined by states near the mobility edges.

$$\Delta \sigma_{LT} = \left[Gq\mu_{LT} / C_h^0 G_v E_v^* \right] \tag{1.25}$$

where μ_{LT} is an asymptotic mobility reached at low temperatures.

We have the equations

$$E_v^{*0} = E^- - E_\mu$$
$$E_c^{*0} = E^+ + E^- + E_{F0}\big|_{T=0} \tag{1.26}$$

where the superscript '0' indicates the value of the quantity at T = 0 K and results from the fact that it is the value of the energy at T= 0 K that is determined from a measurement of activation energy if the energy varies linearly with temperatures.

These equations are consistent with the characteristics of Type I photoconductivity. If they are applied to a series of photoconductivity curves as function of light intensity and temperature for a given amorphous material, values of N_v, G_v, G_c, K N_{FO}, K", E_v^{*0} and E_c^{*0} can all be derived provided values are assumed for μ_0 and C_h^0. For Type I photoconductors using $\mu_0 = 10 cm^2 v^{-1} s^{-1}$ and $C_h^0 = 10^{-9} cm^3 s^{-1}$, the values obtained for different materials of this type are approximately the same. Type II photoconductivity is characterised by transitions 3. For type II photoconductors transitions 3 dominate photoconductivity over all the measurable range without transforming to a transition 2 dominant region.

Scaling of parameters

Regardless of the specific composition of the material, it is found that the energy parameters of chalcogenide glasses scale with the absorption gap E_g [90]. A survey of some 20 amorphous semiconductors showing both type I and type II photoconductivity, shows that all of them fall, with some small scatter, about a line representing $E_\sigma = 0.46E_g$. Furthermore, for a small group of materials on which complete photoconductivity, and

thermoelectric power data are available, show that $E_c^* = 0.79E_g$, $E_{F0} = 0.36E_g$, $E_v^* = 0.11E_g$, $E_\sigma = 0.49E_g$ and $E_\mu = 0.13\ E_g$.

For many of the amorphous materials the magnitude of photoconductivity also scales with the optical energy gap. An understanding of this behaviour can be obtained by recognising that the maximum photoconductivity should be describable approximately by Eqn. (1.23) with T~ T_m. If all the preexponential factors of this equation were roughly the same for the different materials, then the major temperature dependence of photoconductivity at T_m would be given by the exponential term. Then

$$\Delta\sigma_{max} \propto \exp[-(E_v^{*0} + E_\mu)/kT_m$$

$$\propto \exp\left[-\frac{aE_g}{kT_m}\right] \tag{1.27}$$

[The value of a is approximately 0.24 using $E_v^* = 0.11E_g$ and $E_\mu = 0.13E_g$]

$$\text{or} \quad T_m.\ln\Delta\sigma_{max} \propto -a.E_g \tag{1.28}$$

$\Delta\sigma_{max}$ is the maximum photoconductivity at temperature T_m. A plot between E_g and the product $T_m.\ln\sigma_{max}$ for most of the amorphous chalcogenide systems can be fitted to a straight line. This feature can be used to analyse their behaviour in the light of ABFH model.

1.10 Electrical switching in amorphous semiconductors

The phenomenon of electrical switching in chalcogenide glasses has been an area of intense research ever since Ovshinsky reported reversible switching in amorphous semiconductors[91-101]. Switching could find applications in areas like information

storage, electrical power control etc. Several tellurium containing amorphous semiconductors such as CdTe, GaTe, AsTe, As-Te-Se etc. in thin film form are reported to exhibit current controlled electrical switching[102-107]. Investigations in this area help in understanding the mechanism of switching which is necessary to select and modify materials for specific applications.

Switching is the rapid and reversible transition between a highly resistive OFF state and a conductive ON state driven by an external electric field and characterised by a threshold field. While analysing the OFF state V-I behaviour of a material possessing switching property it can be seen that the V-I characteristic is linear only for a small region at low electric fields. Then the material goes into a quasi equilibrium state where V-I behaviour shows exponential dependence of the form $I \propto V^n$ where n>2. In this region the material switches to a highly conductive state.

1.10.1 Threshold and Memory Switching

Depending on the material, switching can be of threshold type (ON state persists only while a current flows down to a certain holding voltage) or of memory type (ON state permanent until a suitable reset pulse is applied) . Fig.1.8 shows V-I characteristic of both threshold and memory switching possessed by materials. In threshold switching materials, the ON state requires a small holding current (I_h) and a voltage (V_h) to sustain it. Once the switching current is removed, the material reverts back to the low conducting OFF state. In materials exhibiting memory type switching the ON state is restrained even after the removal of the applied field. The application of suitable current pulse will restore the original OFF state. In both cases, switching occurs with a delay time reaching values of the order of 10^{-9} sec, when the voltage across the sample is about 50% higher than the threshold voltage[92].

The crystallisation of the glasses from the melt state is important to determine the switching mechanism rather than from the glassy state. Very easy glass formers may not
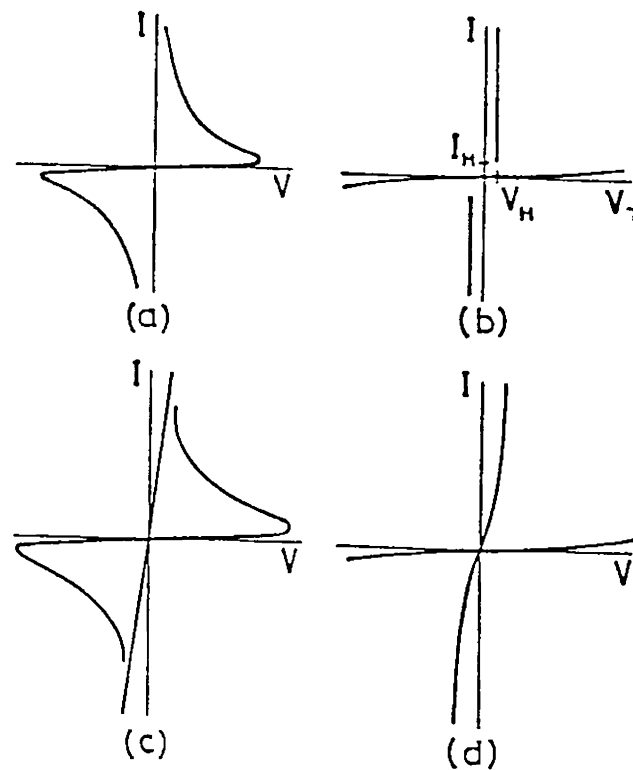
Fig.1.8 The general classification of switching phenomenon exhibited by chalcogenide glasses (a) negative resistance device (b) switching device (c) negative resistance device with memory (d) switching device with memory.

exhibit switching under normal conditions as they prefer to go to glassy state upon cooling. Glasses which can form under very fast cooling may exhibit memory switching[104-105, 108-114].

1.10.2 Switching Models

Different models have been proposed to account for electrical switching process in amorphous alloys based on electronic, thermal, and electrothermal mechanisms[110-112]. These models, in general, assume that threshold switching is electronic in origin whereas memory switching is of thermal origin.

In the case of chalcogenide semiconductors the switching behaviour depends primarily on the electronic structure of the material[98]. Glasses that undergo threshold type switching have relatively large densities[10^{18}-10^{19} cm^{-3}] of positive and negatively charged traps. Under normal conditions these traps called C_3^+ andC_1- sites are present in equal concentrations in the material, and they pin the Fermi level near the centre of the energy gap. Once these traps are filled by generation or injection of electrons or holes under high field conditions, it can be expected that the actual carrier mobility becomes equal to the conductivity mobility in the OFF state. Then the lifetime of excess carriers increase abruptly and an avalanche of carriers reach the conduction band. This leads to a sudden drop in the voltage across the sample and the material switches to a conducting state.

In threshold type switching a redistribution of charge carriers having very different mobilities and transmission rates occur through the electrode interfaces. This gives rise to a space charge and field enhancement near one electrode and to a small value for V_h, the holding voltage after switching. It has been observed that in general the temperature being steady, the threshold voltage is not affected significantly upon the creation of high density of electron-hole pairs by photon or electron bombardment, even though current is increased considerably. But with increase in temperature threshold voltage is found to decrease with an increase in current[115-119].

Memory switching is considered as a consequence of the formation of conducting crystalline channels in the material. The high resistivity of the OFF state resulting from the trap limited mobility inhibits large Joule heating effects. In addition to Joule heating effects, the bulk space charge and the presence of large concentrations of crosslinking atoms together induce crystallisation.

Boer and Ovshinsky[112] presented the concept of electrothermal instability during switching. They solved the thermal balance equation

$$C.\rho.dT/dt = K.\nabla^2 T + \sigma.E_A^2 \qquad (1.29)$$

to calculate the breakdown temperature for switching[119-121]. Here C is the specific heat capacity, ρ is the density, E_A is the applied electric field, K is the thermal conductivity and σ is the electrical conductivity.

According to their analysis the actual switching transition transition can not be a simple thermal runaway (thermistor transition). It would require temperature in the current channel far in excess of those which can be reached without material destruction, and one should be able to stabilise the transition with sufficiently large load resistor.

1.11 X-ray photoelectron spectroscopy (XPS)

X-ray photoelectron spectroscopy is a modern development of early experimentation on photoelectric effect . Photons of sufficient energy would ionize atoms or molecules as

$$M + h\nu \rightarrow M^+ + e^- \qquad\qquad (1.30)$$

The kinectic energy of the ejected photoelectron depend only on the wavelength of the incident photons and not on their intensity. The Einstein photoelectric equation, which is essentially an energy balance equation, relates the energy of the incident photon, $h\nu$ with the ionization potential I of the target and the kinetic energy K.E of the ejected photoelectron. It is given by

$$K.E = h\nu\text{-}I \qquad\qquad (1.31)$$

By analysing the K.E of ejected electrons using appropriate electric fields the ionization potential is determined, and thereby the binding energy of levels can be evaluated.

XPS is a powerful tool for nondestructive surface analysis of materials and it enables one to detect the individual atomic constituents of a sample and their chemical

states. It is extensively used now a days to deduce unknown chemical structures and for analysing both organic and inorganic species

XPS is a direct method for understanding the electronic structure of molecular species. Since valence electrons are directly involved in bonding , they are very sensitive to substituents and other structural features; but since the molecular orbitals they occupy are multicentred, it is not usually possible to identify the individual elements of a molecule from its valence shell XPS spectrum. This difficulty is compounded by the fact that many different types of valence shell orbitals have very similar energies with resultant overlap of adjescent bonds in the photoelectron spectra. However, core electrons within a molecule do retain their atomic identity to a great extent so that XPS can still be used to perform an elemental analysis of molecular species. The presence of a particular element is inferred from the XPS spectrum by the presence of a peak characteristic of the K-shell or other inner shell electrons of the element[122-124]

XPS data can be used to determine the binding energies and relative concentrations of the constituent elements of a compound. It can provide information about the presence of nonbonding electrons, bonding states and the energy values separating bonding and non-bonding states[125-128]. Details of XPS data analysis and interpretation are available in literature[129-132].

In the case of chalcogenides, atoms are covalently bonded and are arranged in an open network with interaction extending upto the third or fourth nearest neighbours. The most important aspect of this short range order is that the number and type of immediate neighbours and their spatial arrangement about a given reference atom do affect the energy levels of its electrons and the corresponding changes can not be predetermined. Other spectroscopies like UV-Vis-NIR can not give information about the binding energy of different electronic levels.

1.12 References

1. G. Lucovsky and T.M Hayes " *Amorphous Semiconductors*" ed M.H Brodsky, Springer , Verlag, Berlin (1985)

2. N.F Mott E.A Davis, *"Electronic preocesses in non crystalline materials "* Clarendon Press" (1971)

3. R.H.Bube *"Photoelectronic properties of semiconductors"* Cambridge University Press (1992)

4. S.R Elliot: *"Physics of amorphous materials"* 2nd ed. Longman, London (1990)

5. A.F.Ioffe and A.R Regel, *Prog. Semiconductors* **4** (1960) 237

6. S.R Elliot *Nature* **354** (1991) 445

7. A.C Wright, R.A Hulme, D.I Grimley, R.N Sinclair, S.W Martin, D.L Price and F.L Galeener *J.Non-Cryst. Solids* **129** (1991) 213

8. W.H. Zachariasen *J.Amer.Chem.Soc.***34** (1932) 3841

9. N.F Mott, *Adv.in Phys.* **16** (1967) 49

10. R.M.White, *J.Non-Cryst Solids* **16** (1974) 387

11. J.C Phillips, *Phys.Today* (February, 1982) 27

12. A.Srinivasan, K.N Madhusoodanan, E.S.R Gopal and J.Philip *Phys.Rev.***B45** (1992) 8112

13. A.Giridhar, P.S.L Narasimham and S. Mahadevan *J.Non-Cryst Solids* **37** (1980) 165

14. G.Mathew, K.N Madhusoodanan and J.Philip *Phys.Stat.Sol(a)* **168** (1998) 239

15. A.Giridhar and S.Mahadevan *J.Non-Cryst Solids* **51**, 1982 305

16. K.Tanaka, *Phys.Rev.***B 39** (1989) 270

17. J.C Phillips *J.Non-Cryst. Solids* **43** (1979) 153

18. M.F Thorpe *J.Non-Cryst Solids* **57** (1983) 355

19. J.C.Phillips and M.F Thorpe, *Solid State Commun.* **53** (1985) 699

20. J.Z Liu and P.C.Taylor, J.Non-Cryst.Solids **114** (1989) 25

21. H.Fritzsche, *Physics Today* (October 1984) 43

22. M.H Cohen, H.Fritzsche and S.R Ovshinsky *Phys.Rev.Lett* **22** (1969) 1065

23. H.Fritzsche in " *Electrical and structural properties of amorphous semiconductors*" Academic Press , London, (1973) 55

24. H.Fritzsche in *"Amorphous and liquid semiconductors*" ed. J.Tauc , Plenum Press, New York (1974) 221

25. D.Adler, Naturewissen schaften **69** (1982) 574

26. E.A Davis and N.F Mott *Phil.Mag* **22** (1970) 903

27. N.F Mott *Phil..Mag* **26** (1972) 505

28. N.F Mott *Contemp.Phys.***26** (1985) 203

29. P.W Anderson, *Phys.Rev.Lett* **34** (1975) 953

30. R.A Street and N.F Mott, *Phys.Rev. Lett* **35** (1975) 1293

31. N.F Mott, E. A Davis and R.A Street , *Phil.Mag* **32** (1975) 961

32. M.Kastner and H.Fritzsche *Phil.Mag* **B 37** (1978) 199

33. M.Kastner, D.Adler andv H.Fritzsche *Phys.Rev.Lett* **37** (1976) 1504

34. R.A Swaline :*"Thermodynamics of solids"* John Willey, New York (1972)

35. A.C Write and A.J. Leadbetter *Phys.Chem.Glass* **17** (1976) 122

36. D.E Polk, *J.Non-Cryst. Solids* **5** (1971) 365

37. G.N Greques and E.A Davis *Phil.Mag* **29** (1974) 1201

38. M. Long, P.Galiron, R.Alben and G.A.N Connel, *Phys.Rev.***B13** (1976) 1821

39. J.C Phillips J.*Non-Cryst. Solids* **35** (1980) 1157

40. R .Grigorovici, *J.Non-Cryst. Solids* **1** (1969) 303

41. G.Lucovsky " *Physical properties of amorphous materials*" ed : D.Adler, Plenum Press, New York. (1985)

42. L. Ley, M. Cordona and R.A Pollk " *Photoemission in solids -II* " Springer- Verlag , Berlin (1979)

43. P.P Seregin, A.R .Regel, A.A Andreev and F.S Wasredinov, *Phy.Stat.Solidi* **74a** (1982) 373

44. R.C Mackenzie *"Differential thermal analysis"* ed : R.C.Mackenzie , Academic Prss, New York (1970).

45. P.Nagels *"Amorphous semiconductors"* ed: M.H Brodsky. Springer Verlag , Berlin (1985)

46. R.Zallen " *The physics of amorphous solids"* John Wiley (1983)

47. H. Scher and E.W Montrell *Phys.Rev.* **B 12** (1975) 2455

48. W.A Phillips (ed), *"Amorphous solids: low temperature properties"* Springer Verlag (1981)

49. P.W Anderson, B.I Halperin and C.M Varma *Phil.Mag* **25** (1971) 1

50. N.H Ritland, *J.Am. Ceram.Soc.* **37** (1954) 370

51. R.Berman, Proc. *R.Soc.London* **A208** (1951) 96

52. A.Vasko, D.Lezal and I. Srb *J.Non-Cryst Solids* **4** (1970) 311

53. R.C Zeller and R.O Pohl *Phys.Rev.***B4** (1971) 2029

54. S.Alexander, O.E Wohlman and R. Orbach , *Phys. Rev.***B 34** (1986) 2726

55. J.Tauc, *Mat. Res. Bull* **5** (1970) 721

56. J.D Dow and D.Redfield, *Phys.Rev* **B 5**, (1972) 594

57. R.A .Street, *Solid State Commun* **24** (1977) 363

58. G.O Jones, *"Glass ,"* 2nd ed, Champan and Hall, London, (1971)

59. D. Turnbull, *Contemp. phys* **10** (1969) 473

60. E.S.R Gopal, *Proc. 30 Years' commemoration. Saha Institute of Nuclear Physics,* Calcutta , India (1983) 37

61. D.Turnbull " *Undercooled alloy phases"* ed: E.W Collings and C.C Koch, Metallurgical Soc. Warrendale PA (1986) 3

62. F. Yonezawa, *"Solid state physics"* ed: H. Ehrenreich and D.Turnbull, 45 Academic Press Inc-199

63. R.B Schwarz and W.L Johnson, *Phys.Rev. Lett* **51** (1983) 415

64. C.C. Koch, O.B Cavin, C.G Mckamey and J.O Scarbrough, *Appl. Phys.Lett* **43** (1983) 43

65. S.B Seddon, *J.Non-Cryst. Solids* **184** (1995) 44

66. B.T Kolomites, E.A Lebedev and N.A Rogachev *Fiz.Tech. Poluprov.* **8** (1974) 545

67. S.Okano, M.Suzuki, T.Imura, N.Fukada and A.Hiraki *J.Non-Cryst. Solids* **59-60** (1983) 969

68. R.Misra, S.Goel, A.K Agnihotri and A.Kumar *J.Mat.Sc.Lett* **11** (1992) 212

69. Hamakawa " *Non crystalline semiconductors*" ed M.Pollak, Vol. I CRC Press (1987)

70. A.Madan and M.P Shaw "*The physics and applications of amorphous semiconductors*" Academic Press (1988)

71. J. Gabona "*Glass: Current issues*" (1985)

72. G.Eisenman " *Glass electrodes for hydrogen and other cations- Principle and practice*" Marcel Dekker (1967)

73. Z. Cimple and F. Kosek *J.Non-Cryst. Solids* **90** (1987) 577

74. A.C.M Chen, A.M Dunham and J.M Wiang *J.Appl.Phys* **44** (1973) 1436

75. R.H Bube "*Photoconductivity of Solids*" Krieger Publ.Co, New York (1978)

76. J. Mort and D.M Pai "*Photoconductivity and related phenomena*" Elsevier, New York (1976)

77. K.Weiser, R.Fisher and M.H Brodsky. "*Proc. of the 10 th int. semiconductors Conf.* Cambridge U.S, AEC, Oak Ridge (1970)

78. E.A Fagen and H.Fritzsche *J.Non-Cryst Solids* **4** (1970) 480

79. J.G Simmons and G.W Taylor *J.Non-Cryst Solids* **8-10**, (1972) 947

80. J.G Simmons and G.W Taylor *J.Phys.* **C6**, (1973) 3706

81. G.W Taylor and J.G Simmons *J.Phys* **C7** (1974) 3067

82. T.C Arnoldussen, R.H Bube, E.A Fagen and S.Holmberg *J.Non-Cryst Solids* **8-10** (1972) 933

83. T.C Arnoldussen, R.H Bube, E.A Fagen and S.Holmberg *J. Appl. Phys* **43** (1972) 1798

84. T.C Arnoldussen , C.A Menzes, Y.Nakagawa and R.H Bube *Phys.Rev.***B9**, (1974) 3377

85. R.H Bube, J.E Mahan, R.T.S Shiah and H.A Vander Plas, *Appl.Phys.Lett* **25** (1974) 419

86. P. Bhattacharya " *Semiconductor optoelectronic devices*" Prentice Hall of India Pvt. Ltd. (1995)

87. C.J Park, J.E .Mahan, R-T-S Shiah, H.A.Vander Plas and R.H .Bube , *J.Appl.Phys* **46** (1975) 5307

88. R.H.Bube, *RCA Review* **36** (1975) 467

89. W.Shockley and W.T Read *Phys.Rev* **B 87** (1952) 835

90. R.T.S Shiah and R.H. Bube *J.Appl.Phys.* **47** (1976) 2005

91. S.R Ovshinsky *Phys.Rev. Lett* **21** (1968) 1450

92. S.R.Ovshinsky and H.Fritzshe *IEEE Trans.on Electron Devices* **20** (1973) 91

93. R.Neale and J.A Aseltine *IEEE Trans.on Elecron Devices* **20** (1973) 195

94. S.R Ovshinsky and H.Fritzsche *Met.Trans.* **2** (1971) 641

95. M.H Cohen, R.G. Neale and A.Paskin, *J.Non-Cryst. Solids* **8-10** (1972) 885

96. A.G.Steventon, *J.Non-Cryst Solids* **21** (1976) 319

97. K. Nakashima and K.C . Kao *J. Non-Cryst Solids* **33** (1979) 189

98. D. Adler , H. K Henisch and N.F Mott, *Rev.Mod.Phys.* **50** (1978) 209

99. D. Adler and S.C Moss *J. Vac.Sci & Technol.* (1972) 1182

100. A.E Owen and J.M Robertson, *IEEE Trans. on Electron Devices* **20** (1973) 105

101. J. Bicerano and S.R Ovshinsky *J.Non-Cryst Solids* **75** (1985) 75

102. G.A Denton, G.M Friedman and J.F Schetzina *J.Appl. Phys.* **46** (1975) 3044

103. J.Vazquez , E. Marquez , P.Villares and R. G Jimenez *Materials Letters* **4** (1986) 60

104. R.L Hargraves P.R Mason and J.C Anderson *J.Phys.D : Appl.Phys.* **7** (1974) 85

105. S.S.K Titus, Chaterjee R , Asokan S and A.Kumar , *Phys.Rev.***B48** (1993) 1460

106. S.Prakash, S.Asokan and D.B. Ghare, *Semicond.Sci.Technol.* **9** (1994) 1484

107. J.A savage, *J.Non-Cryst. Solids* **11** (1972) 121

108. A.C Warren, *J.Non-Cryst.Solids* **4** (1970) 613

109. C.F Drake and I.F Scanlan *J.Non-Cryst Solids* **4** (1970) 234

110. W.D Buckley and S.H Holmberg *Solid State Electronics* **18** (1975) 127

111. H.K Henisch, E.A Fagen and S.R Ovshinsky *J. Non-Cryst. Solids* **4** (1970) 538

112. K.W Boer and S.R Ovshinsky *J.Appl.Phys.* **41** (1970) 2675

113. Z.U Borisova; *Glassy Semiconductors* Plenum, New York (1985)

114. D.F Weirauch, *Appl.Phys.Lett* **16** (1970) 72

115. K. Subhani, M.S Shaw and D.Adler *Proc. Int.Conf. on Amorphous Semiconductors*
     Ed: Spear W.E, Univ. of Edinburgh (1977)

116. M.P Shaw, S.C Moss, S.A Kostylev and L.H Slack, *Appl.Phys.Lett* **22** (1973) 114

117. K.Homma, *Appl.Phys.Lett* **18** (1971) 198

118. H.K Henisch W.R Smith and W.Wihl *"Amorphous and liquid semiconductors* ed:
     J.Stuke and W.Brenig, Taylor and Francis, London (1974)

119. D.Adler and C.J Yoffa, *Phys.Rev.Lett* **36** (1976) 1197

120. S.K Shinakawa, Y. Inagaki and T. Arizumi *Jap.J.Appl. Phys.* **12** (1973) 1043

121. G.C Vezzoli and I. M Pratt *Thin Solid Films* **12** (1972) 161

122. C.R Brundle and A.D Baker *"Electron Spectroscopy Vol.I* Academic Press, New
     York, (1977)

123. A.D Baker and D. Betteridge *"Photoelectron spectroscopy"* (Oxford: Pergamon
     Press)

124. R.Oswald, E. Kasper and K.H Gaikler. *J.Elect. Spect and Rel.phenom* **61** (1993)
     251

125. G.Jakovidis, J.D Riley and R.C.G Leckeu *J.Elect .Spect and Rel.Phenom* **63** (1993) 171

126. M.W Conor and C.Colmenares *J.Non-Cryst. solids* **201** (1996) 76

127. F. Parmigiani, L.Rollandi, G.Samoggia and L.F Depro, *Solid State Commun* **100** (1996) 801

128. K. Siegbhan *Nature* **210** (1966) 4

129. A. Fujimori *Phys.Rev.***B27** (1983) 3992

130. A.J Signorelli and R.G Hayes *Phys.Rev.***B8** (1971) 81

131. G.E .Mullenberg " *Hand book of x-ray photoelectron spectroscopy*" Minnesota Perkin Elmer (1978)

132. D.F Mullica, H.O Perkius, C.K.C Lok and V.Young "*J.Elect.Spect.and Rel. phenom.*" **61** (1993) 337

Chapter 2

Experimental method and instrumentation

2.1 Introduction

The details of experimental technique used for the investigations presented in this work are described in this chapter. Experimental setups for a.c and d.c photoconductivity measurements, setup for electrical switching measurements, details of photoconductivity cell fabrication, technical details of x-ray photoelectron spectroscopy(XPS) measurements etc. are outlined in this chapter. The method of preparation of glass samples in the bulk form is also described. The results presented in chapters 3, 4, 5 6 and 7 have been obtained by carrying out measurements employing the experimental techniques outlined in this chapter.

2.2 The photoconductivity setup

The basic requirements for a photoconductivity measurement setup are (i) a radiation source of sufficient intensity in the required spectral range, (ii) optical unit such as a monochromator to select the appropriate wavelength of the radiation for irradiating the sample, (iii) an intensity modulator such as an optical chopper for a.c measurements, if required. (iv) conductivity cell in which sample is mounted and irradiated with the light beam and (v) necessary instruments to measure the signal produced. A general schematic diagram of a typical photoconductivity setup is shown in Fig.2.1. A more detailed description of each of these units is given in the following paragraphs.

```
┌──────────┐   ┌──────────┐   ┌──────────┐   ┌──────────┐   ┌──────────┐
│  Light   │   │ Monochro-│   │ Intensity│   │Conductivity│  │ Measuring│
│  Source  │───│  mator   │───│ modulator│───│  cell -  │───│instruments│
│          │   │          │   │          │   │  Sample  │   │          │
│          │   │          │   │          │   │  holder  │   │          │
└──────────┘   └──────────┘   └──────────┘   └──────────┘   └──────────┘
```
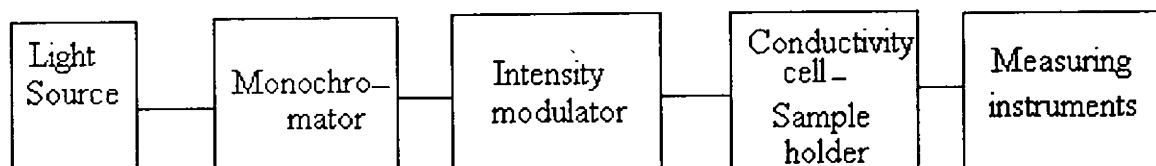
Fig.2.1 A general schematic diagram of photoconductivity measurement setup

2.2.1 Radiation source and monochromator

Incandescent or arc lamps and lasers are the two popular types of light sources that can be used for photoconductivity measurements. High pressure Xe arc lamps, high pressure Hg lamps, tungsten lamps etc. are the commonly used polychromatic sources. There are two major classes of radiation sources used in photoconductivity measurements viz. incoherent sources and coherent sources.

Incoherent sources in u.v-vis-nir region tend to fall into the following two major categories (a) incandescent emitters (b) arc sources . The emission of an incandescent source can be approximated by radiation emanating from a black body at a given temperature. Tungsten lamp provides one of the simplest and most economical sources of continuous radiation throughout the visible and near infrared regions. The most popular incoherent source is the high pressure Xenon lamp. This lamp operates at pressures of 50-70 atm. and is a very efficient emitter of intense radiation from 230 to 700 nm. The most promising source of tunable coherent radiation in uv-visible region is a dye laser. A suitable monochromator can be used to select the appropriate wavelength of the radiation. Both prism and grating monochromators are popular. A suitable lamp-monochromator combination can provide continuous tunability of wavelength from the near infrared to the

ultraviolet. Obviously, suitable optical elements need to be selected depending on the wavelength range of interest.

In our measurements the light sources used are a 300 W tungsten lamp and a 1 kW Xe arc lamp. A McPherson monochromator(Mod.275) has been used for obtaining the desired wavelength for irradiating the sample. This monochromator has a concave holographic grating as the dispersive element and provides a resolution better than 0.1 nm.

2.2.2 Intensity modulator/Optical chopper

A mechanical chopper driven by a motor whose speed can be controlled precisley is the most popular light intensity modulator for a.c photoconductivity measurements. Such choppers provide an almost 100% modulation depth. The optical chopper used in the present measurements is an SRS Model 540 which provides a maximum modulation frequency of 4 kHz. The chopper control unit provides a synchronous signal at the frequency of the chopper with which a lock-in amplifier can be triggered.

2.2.3 Photoconductivity cell

The photoconducting properties of bulk chalcogenide glasses have dependence on composition of the material, temperature, incident wavelength, intensity of light etc.[1]. In order to to carry out these investigations systematically , a versatile photconductivity cell has been designed and fabricated, the details of which are outlined below. A sketch of the cell is given in Fig.2.2. Various parts of the photoconductivity cells are listed in this figure.

Photoconductivity cell mainly consists of the following parts (i) an outer chamber (ii) a cylindrical tube which acts as liquid nitrogen reservoir for the purpose of making low temperature measurements (iii) a sample holder and a glass window. The outer chamber is made of an M.S pipe of outer diameter 20 cm , thickness 6 mm and height 40 cm. M.S
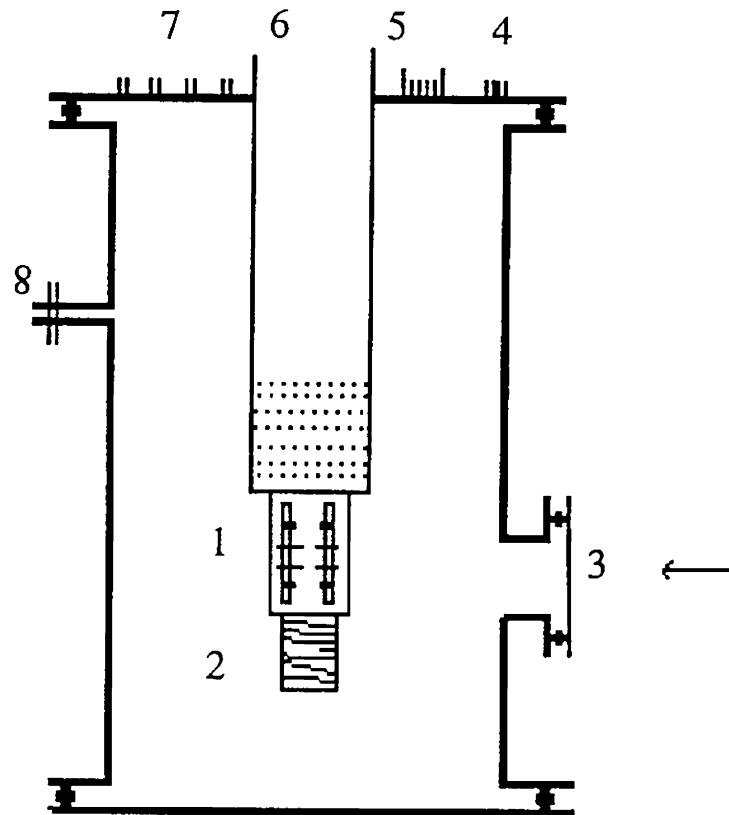
Fig.2.2 A schematic diagram of the photoconductivity cell

1) Sample holder, 2) Heater, 3) Glass window, 4) Heater supply, 5) Connector for temperature sensor, 6) Liquid nitrogen reservoir, 7) BNC connectors, 8) Connector to vacuum pump.

flanges are welded at the top and bottom of this pipe. The flanges have O ring grooves.

The chamber is provided with a vacuum line which can be connected to a rotary pump so that the cell can be evacuated whenever necessary.

External electrical connections to the cell are provided through a port provided on the top of the plate of the chamber. This port is provided with four BNC connectors for

connections from the sample, a D-type connector for taking the signal from the temperature sensor and another connector for heater supply.

The liquid nitrogen reservoir is made of an SS tube which is welded at the center of the top plate. The sample holder which is made of copper is attached to bottom of this reservoir. Since copper is a good thermal conductor with a high value for specific heat capacity, temperature gradients will be minimum across the sample holder. The mass of the sample holder is a critical factor in controlling the temperature. High thermal mass enables one to achieve in very slow rates of heating and cooling. The mass of the sample holder is evaluated after considering the specific heat capacity, power delivered by the temperature controller to the heater, the required rate of rise of temperature and the heat loss from the different portions of the unit. The quantity of liquid nitrogen required to cool the sample to 77 K is also a factor while designing the system for doing low temperature measurements.

2.3 Measurement of photoconductivity

Photoconductivity measurements can be carried out either by d.c (steady state) method or by a.c (pusled excitation) method. These two methods are described separately in the following paragraphs.

2.3.1 d.c Method

In the steady state method, the dark current(I_d) and the d.c photocurrent under steady state illumination(I_{ill}) are measured. The photocurrent (I_{ph})is given by[2]

$I_{ph} = I_{ill} - I_d$.

The block diagrams of the experimental setups for measuring d.c photoconductivity are shown in figures 2.3 and 2.4. It can be done either by the two probe or the four probe method depending on the resistivity and geometry of the sample. Contact resistance can be neglected in the case of samples with high resistivity and two probe technique is

sufficient if the sample has a regular shape. For samples with low resistance, contact resistance can not be neglected and for them four probe technique is preferred. This method eliminates the effect of contact resistance. Moreover, this is more suitable
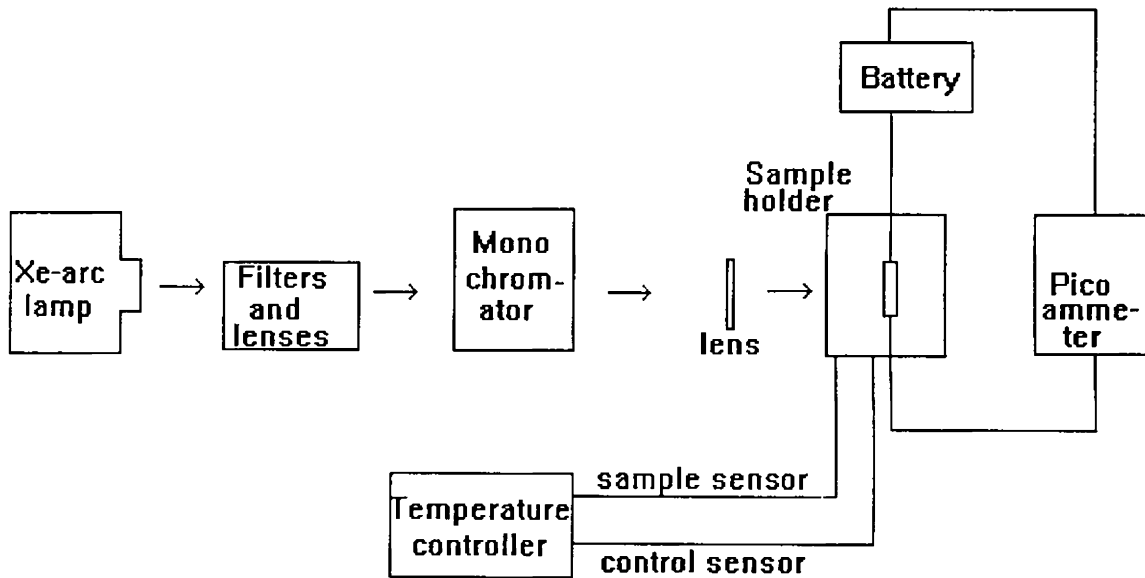
Fig.2.3 Experimental setup for two probe method for measuring d.c photoconductivity

for samples without a definite geometrical shape. The resistivity of a small area specimen is given by $\rho = 2\pi\delta R/\ln.2$ where δ is the thickness of the sample[3]. Of the four probes available, two are used to pass a steady current through the sample and the other two are for measuring the voltage generated across the sample. The larger or thinner is the sample, the closer can the voltage probes be placed to the current probes, in which case the

conductivity of the sample can be measured accurately. Area of contact of the electrodes on the sample should be small compared to the distance between the contacts.
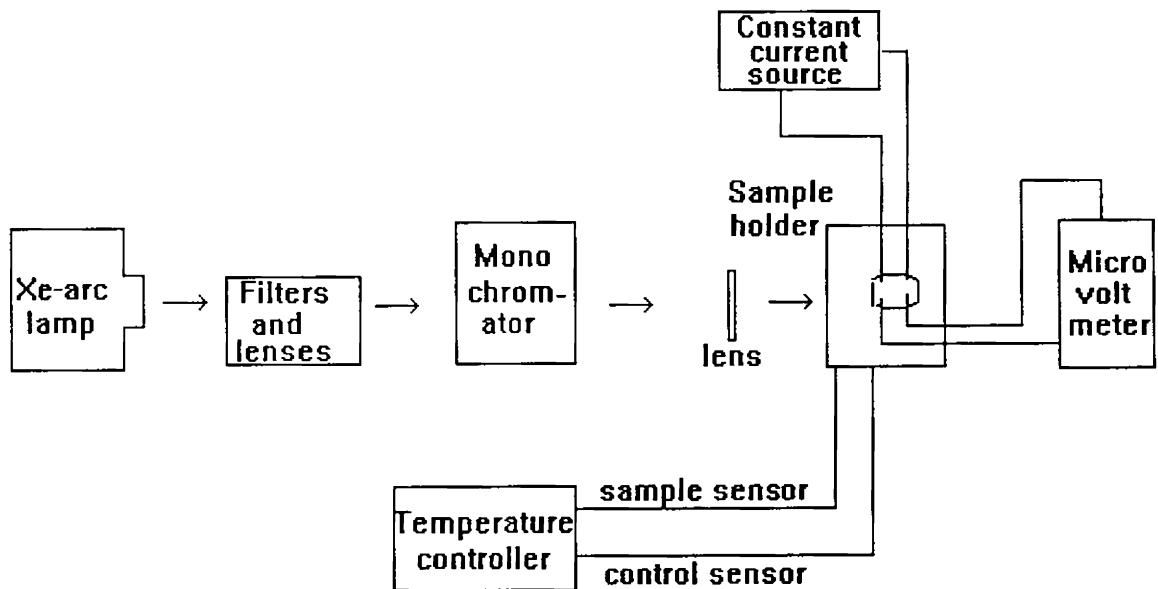
Fig.2.4 Experimental setup for measuring d.c photoconductivity by four probe method.

Since most of our samples are having high resistivity values of the order of 10^8 ohm-m, two probe technique has been adopted for measurements. The samples are polished   and shaped to exact square or rectangular shapes. The electrodes can be connected either in coplanar or sandwich mode. In our measurements for bulk samples the sandwich

configuration has been used. The sample is sandwiched between two conducting glass plates which are SnO_2 coated. In this arrangement the sample can be illuminated through one of the electrodes. The contacts are found to be ohmic from a study of the V-I characteristics of the contacts.

A Keithley autoranging picoammeter(Model 485) is used for current measurements. The incident power is measured using a KIMMON power meter(Model PT-3000)

2.3.2 a.c Method

The a.c method has certain advantages over the steady state (d.c) method. This method eliminates the effect of any stray light, dark current or any other unmodulated signal or any signal modulated at any other frequency[4-6]. Chopped radiation from a 1kW Xe arc lamp(Spectroscopy Instruments) has been used as the excitation source. An SRS 830 DSP lock in amplifier is used for measuring photocurrent signals. The chopping frequency of incident light is fed to the lock in amplifier for its synchronization. The block diagram of the setup for a.c method is shown in Fig.2.5.

Carrier lifetime from a.c photoconductivity measurements

The lifetime of generated carriers can be obtained from a.c photoconductivity measurements by frequency resolved photocurrent(FRPC) measurements. In FRPC the photocurrent is measured by varying the chopping frequency of incident light from 1 Hz onwards and the frequency vs photocurrent plot is drawn. It can be found that the photocurrent attains a threshold maximum value for a particular frequency(f_{max}) above and below which the photocurrent shows lower values. The carrier lifetime(τ) is then given by $\tau = 1/2\pi f_{max}$
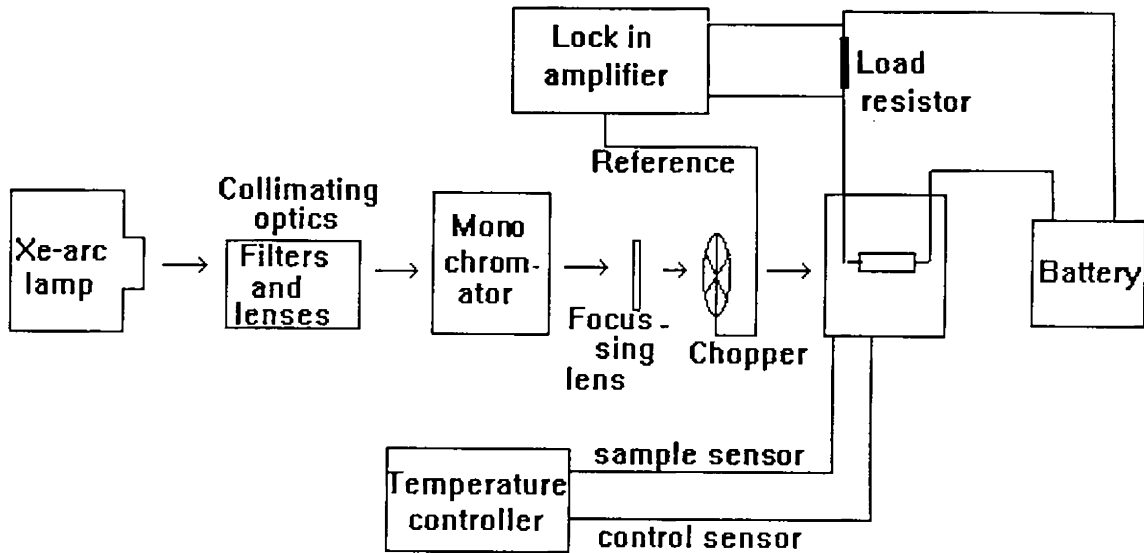
Fig.2.5 Block diagram of the a.c photoconductivity measurement setup

Spectral variation of photoconductivity

While studying the spectral dependence of photoconductivity with a lamp monochromator system, there is the problem of spectral variation of source intensity. This should be normalized to get the exact spectral behaviour. The power of the incident radiation(P_{inc}) is measured for this end. Then by knowing the wavelength(λ) of incident radiation the variation of photocurrent with wavelength can be normalized. If I_{ph} is the photocurrent, then the normalized photocurrent is given by (I_{ph}/q) / ($P_{inc}\lambda$ /hc). Actually this quantity gives the quantum efficiency of the sample at that incident wavelength.

2.4 Electrical Switching Measurements

The block diagram of experimental setup used for electrical switching measurements in amorphous semiconductor samples is shown in Fig.2.6. [7]. Basically, electrical switching measurement setup is the same as that of electrical conductivity. Care is taken to ensure that one of the contact terminals is of pointed type. This is essential to ensure the reproducibility of results.

In order to get the V-I characteristics, a known current is sent through the sample from a constant current source. The voltage developed across the sample is measured by a digital voltmeter. The current through the sample is varied from low values to higher
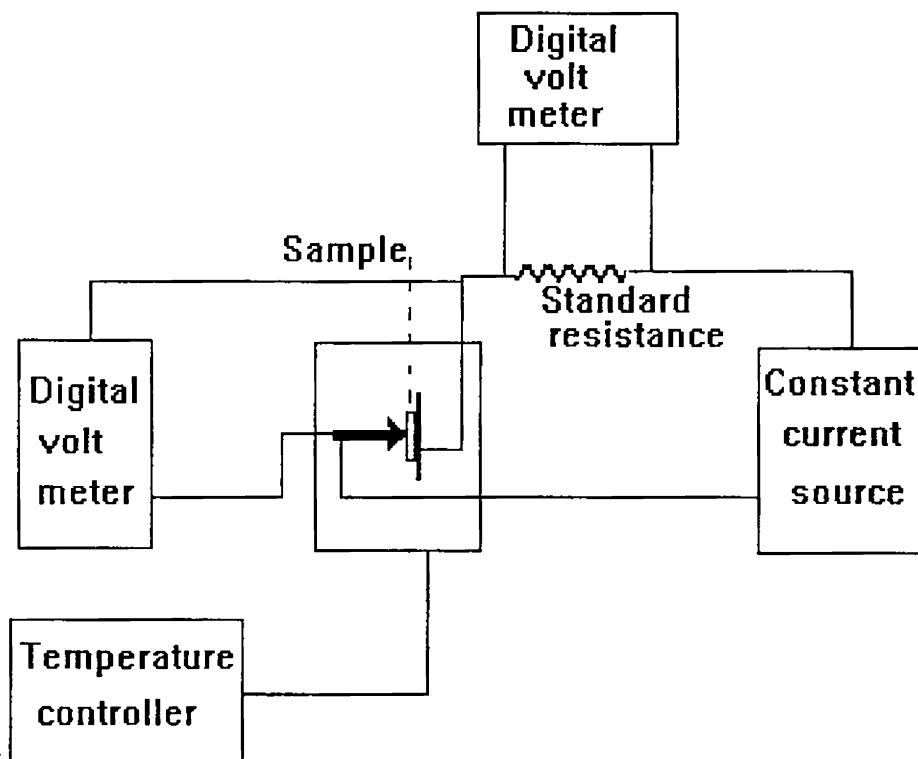
Fig.2.6 Block diagram of experimental setup for electrical switching measurements.

values in steps and the V-I characteristics are plotted. The pointed electrode is positioned at different points on the surface of the sample and measurements are always repeated to check the reproducibility.

Initially the current and voltage show the linear variation (ohmic behaviour). For a particular value of current, the voltage across the sample attains a threshold (V_{th}) value. Further increase in current results in a decrease of voltage and the sample deviates from the ohmic behaviour to a negative resistance region which leads to a high conducting state.

2.5 X-ray photoelectron spectral analysis(XPS)

Surface analysis of a material by XPS involves irradiation of the sample in vacuum with monoenergetic soft x-rays and sorting the emitted electrons by energy. The spectrum so obtained is a plot of the number of emitted electrons per energy level versus their kinetic energy. Each element has unique elemental spectrum and the spectral peaks from a mixture are approximately the sum of the elemental peaks from the individual constituents. Since the mean free path of the emitted electrons is very small the electrons which are detected originate from only the top few atomic layers of the sample[8,9]. A schematic representation of a typical XPS machine is given in Fig.2.7. Since XPS measurements are very delicate and highly sensitive to impurities and environmental changes, extreme care should be taken while recording the spectrum. Some of the relevant points to be taken care of are outlined below[10-11].

Mounting of the sample

In majority of XPS applications sample preparation and mounting are not critical. Typically the sample can simply be mechanically attached to the specimen mount and analysis begin with the sample in the as received condition. Sample preparation is even discouraged in many cases especially when the natural surface is of interest, since almost all procedures will tend to modify the surface composition. Ordinarily any volatile

material must be removed (if there is no special interest in the volatile material) from the sample before analysis. Removal of volatile material can be done by a long term pumping in a separate vacuum system or by washing it with a suitable solvent.

Ion sputtering, etching or other erosion techniques such as use of oxygen atoms on organic materials, can also be used to remove surface contaminants. Argon-ion etching is also commonly used to obtain information on composition as a function of depth into the specimen.

Calibration of the XPS machine

To ensure the accuracy of the XPS data the instrument is calibrated regularly throughout the data gathering process. The energy scale is periodically calibrated using a high
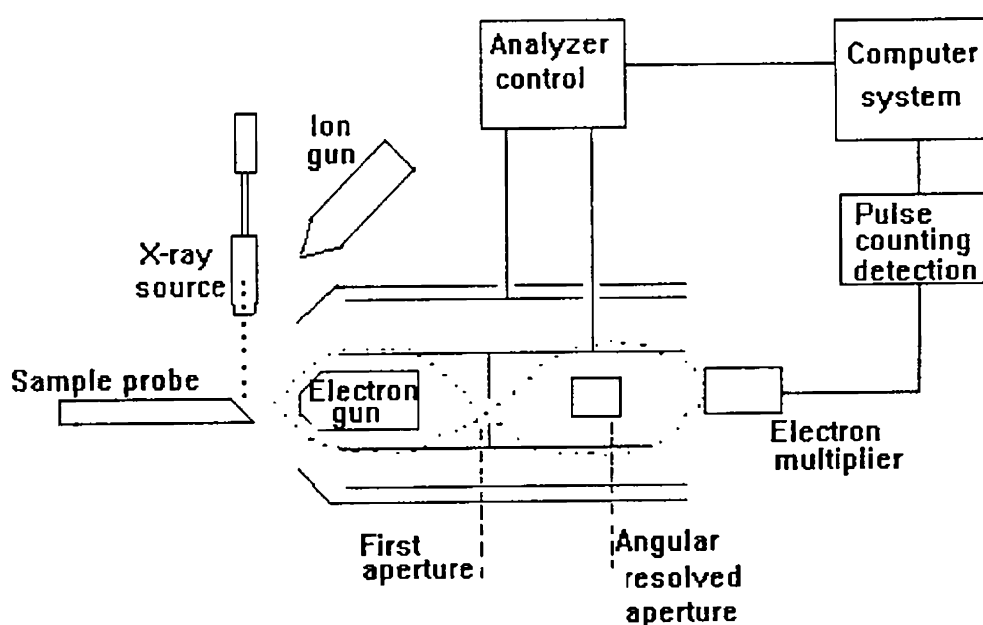
Fig.2.7 A general schematic diagram of an XPS machine

precision digital voltmeter. The best way to check the calibration is to record suitable lines from a known conducting specimen. Typically the Au_{4f} or Cu_{2p} lines are used for calibration. The lines should be recorded with a narrow sweep width in the range of 5-10 eV and pass energy of 20 eV or less. The peak position is determined accurately bydrawing cords parallel to the baseline and drawing the best straight line or simple monotonic curve through the midpoints of the cords.

For the measurements presented in this work, the XPS machine used is a VG Scientific Ltd.(UK). The radiation used is $MgK\alpha$.

2.6 Preparation of samples

Bulk glass of the required material is prepared by the conventional melt quenching technique[8-9]. Spectroscopicaly pure(99.999%) constituent elements are weighed in appropriate proportions. These are taken in a quartz ampoule, evacuated and sealed. The ampoule is then kept in a rotary furnace for nearly 24 hours at a temperature well above the melting point of the constituents. There is provision for periodic rotation and by this the melt get mixed uniformly. The ampoule is then quenched in ice water . The cooling rate is around 500° C per second. Then the ampoule is annealed for nearly one hour at a temperature below the glass transition temperature of the sample. The amorphous nature of the sample is checked by X-ray diffractometry. The sample is then cut and polished so that it has definite geometrical shape.

2.7 References

1. B.T.Kolomiets and V.M Lyubin, *Phys.Staus Solidi(a)* **17** (1973) 11

2. S.K.Tripathi and A.Kumar *J. Non-Cryst. Solids* **104** (1988) 229

3. H.H.Weider, *"Laboratory notes on electrical and galvanomagnetic measurements"* Elsevier Scientific Publishing Company New York (1979)

4. D.Wagner P.Irsigler and D.J Dunstan *J.Phys C: Solid State Phys.* **17** (1984) 6793

5. C.Main, D.P Webb, R.Bruggemann and S.Reynolds *J.Non-Cryst Solids* **137-138** (1991) 951.

6. R.Kaplan *J.Phys: Condens.Matter* **7** (1995) 6847

7. R.Chatterjee, K.V. Acharya, S.Asokan and S.S.K Titus, *Rev. Sci. Instrum* **65** (1994) 2382

8. S.R.Elliot *"Physics of amorphous materials"* 2nd Ed. Longman, London (1990)

9. R.Zallen *"The physics of amorphous Solids"* John Wiley (1983)

10. A.D.Baker and D.Betteridge *"Photoelectron spectroscopy"* Oxford: Pergamon Press (1972)

11. G.E. Mullenberg *" Hand book of x-ray photoelectron spectroscopy"* Minnesota: Perkin Elmer Corporation (1978)

Chapter 3

Photoconductivity in Ge-In-Se glasses

3.1 Introduction

Electrical properties of chalcogenide glasses do not, in general, get affected appreciably by the incorporation of impurities because the random network of atoms can accommodate an impurity without creating an extra electron or hole. This concept is based on the fact that an impurity can satisfy its valence requirements by adjusting its nearest neighbour environment and thus causing negligible effect on the electrical properties[1]. Another argument is that the high density of localized states present in the forbidden energy gap effectively pins the Fermi level. However, experimental results reported by various authors have shown that there are cases in which addition of impurity atoms do change the electrical properties of chalcogenide glasses significantly[2-5]. It has been found that the effect of impurities depend strongly on the composition of the glass, the chemical nature of the impurity and the method of doping. Impurity concentration is a critical factor in such cases because all impurities cannot behave in an electrically active manner. Several of the physical properties are found to improve by the addition of certain impurities. Therefore investigations on the influence of impurities on the properties of chalcogenide glasses are of relevance both from basic science and application points of view.

This chapter presents the results of our investigations on the photoconducting properties of a ternary chalcogenide system, namely Ge-In-Se. Actually this system consists of the basic Ge-Se network with indium acting as an impurity.

In most of the glasses containing IV-VI or V-VI elements, the chemical thresholds are seen to coincide with the mechanical thresholds, making it difficult to isolate the

effects of chemical ordering from those of topological origin in such systems. In the Ge-In-Se system bulk glasses are formed whose average coordination number (Z) cover the mechanical and chemical thresholds as predicted by various models[6-14]. $Ge_xIn_5Se_{95-x}$ glasses with 12< x <32 give rise to average coordination values(Z) ranging from 2.39 to 2.79. The motivation for selecting this system is that they form good glasses in the entire range covering the predicted critical compositions 2.41, 2.67 and 2.73. Moreover, this is a system in which the three thresholds do not overlap. At Z= 2.41 a topological threshold was predicted by Phillips and Thorpe[6,7] whereas at Z= 2.67 a dimensional transition threshold was proposed by Tanaka[8]. The details of these models have already been discussed in Chapter 1. The chemical threshold at Z= 2.73 which corresponds to the stoichiometric composition can be understood in terms of the Chemically Ordered Covalent Network (COCN) model[9,13-14] which has also been discussed at length in Chapter 1. At Z= 2.41 the glass network changes from a floppy polymeric glass to a rigid network. At Z= 2.67 it has been established from topological considerations including medium range order that the glass network changes from a two dimensional layered structure to a three dimensional rigid network arrangement due to complete cross linking.

Many of the physical properties such as optical band gap, glass transition temperature, thermal diffusivity, elastic constants etc. are found to exhibit threshold values at one or more of the above mentioned critical compositions[15-17]. Simulations by H.He et.al[15] on a 3D network of two fold, three fold and four fold coordinated atoms indicate that a distinct increase in the elastic constants C_{11} and C_{44} begin to occur around Z=2.41. The topological transitions and chemical ordering in Ge-In-Se glasses have been investigated by Giridhar et.al.[16]. They reported a minimum in the mean atomic volume at Z=2.45 and a peak at Z= 2.63 which are attributed to the floppy to rigid transition and structural transition respectively occurring in network glasses. Also they observed peaks at the stoichiometric compositions around Z = 2.73. The same authors have investigated

composition dependence of glass transition temperature(T_g) in the Ge-In-Se system and found a slope change at $Z = 2.4$ and a maximum at coordination number $Z = 2.73$ corresponding to the stoichiometric or tie-line composition of the system[17].

In this Chapter we present the results of our investigations on the composition dependence of photoconductivity and carrier lifetime in Ge-In-Se glasses. Variation of these properties with temperature have also been measured and analyzed. Spectral behaviour of photoconductivity has been studied and the quantum efficiency of various compositions have been calculated. The photoconductivity behaviour of this system has been analyzed in terms of the ABFH model and the results are presented.

3.2 Sample preparation and experimental details

Bulk $Ge_xIn_5Se_{95-x}$ (x = 12-32) glasses have been prepared by the melt quenching technique, as outlined in Chapter 2. The amorphous nature of the samples have been confirmed by XRD technique. The XRD patterns of two samples are shown in Fig.3.1. There is no observable sharp peak in the diffractograms, which is characteristic of amorphous materials. The average coordination numbers have been evaluated using the standard procedure[18] adopting the 8-N rule to arrive at the coordination numbers of Ge, In and Se. However, it is known that 8-N rule is valid only for elements from the groups IV-VII; instead a formula of the type $Z=8-n$ has been suggested[19] to evaluate the Z values of compositions containing elements from groups I-VII. Based on this for acomposition with the general formula $Ge_xIn_ySe_p$ (x+y+p = 1), the values of Z can be written as

$$Z= 8-(4x-3y-6p) \tag{3.1}$$

Referring to ref.[19] for further details, for the Ge-In-Se system under consideration, it is seen to be tetrahedrally coordinated and the formal charge transfer would be from Se,

leaving the normally four fold coordinated Ge unchanged. For the evaluation of average coordination number of Se, $Z_{av(Se)}$, this gives the formula
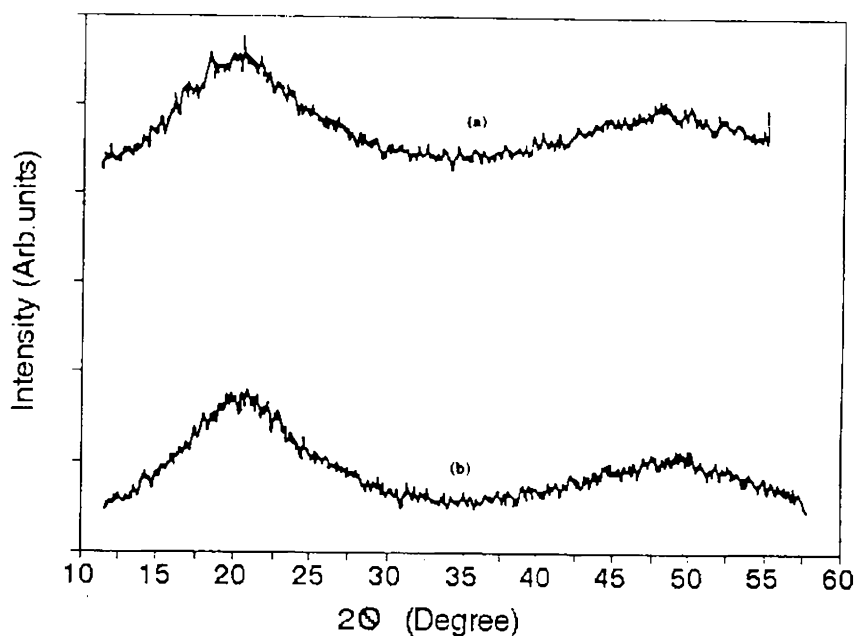
Fig.3.1 XRD patterns of two compositions of Ge-In-Se system. (a) $Ge_{12}In_5Se_{83}$ (b) $Ge_{32}In_5Se_{63}$

$$Z_{(av)(Se)} = (Z-4x-4y)/p \qquad (3.2)$$

Also,

$$Z_{(av)(Se)} = (2p_2+3p_3+4p_4)/4 \qquad (3.3)$$

where p_2, p_3 and p_4 are the numbers of two, three and four fold coordinated Se atoms respectively. Rearrangement of these equations yield

$$p_3+2p_4 = y \qquad (3.4)$$

71

which shows that the number of extra chalcogen bonds relative to the normal two fold coordination is uniquely determined by In concentration. Thus equation(3.2) can be written as

$$Z_{av(Se)} = [2(p_2+p_3+p_4)+p_3+2p_4]/p \qquad (3.5)$$

ie, $\quad Z_{av(Se)} = (2p+y)/p \qquad (3.6)$

Equating(3.5) and (3.6) we get Z= 4x+5y+2p, a value already obtained in which a coordination 5 was used for In, based on the 8-N rule. A tetrahedral coordination has been assigned for In [20,21] in chalcogenide glasses.

Photoconductivity and carrier lifetime have been measured as already described in Chapter 2. Also three compositions of this system have been analyzed by XPS.

Bulk samples having rectangular shape with surface area 5 x 3 mm^2 and thickness 0.5 mm have been prepared for the present measurements. The sample is sandwiched between two SnO$_2$ coated conducting and transparent glass plates, which act as electrodes. Sample can be illuminated through one of these electrodes. A 1kW Xe arc lamp is used as the source of light. The power density of light used for photoconductivity and carrier lifetime measurements is 25 mWcm^{-2}

3.3 Results and Discussion

3.3.1 Pulsed excitation (a.c) and steady state(d.c) photoconductivity measurements

Photoconductivity measurements have been carried out by both pulsed excitation and steady state methods. Fig.3.2 shows the plot of 1/T vs $\sigma_{ph(a.c)}$ for three samples of the Ge-In-Se system and of pure Ge$_{20}$Se$_{80}$, where $\sigma_{ph(a.c)}$ is the a.c photoconductivity and T is the temperature. Photoconductivity increases with temperature initially and attains a

maximum value at a particular temperature(T_m) and then decreases in all these samples. The same type of photoconductivity behaviour is found in d.c photoconductivity measurements as well which is shown in Fig.3.3. In Fig.3.4 the variation of (σ_{ph}/σ_{dc}) with temperature is plotted for $Ge_{12}In_5Se_{83}$ where σ_{dc} is the dark conductivity. The parameter (σ_{ph}/σ_{dc}) is known as the photodetectivity or photosensitivity. This quantity is an
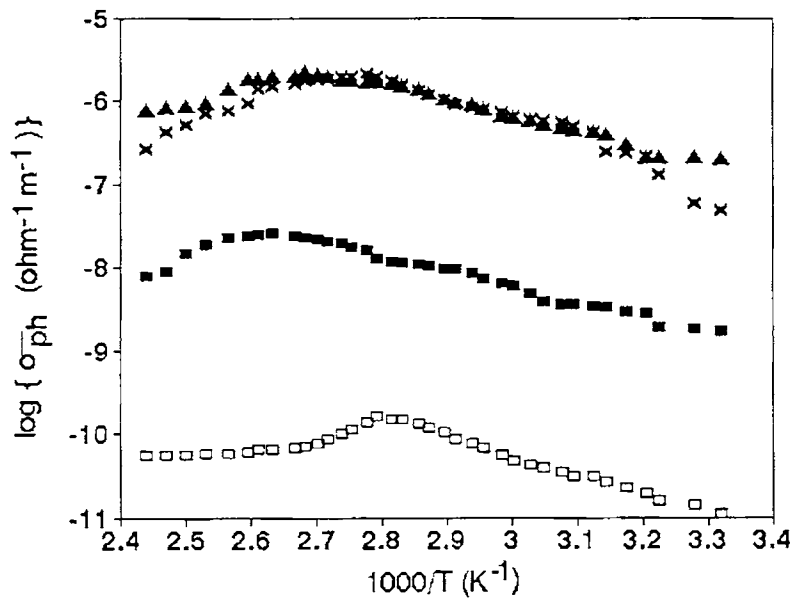
Fig.3.2 Variation of photoconductivity with temperature from a.c photoconductivity measurements. (□□□......$Ge_{20}Se_{80}$, ■■■ ....$Ge_{28}In_5Se_{67}$,(Z=2.7) ×××× ....$Ge_{16}In_5Se_{79}$(Z= 2.47) , ▲▲▲▲.......$Ge_{12}In_5Se_{83}$ (Z=2.39). Chopping frequency is 10 Hz. Uncertainty in the values are less than 4%.

important parameter for a photoconductor as it determines its suitability to be used as a photodetector. It is clear that the dark conductivity should be low to get higher photosensitivity. This quantity is found to decrease with increase of temperature. Fig.3.5 shows the variation of photoconductivity with intensity of illumination. Photoconductivity exhibits a linear dependence on intensity at low intensities and with increase in intensity it is found to get almost saturated. From the temperature dependent study of
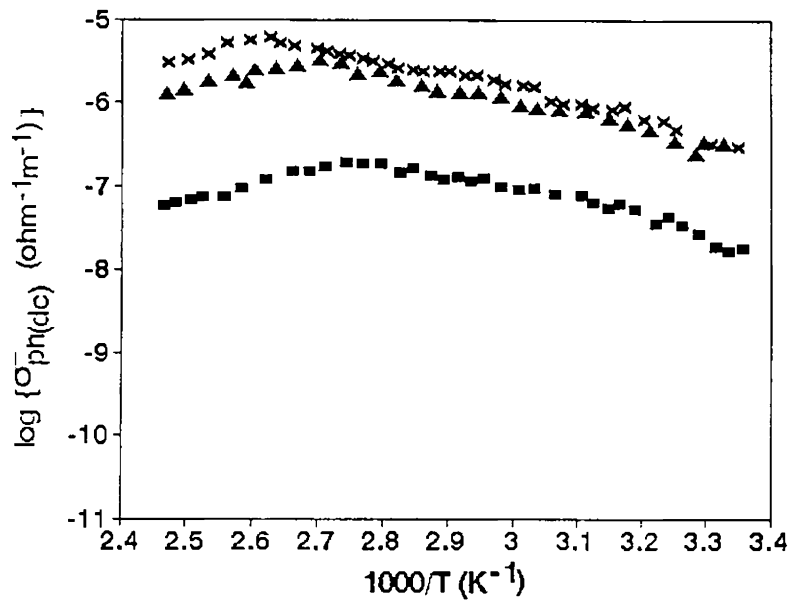
Fig.3.3 Temperature variation of photoconductivity from d.c measurements for three samples (■■....$Ge_{28}In_5Se_6$-, ×××x....$Ge_{16}In_5Se_{79}$, ▲▲▲▲.....$Ge_{12}In_5Se_{83}$).Uncertainty is less than 6%.
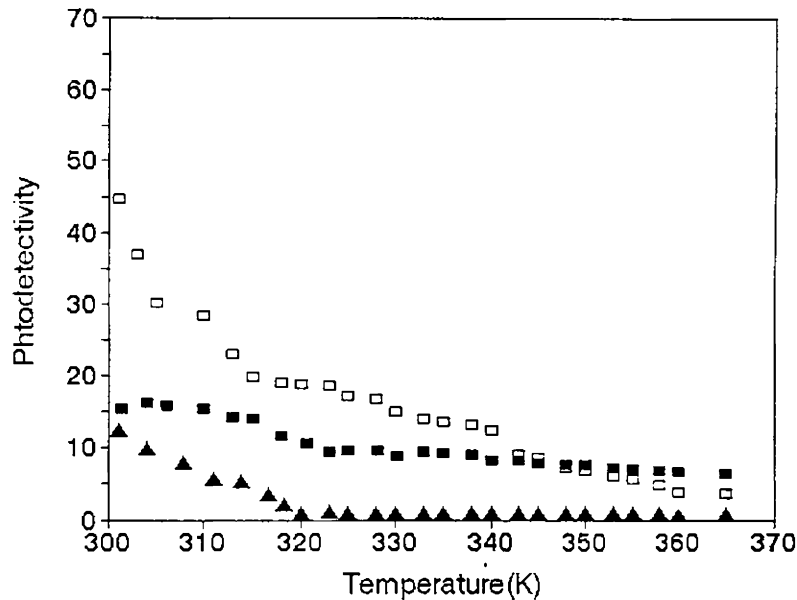
Fig.3.4 Variation of photodetectivty(σ_{ph}/σ_{dc}) with temperature for $Ge_{12}In_5Se_{87}$ (Z=2. 39)...□□, $Ge_{22}In_5Se_{73}$.(Z=2. 59)..■■ and $Ge_{32}In_5Se_{63}$ (Z=2.79) ...▲▲▲▲. Other compositions also exhibit similar variations.

photoconductivity in Ge-In-Se system it has been found that they are type I photoconductors as outlined by the ABFH model[22-24]. Type I photoconductors have a maximum photoconductivity at a particular temperature(T_m), and above and below this T_m, photoconductivity decreases. The maximum photoconductivity has different magnitudes for different compositions. Photoconductivity decreases with increasing temperature for temperatures above T_m, while it increases with temperature for temperatures below T_m in the vicinity of the maximum. When the temperature is low, the variation in photoconductivity is very small and approaches almost a steady state for all the
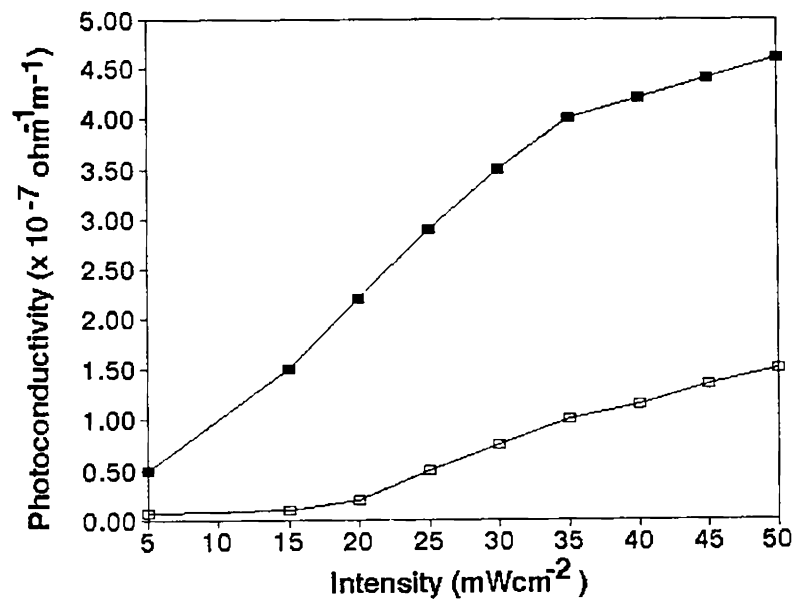
Fig.3.5 Variation of photoconductivity with intensity of illumination for (■■■ ....)$Ge_{13}In_5Se_{82}$ sample(Z = 2.41) and for (□□□ ....) $Ge_{16}In_5Se_{79}$(Z = 2.47). Other samples show similar variations.

compositions. The measurements have been carried out in a low intensity regime where a linear dependence on intensity is observed for photoconductivity. The results can be analyzed with the help of ABFH model which takes into account transitions from valence and conduction band states as well as that from localized states near the valence and

conduction band edges and localized states in the middle of the gap near the Fermi level[24-25].

Type I photoconductivity is explained on the basis of recombination transitions from (i) localized to extended states (high temperature region for $T > T_m$), (ii) localized to localized states (for $T < T_m$ near T_m) and (iii) localized states at the conduction band edge to conduction band extended states or localized states at the valence band edge to valence band extended states. There are two possibilities for localized to localized transitions namely transitions involving localized states at the valence band and conduction band edge and localized states near the Fermi level. The latter one which gives a linear dependence for photoconductivity on intensity is predominant in the present case. In glassy samples the localized states near the band edges arise due to disorder associated with variations in the bond angle, bond length and dihedral angle whereas the localized states near the Fermi level are associated with bonding defects such as C^0, C^+ and C^-[24]. Photoconductivity is greater than dark conductivity up to the temperature T_m. Therefore it can be concluded that carrier generation and recombination mechanisms in these materials are such that the concentration of photogenerated carriers is greater than that of thermal equilibrium carriers in these ranges of temperatures.

In type I materials, for temperatures above T_m, the photoconductivity decreases with 1/T with a variation that can be characterized by a single activation energy E^+ given by

$$\Delta\sigma \propto \exp[E^+/kT] \qquad (3.7)$$

For temperatures just below T_m, photoconductivity increases with 1/T and the corresponding activation energy E^- is given by

$$\Delta\sigma \propto \exp[-E^-/kT] \qquad (3.8)$$

Values of E^+ and E^- are found to be ≈ 0.173 eV and ≈ 0.191 eV respectively for the $Ge_{16}In_5Se_{79}$ sample. The E^+ and E^- values scale with the optical band gap with a factor 0.2.

The sum of E^+ and E^- is found to be less than ΔE, the conductivity activation energy. These characteristics are followed by several other type I materials[24]

In the frame work of ABFH model for type I photoconductors, the relation between maximum photoconductivity σ_{max} and E_g can be expressed as [25-26]

$$\sigma_{max} \propto \exp [-(E_v^* + E_\mu)/kT_m] \tag{3.9}$$

Generally E_v^*, the valence band edge activation energy and E_μ, the mobility activation energy scale with the optical band gap E_g. Therefore,

$$\sigma_{max} \propto \exp[-a.E_g/kT_m] \tag{3.10}$$

$$\text{or} \quad T_m.\ln\sigma_{max} \propto -a.E_g \tag{3.11}$$

A plot between E_g and $T_m.\ln\sigma_{max}$ is shown in Fig.3.6. The points can be fitted to a straight line, which is a clear demonstration for the type I behaviour exhibited by the Ge-In-Se system.
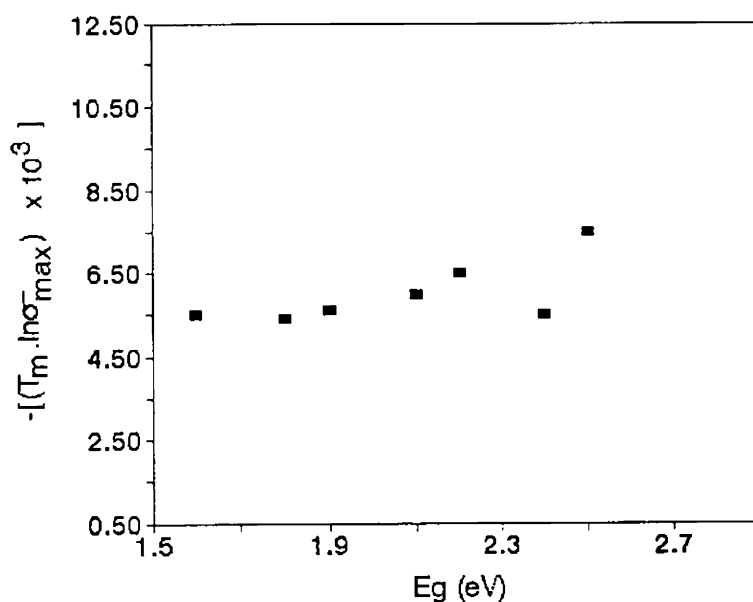
Fig.3.6 Plot between E_g and the product $-[T_m.\ln\sigma_{max}]$ for the $Ge_xIn_5Se_{95-x}$ system.

3.3.2 Composition dependence of photoconductivity

Investigation of composition dependent variation of various properties help to select the most suited material for a specific application. It may also give an insight into the modifications required to produce a material with pre assigned properties.

In general, compared to the pure Ge-Se glass, the photoconductivity of Ge-In-Se system is found to be enhanced by nearly four orders of magnitude as is clear from Fig.3.2. The composition dependence of photoconductivity for the $Ge_xIn_5Se_{95-x}$ glasses is shown in Fig.3.7. In Fig.3.8 the photodetectivity(σ_{ph}/σ_{dc}) is plotted for various compositions.

The enhancement in photoconductivity of Ge-In-Se with the addition of indium can be attributed to the increase of the density of charged defect states formed in the energy gap[27]. The difference between the electronegativities of indium and selenium is the most
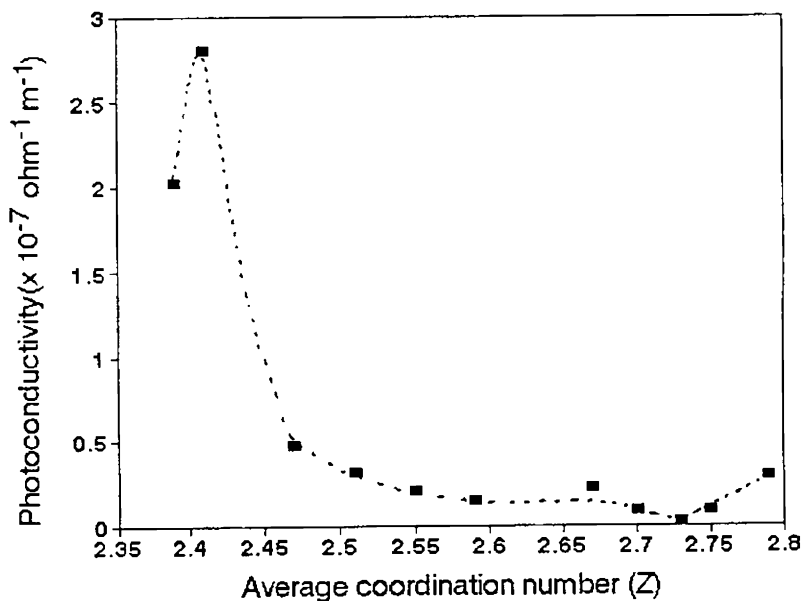
Fig.3.7 Composition dependence of photoconductivity in $Ge_xIn_5Se_{95-x}$ system

probable cause for the generation of charged defect centres. Hopping of the carriers between the defect centres result in the enhancement of photoconductivity. Though photoconductivity increases with addition of indium, photodetectivity is found to be decreased as shown in Fig.3.8

The composition dependent variation of photoconductivity can be understood from Fig.3.7 in terms of the variation in coordination number as well as variation in Ge content.
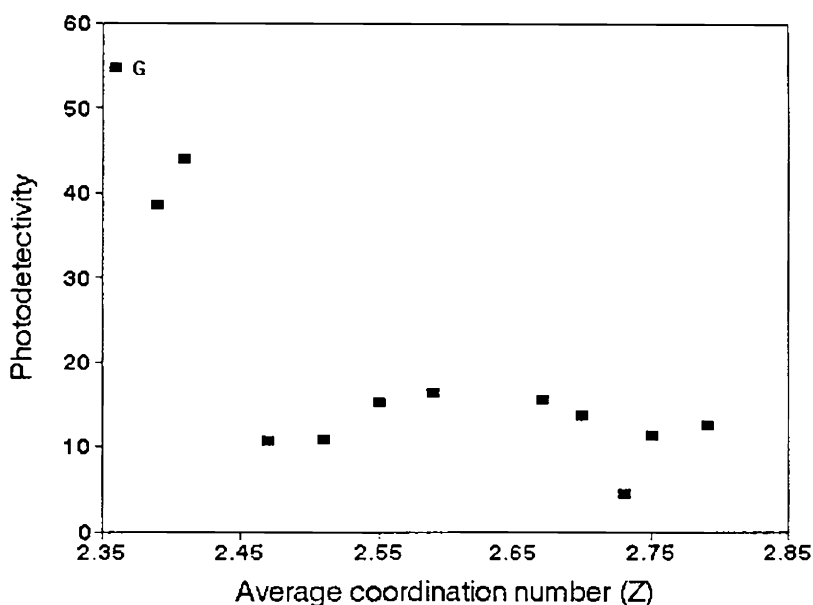
Fig.3.8 Variation of photodectivity (σ_{ph}/σ_{dc}) with coordination number(Z). Point marked as **G** represent the photodetectivity of $Ge_{20}Se_{80}$.

Selenium based chalcogenide systems are dominated by flexible two fold coordinated Se atom chains. Addition of other elements increases the cross linking between selenium chains with the formation of different types of bonds. According to the COCN model the formation of heteropolar bonds is favoured over homopolar bonds[13-14, 28]. The bond energies of the heteropolar bonds are, on the average, higher than those of homopolar bonds.

The Ge_xSe_{100-x} system can be considered as consisting of Ge-Se heteropolar bonds dispersed either in excess of Ge-Se bonds or Se-Se bonds. Addition of indium causes change in the nature of the structural units. The Ge-In-Se glasses are assumed to be composed of cross-linked structural units of tetrahedral $GeSe_2$ and pyramidal In_2Se_3 and excess, if any, of Ge(for Ge rich compositions) or Se (for Se rich compositions). Upon analysis of different compositions it can be seen that the glass with Z= 2.73 consists only of structural units of $GeSe_2$ and In_2Se_3 with neither Se or Ge present in excess. This composition is referred to as the tie line or stoichiometric composition of the system and can be represented by $(GeSe_2)C(In_2Se_3)1-C$ where C and 1-C are the respective fractional contents of $GeSe_2$ and In_2Se_3. If the stoichiometric composition is taken as reference, glasses with Se content greater than that on the tie-line are referred to as Se rich compositions and those with less Se content as Ge rich glasses. The stoichiometric composition consists of only energetically favoured heteropolar bonds with neither Ge or Se in excess. This stoichiometric composition (Z=2.73) corresponds to the chemical threshold of the system. Composition dependent variation of photoconductivity shows that at the chemical threshold photoconductivity assumes minimum value. The chemical ordering and high average energy of bonds in this composition are the reasons for this behaviour. A maximum in optical band gap(E_g) and glass transition temperature (T_g)[16] have been reported at this composition. Also a clear change in photoconductivity has been observed at Z= 2.41. As predicted by the mechanical constraints model proposed by Phillips and Thorpe [6,7] this composition corresponds to the one at which the system undergoes a topological transition from a floppy to rigid network. At this critical composition there is an appreciable enhancement in the density of the sample. For this critical composition the interatomic bonds become rigid and the elastic forces begin to bulid up fast. The network at this composition takes the form of a fully interconnected rigid network with a number of floppy inclusions in it. These floppy inclusions acting as defects providing defect states may be the cause for enhancement in photoconductivity at this critical composition.

3.3.3 Spectral variation of photoconductivity and quantum efficiency

The spectral variation of photoconductivity in Ge-In-Se system for three representative samples are shown in Fig.3.9. The normalized photoconductivity is found to exhibit a rapid rise around the region of absorption edge and then nearly saturates for the wavelengths investigated. The behaviour is not affected by reversing the polarity of the electrodes. Though the photoconductivity saturates near the absorption edge, it is difficult to calculate the exact optical band gap from this data. Since the photocurrent is normalized for the variation of intensity of source with wavelength, the quantity plotted along the y-axis represents quantum efficiency[29-30]. The plots can also be considered as the
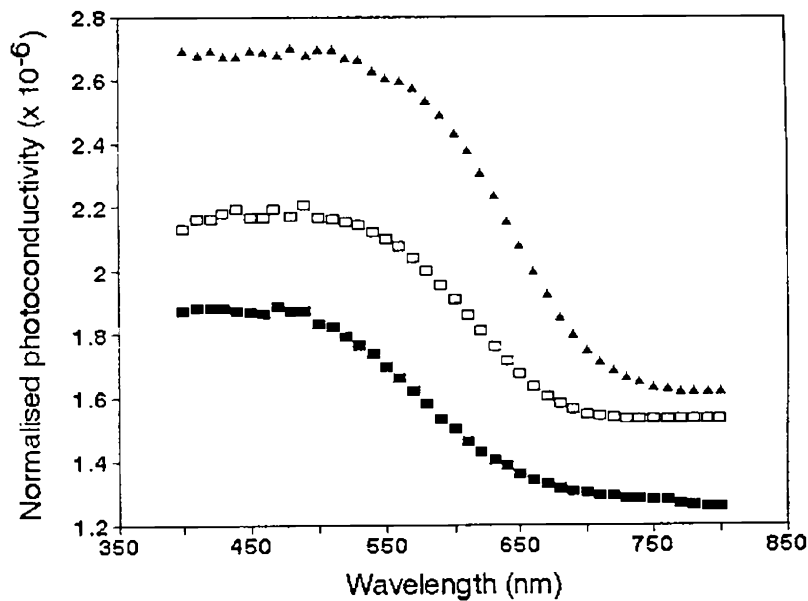
Fig.3.9 Spectral variation of normalised photoconductivity for three compositions of $Ge_xIn_5Se_{95-x}$ system (▲▲▲▲.....x = 12 (Z = 2. 39), □□□ .....x = 22(Z=2. 59), ■■■....x = 30 (Z = 2.75)

spectral variation of quantum efficiency of the material. Composition dependence of quantum efficiency for an incident wavelength of 600 nm is shown in Fig.3.10. Quantum
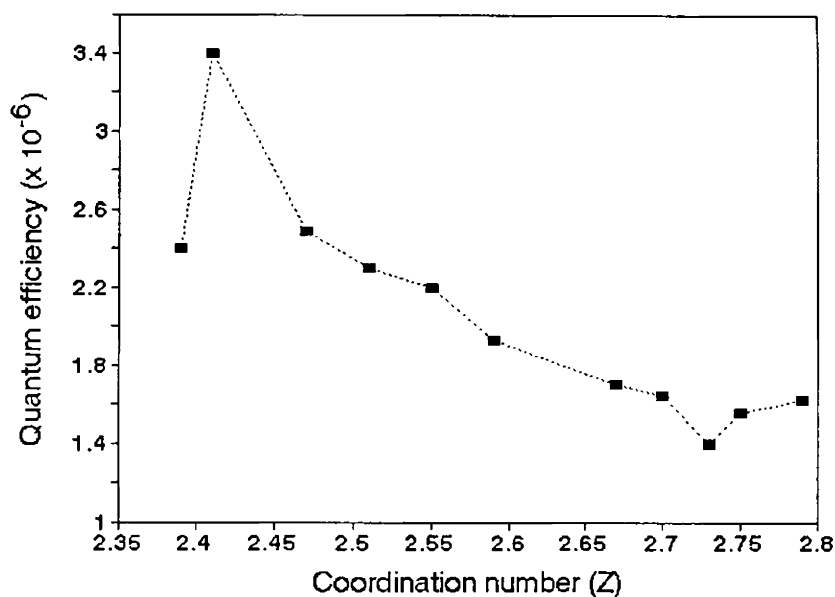
Fig.3.10 Composition dependent variation of quantum efficiency in $Ge_xIn_5Se_{95-x}$ (x= 12-32) system at 600 nm. The region 550-650 nm gives the same type of behaviour

efficiency is found to be of the order of 10^{-6}. Such a low value indicates that about 10^6 photons are needed to generate one carrier which can contribute to the photoconductivity. Temperature variation of spectral dependence of photoconductivity for $Ge_{22}In_5Se_{73}$ sample is shown in Fig.3.11. There is no appreciable shift in the region where the photoconductivity peaks. Other samples also show similar variation with temperature. The spectral sensitivity $dI_{ph}/d\lambda$ has been calculated for all the compositions and plotted in Fig.3.12. This quantity is found to have poor composition dependence. High spectral sensitivity is an essential quality for a photoconductor for applications like photodetective devices.
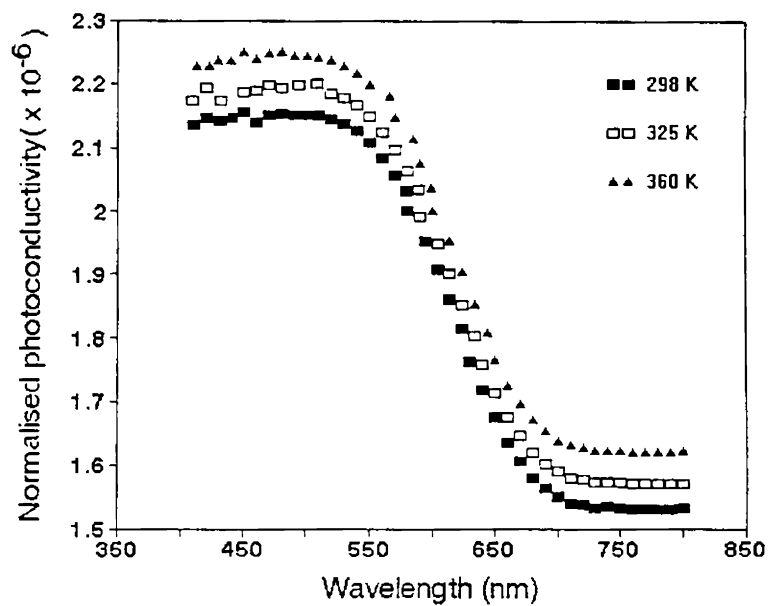
Fig.3.11 Spectral variation of photoconductivity at three different temperatures for the $Ge_{22}In_5Se_{73}$ (Z = 2.59) sample.
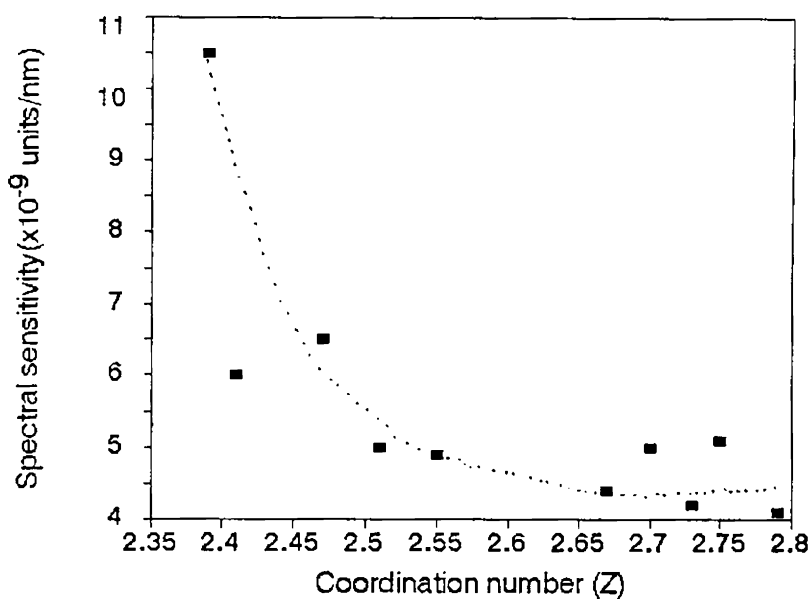
Fig.3.12 Composition dependence of spectral sensivity in the $Ge_xIn_5Se_{95-x}$ system.

3.3.4 Frequency resolved photoconductivity(FRPC) measurements and carrier lifetime

In order to determine the carrier lifetime in the samples we have measured a.c photoconductivity by varying the intensity modulation frequency of the illuminating radiation. Modulation frequency vs photoconductivity plotts are shown in Fig.3.13 for different compositions of the Ge-In-Se system. The photoconductivity in each plot is normalized with respect to its maximum value. The carrier lifetime can be calculated using the formula $\tau = 1/2\pi f_{max}$ where f_{max} is the frequency at which photoconductivity shows a peak in its value[31-32]. Carrier lifetime is found to vary with temperature and intensity. The plots of FRPC data for Ge-In-Se with varying temperature and light intensity are shown in Fig.3.14 and 3.15 respectively. The position of f_{max} shifts to higher frequencies with
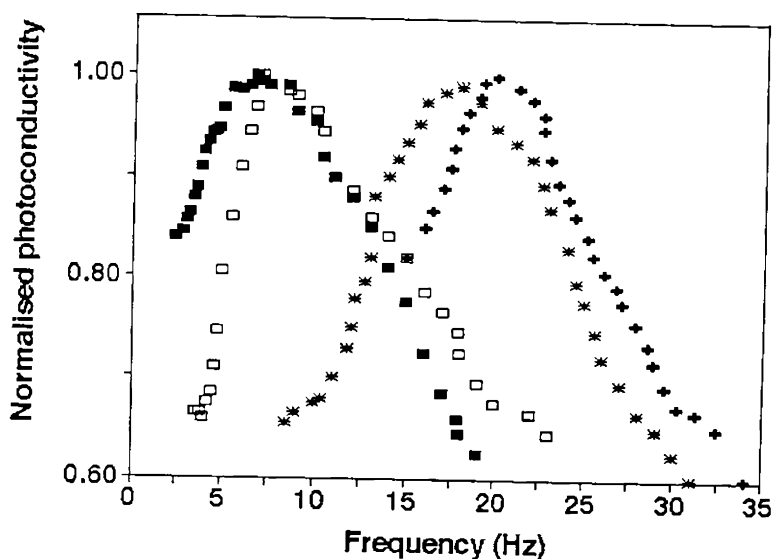
Fig.3.13 FRPC measurements for four different compositions of the $Ge_xIn_5Se_{95-x}$ system
(■ ■ ■......x = 30 (Z= 2.75), □ □ □!.....x = 29   (Z =2.73), ****........x = 18
(Z= 2.51),   ++++............x = 12   (Z= 2..39)
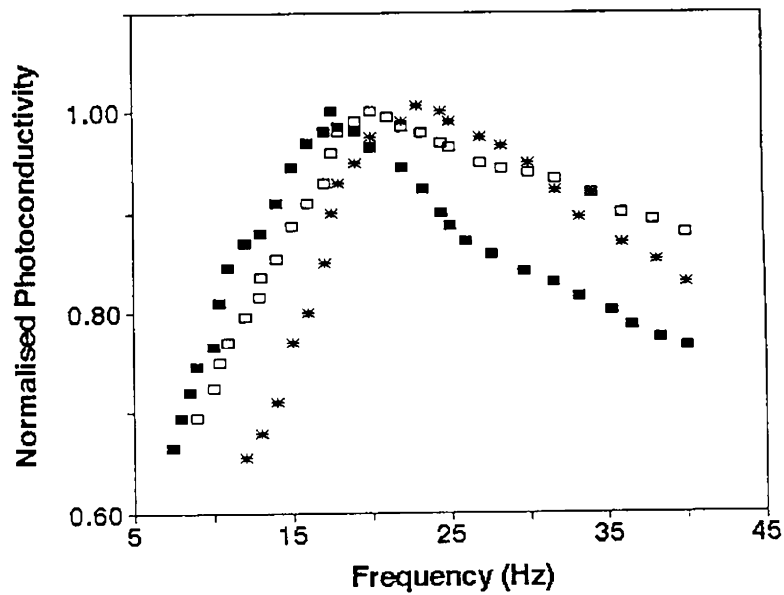
Fig.3.14 FRPC measurements at three different temperatures for $Ge_{18}In_5Se_{77}(Z=2.51)$
(■■■....300 K, □□□....340 K, ****.......380 K)
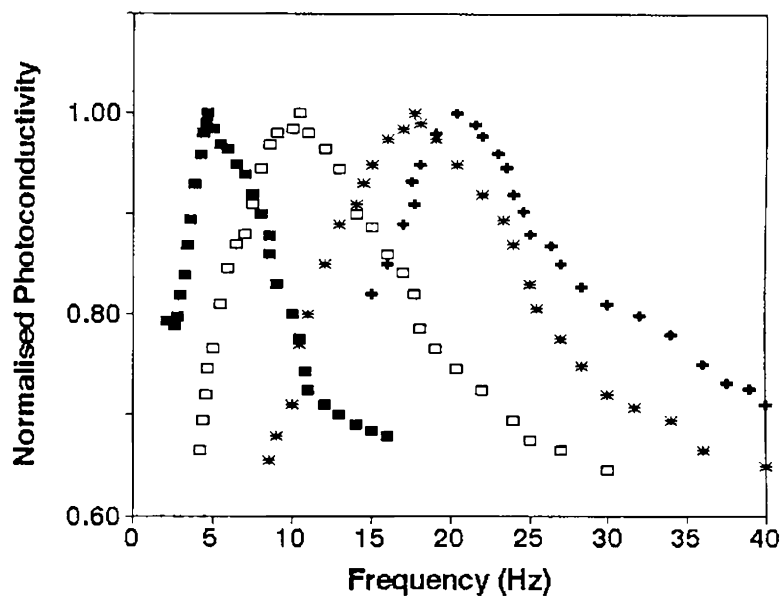
Fig.3.15 FRPC measurements at various intensities for $Ge_{18}In_5Se_{77}$ ($Z=2.51$) (■■■.....5 mWcm^{-2},
□□□..15 mWcm^{-2}, ****........20 mWcm^{-2}, ++++.........30 mWcm^{-2})

increasing temperature or intensity. Figures 3.16 and 3.17 show the variation of carrier lifetime with temperature and intensity. Other compositions exhibit similar type of variations. The carrier lifetime decreases with increase in intensity or temperature for all the compositions investigated. Intensity of excitation light is proportional to the generation rate G, and the dependence of lifetime on G can be expressed as[33-34]

$$\tau = AG^v \tag{3.12}$$

The slope of the plot ln τ against ln G shown in Fig.3.18 should give the value of v. Knowledge of the value of the exponent v will help to determine the kind of recombination occurring between the photoexcited carriers[35]. It has been suggested that in the geminate type of recombination the distribution of lifetimes will be insensitive to generation rates whereas in the distant pairs(DP) model [33-35], where it is assumed that recombination
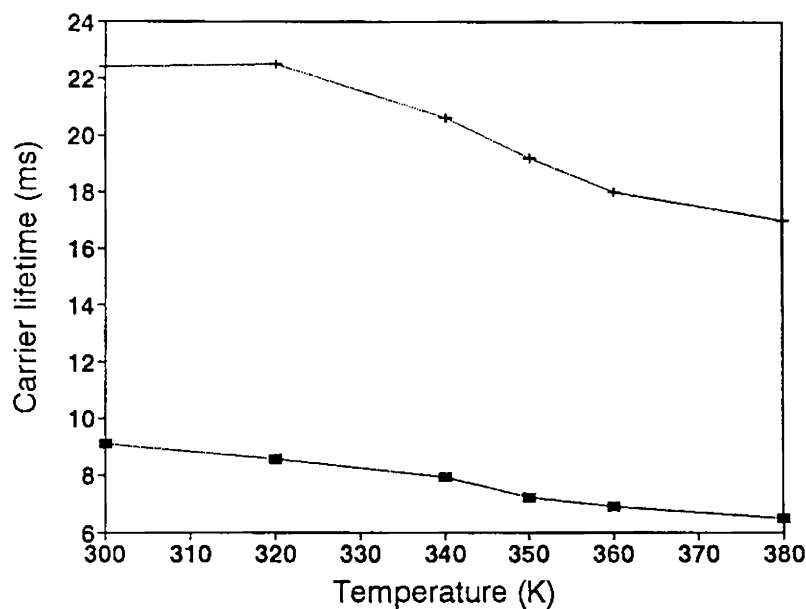
Fig.3.16 Variation of carrier lifetime with temperature for two compositions. Other compositions show similar variations(++++....... $Ge_{30}In_5Se_{65}$, Z= 2.75 and ■■■........$Ge_{18} In_5 Se_{77}$, Z= 2.51)
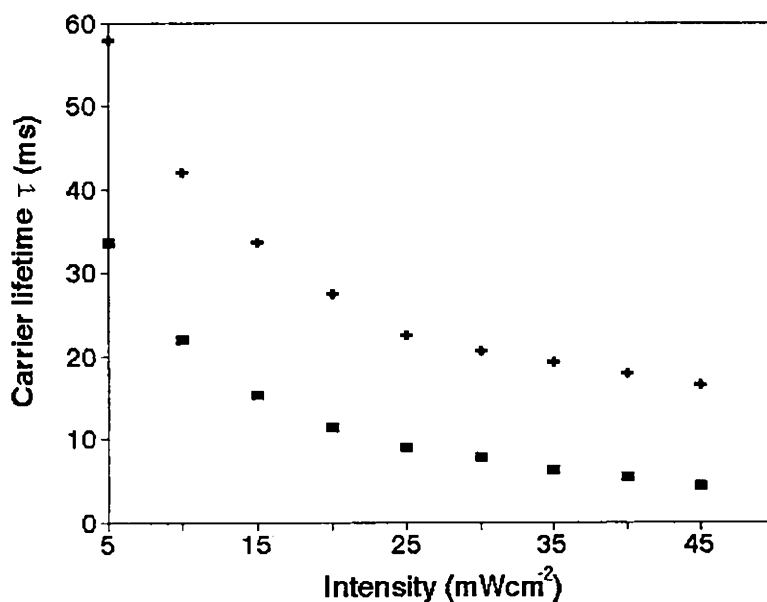
Fig.3.17 Variation of carrier lifetime with intensity(++++.........Ge$_{30}$In$_5$ Se$_{65}$, ■ ■■....Ge$_{18}$ In$_5$ S$_{e77}$)
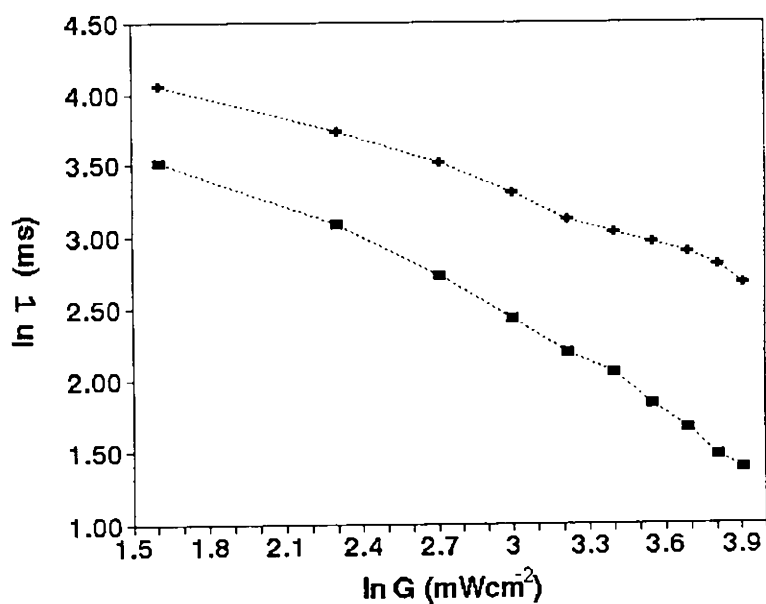
Fig.3.18 Plot showing variation of carrier lifetime with carrier generation rate(■■ ■...Ge$_{18}$In$_5$ Se$_{77}$, Z=2.51) , (++++.........Ge$_{30}$ In$_5$ Se$_{65}$ Z = 2.75)

takes place between nearest available neighbours non-geminately, the lifetime should decrease with increasing generation rate. Fig 3.17 shows that lifetimes are dependent on the generation rate, with a negative slope and therefore can be interpreted as supporting the DP model. Although the DP model is assumed to be valid only at low temperatures, the present measurements which have been carried out at room temperature also agrees with this model. According to Rose[36] if the value of the exponent $v=1$ then the recombination is monomolecular, while $v =0.5$ corresponds to bimolecular recombination. For the present system the value of v lies between 1 and 0.5 (≈0.875 and ≈ 0.6 for the two samples presented here). This is an indication of a continuous distribution of traps or localized states in the energy gap. The position of the peak frequency(f_{max}) is found to be independent of the applied electric field.

Composition dependence of carrier lifetime is shown in Fig.3.19. Carrier lifetime exhibits a maximum corresponding to the chemical threshold composition. It also has a
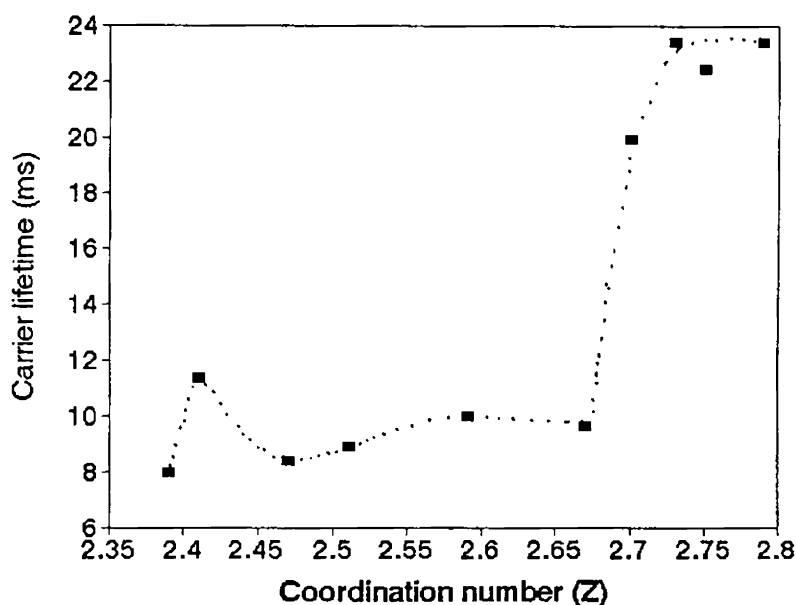
Fig.3.19 Composition dependence of carrier life time plotted with average coordination number in $Ge_xIn_5Se_{95-x}$

88

clear peak at the composition corresponding to Z= 2.41 where a mechanical threshold has been predicted according to the Phillips-Thorpe model[6,7]. Corresponding to the chemical threshold composition photoconductivity exhibits a minimum while carrier lifetime exhibits a maximum. The minimum in photoconductivity has been explained on the basis of COCN model. Due to chemical ordering and high average energy of bonds, photoconductivity assumes a minimum value at the chemical threshold composition. Also, the number of charged defects will be minimum corresponding to this composition, since the valencies of the components are fully satisfied. This results in the disappearance of hopping of carriers and conductivity decreases. Since carrier lifetime is the time that a carrier spends in the conduction band, the decrease in the number of defect states will result in the enhancement of carrier lifetime at the stoichiometric composition.

The excess conductivity due to incident radiation can be represented as[37]

$$\Delta\sigma = e(\Delta n.\mu_n + \Delta p.\mu_p) = e.g(\tau_n.\mu_n + \tau_p.\mu_p) \tag{3.13}$$

where g is the generation rate of carriers and τ is the carrier lifetime. Decrease in carrier generation rate and/or mobility with change of composition may be the reason for the minimum in photoconductivity at the chemical threshold composition where the carrier lifetime has a maximum value.

3.4 XPS analysis

Three compositions of the $Ge_xIn_5Se_{95-x}$ system have been analyzed by XPS. The compositions studied are those with x= 12, 26 and 32. Average coordination number(Z) of the these compositions are 2.39, 2.67 and 2.79 respectively. Figures 3.20, 3.21 and 3.22 show the XPS of Ge, In and Se in the three compositions with the spectra of the elements in pure form. The binding energy(b.e) values of the characteristic levels of pure Ge, In and Se and their b.e values in the three compositions of Ge-In-Se system are shown in Table 3.1

Table 3.1

Binding energies obtained from XPS measuremnts   eV

Sample	Ge 3p₃/₂	In 3d₅/₂	Se 3p₃/₂
Pure element	120.8	443.1	161.9
$Ge_{12}In_5Se_{83}$ (Z=2.39)	121.7 (+0.9)	444.5 (+1.4)	160.6 (-1.3)
$Ge_{26}In_5Se_{69}$ (Z=2.67)	122.7 (+1.9)	445 (+1.9)	159.4 (-2.5)
$Ge_{32}In_5Se_{63}$ (Z=2.79)	122.5 (+1.7)	444.5 (+1.4)	158.4 (-3.5)

The b.e values of selenium are found to decrease in the compounds compared to that in pure selenium. But in the case of germanium and indium, the values increase in compounds compared to that of pure elements.
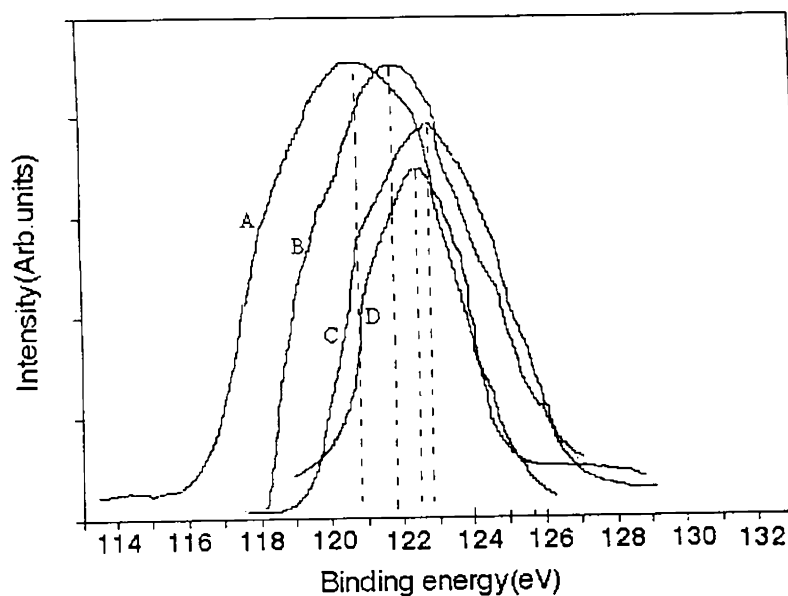
Fig.3.20 XPS of $3p_{3/2}$ levels of   pure germanium(A),   germanium in $Ge_{12}In_5Se_{83}$(B),   in $Ge_{26}In_5Se_{69}$ (C)   and in $Ge_{32}In_5Se_{63}$ (D)
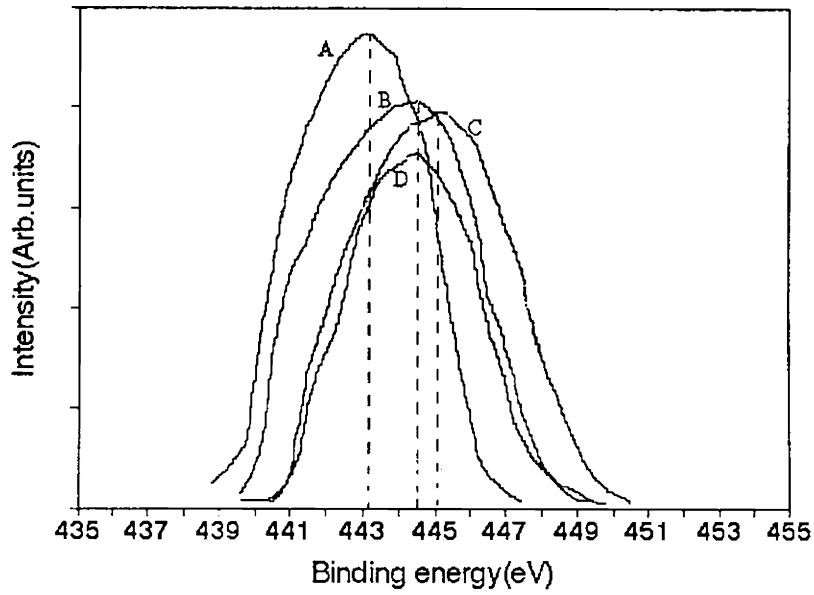
Fig.3.21 XPS of $3d_{5/2}$ levels of pure indium (A) indium in $Ge_{12}In_5Se_{83}$(B) in $Ge_{26}In_5Se_{69}$ (C)
and in $Ge_{32}In_5Se_{63}$(D)
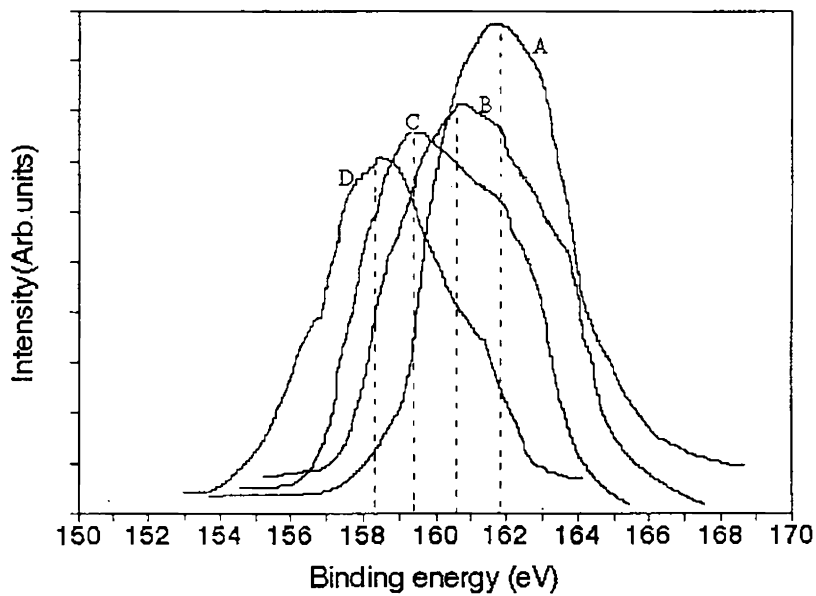
Fig.3.22 XPS of $3p_{3/2}$ levels of pure selenium(A) selenium in $Ge_{12}In_5Se_{33}$(B), in $Ge_{26}In_5Se_{69}$(C)
and in $Ge_{32}In_5Se_{63}$(D)

91

So the b.e shift is negative for selenium in Ge-In-Se whereas it is positive for germanium and indium. The electron transfer from one constituent to another in a compound get reflected in XPS in the form of a chemical shift[38-39]. This is useful in getting information about electronic states of different compositions. Indium and germanium are electropositive compared to selenium and their electrons are transferred more closely to selenium during bond formation. This brings a negative shift for selenium and positive shift for indium and germanium in the b.e of their characteristic levels.

3.5 Conclusions

From our investigations on Ge-In-Se glasses it is found that incorporation of indium causes an increase of photoconductivity of Ge-Se system by nearly four orders of magnitude. At the same time photoconductivity or photosensitivity, which is represented as (σ_{ph}/σ_{dc}) decreases with incorporation of indium. The composition dependent variation of photoconductivity and related properties in Ge-In-Se show that the stoichiometric composition has a minimum in photoconductivity and a maximum in carrier lifetime. At the composition with Z= 2.41 both photoconductivity and carrier lifetime exhibit a clear variation. From FRPC measurements and analysis of carrier generation rate it is found that the carrier recombination is in between that of monomolecular and bimolecular recombinations. This means that there is a continuous distribution of traps in the band gap of the material.

The enhancement in photoconductivity due to indium is explained in terms of the formation of defect centres. The minimum in photoconductivity and maximum in carrier lifetime at the stoichiometric composition are explained on the basis of COCN model.

3.6 References

1. N.F Mott *Adv.Phys* **16** (1967) 49

2. E.A Davis and N.F Mott *Phil.Mag* **22** (1970) 903

3. B.T Kolomiets, A.Lebedev, N.A Rogachev *Fiz.Tech Poluprov* **8** (1974) 545

4. S Okano, M.Suzuki, T.Imura, N.Fukuda and A.Hiraki *J.Non-Cryst. Solids* **59-60** (1983) 969

5. R.Misra S.Goel, A.K Agnihotri and A.Kumar *J.Mat.Sc.Lett* **11** (1992) 212

6. J.C Phillips *J.Non-Cryst Solids* **43** (1981) 37

7. J.C Phillips and M.F Thorpe *Solid State Commun* **53** (1985) 699

8. K.Tanaka *Phys.Rev* **B39** (1989) 270

9. A.Feltz, M.Phole, H.Steil and G.Herms *J.Non-Cryst Solids* **69** (1984) 271

10. B.L Halfpap and S.M Lindsay *Phys.Rev.Lett* **57** (1986) 847

11. M.F Thorpe *J.Non-Cryst Solids* **57** (1983) 355

12. M.Kastner *Phys.Rev.Lett* **28** (1972) 355

13. G.Lucovsky, F.L Galeena and R.C Keezer R.H Geils and H.A Six *Phys.Rev.***B10** (1974) 5134

14. P.Tronc, M.Bensoussan, A.Brenac and C.Sebenne *Phys.Rev* **B8** (1973) 5947

15. H.He and M.F Thorpe, *Phys.Rev.Lett* **54** (1985) 2107

16. A.Giridhar and S.Mahadevan *J.Non-Cryst Solids* **134** (1991) 94

17. A.Giridhar and S.Mahadevan *J.Non-Cryst Solids* **151** (1992) 245

18. S.R Elliot " *Physics of amorphous materials*" Longman, London (1983)

19. J.Z Liu, P.C Taylor *Solid State Commun.* **70** (1989) 81

20. F.Kosek, Z.Cimpl, M.P Mikhailov and A. Karpova, *J.Non-Cryst Solids* **86** (1986) 265

21. H.Fritzche *Proc. 7ᵗʰ int.Conf. Amorphous and liquid semiconductors* Edinburgh ed.W Spear (1977)

22. T.C Arnoldussen, R.H Bube, E.A Fagen and S.Holmberg *J.Appl.Phys.***43** (1972) 1798

23. T.C Arnoldussen, R.H. Bube, E.A Fagen and S.Holmberg *J.Non-Cryst Solids* **8-10** (1972) 933

24. R.T.S Shiah and R.H. Bube *J.Appl.Phys.***47** (1976) 2005

25. R.H.Bube, *RCA Rev.* **36** (1975) 467

26. R.H.Bube *"Photoelectronic properties of semiconductors"* Cambridge University Press (1992)

27. A.Onozuka, O.Oda, I.Tsuboya *Thin Solid Films* **149** (1987) 9

28. R.T Sanderson *"Chemical bonds and bond energy"* vol. 21, Academic Press New York(1971)

29. P.Bhattacharya *"Semiconductor optoelectronic devices"* Prentice Hall of India New Delhi (1995)

30. S.M.Sze *"Physics of semiconductor devices "* Wiley Eastern

31. D.Wagner, P.Irsigler and D.J Dunstan *J.Phys.C: Solid State Phys.* **17** (1984) 6793

32. R.Kaplan *J.Phys: Condens.Matter* **7** (1995) 6847

33. J.Bullot, P.Cordier, M.Gauthier and G.Mawawa *Phil.Mag* **B55** (1987) 599

34. T.M.Searle *Phil.Mag. Lett* **61** (1990) 251

35. M.Bort, W.Fuhs S.Liedtke and R.Stachowitz **64** (1991) 227

36. A.Rose *"Concepts in photoconductivity and allied problems"* Krieger, New York (1978)

37. R.H.Bube *"Photoconductivity in solids"* Krieger, New York (1978)

38. A.D.Baker and D.Betteridge *"Photoelectron spectroscopy"* Oxford, Pergamon Press (1972)

39. G.E.Mullenberg *"Hand book of x-ray photoelectron spectroscopy"* Minnesota: Perkin Elmer Corporation (1978)

Chapter 4

Photoconductivity in Ge-Bi-Se glasses

4.1 Introduction

The effect of incorporation of Bi as an impurity in chalcogenide glasses has been a topic of great interest ever since the synthesis of such glassy systems. A great deal of effort has been expended to understand the role of Bi in controlling the mechanism of electrical conduction in chalcogenide glasses. Chalcogenide glasses are generally p-type semiconductors and are expected to be insensitive to the addition of impurities[1]. For them Fermi level is considered to be pinned due to the equilibrium between the positively and negatively charged dangling bonds which make them insensitive to impurity doping. But there are experimental results which are against this argument[2-5].

In the case of the Ge-Bi-Se system the addition of a critical quantity of Bi brings about a carrier type reversal from p-type to n -type in the basic Ge-Se system[6-8]. The Ge-Se system, which is a p-type semiconductor, changes to n-type with the addition of 7 atomic percent of Bi, which corresponds to an average coordination number Z = 2.47 for the system. Carrier type reversal has been observed in certain Pb doped germanium chalcogenides also[9]. Appreciable variations in different physical properties have been found around the composition with this critical Bi concentration, which occurs in the vicinity of x =7 at.% (Coordination number Z = 2.47) in Ge-Bi-Se glasses with the general formula $Ge_{20}Bi_xSe_{80-x}$.

Composition dependence of various physical properties such as thermoelectric power, electrical resistivity and IR absorption exhibit anomalies near the critical composition corresponding to x = 7 at.%. Measurements by Tohge et.al [7] have shown a gradual decrease in resistivity with increasing Bi content up to 9 at.% and then decreases by about four orders of magnitude between x = 9 and 10 at.% but remain almost constant for x>10 at %. Composition dependence of Seebeck coefficient shows that glass containing 7 at.% of Bi is p-type, similar to other melt quenched chalcogenide glasses but incorporation of 9 at.% of Bi changes it into n-type. In the case of optical band gap(E_g), a decrease by 0.65 eV was reported by incorporation of 2.5 at.% of Bi into $Ge_{20}Se_{80}$ glass. Further addition of Bi causes only very small change in Eg and it remained constant for glasses containing more than 7.5 at.% of Bi. Heat capacity measurements at 323 K show a drastic change in the value of C_p between x=6 and 8 at.%.

The carrier type reversal observed in Bi containing chalcogenide glasses has been accounted for by several authors. Studies of electrical, thermoelectric and optical properties as a function of composition led Tohge et.al [7-8] to explain the transport mechanism on the basis of chemical bonds. Based on EXAFs data, Elliot and Steel [10] have discussed the reasons for this mechanism as due to the formation of partially ionic Bi chalcogen bonds and subsequent unpinning of the Fermi level. Storiopoulous and Fuhs [11] have put forwarded the explanation that a drastic decrease in band gap induces an increase of conductivity and a reversal in the type of the carriers. Analysis based on network modeling led Phillips[8] and Nagels to conclude that carrier type reversal occurs in the vicinity of the percolation threshold and is the result of transport anomalies in the system.

In the present work our aim is the investigation of the composition dependence of photoconductivity and carrier lifetime in $Ge_{20}Bi_xSe_{80-x}$ glasses with x varying 2 to 12 at.%. The average coordination number (Z) of this system varies from 2.4 to 2.52 corresponding

to the above variation in x. Temperature dependence of photoconductivity has also been measured and analysed. The objective in this work is to test whether any special feature is reflected around the critical composition of Ge-Bi-Se glasses at which p-n transition has been reported.

4.2 Experimental method

Bulk semiconducting glasses with the general formula $Ge_{20}Bi_xSe_{80-x}$ ($0<x<12$) have been prepared by the conventional melt quenching technique starting with 5N purity constituents. The cooling rate is approximately $500^0C/Sec$. The amorphous nature of the samples have been checked by X-ray powder diffraction method. Two compositions have been analysed by XPS.

The largest region of glass formation with bismuth was obtained for alloys with 20 to 30 at.% of Ge and 70 to 80 at.% of Se[7]. It is seen that for 20 at.% of Ge, the maximum Bi content that can be incorporated into the glass matrix is 13 at.%, the remaining being selenium. If bismuth content is increased further, the glasses formed may be partially crystallised. Measurements of photoconductivity and carrier lifetime have been carried out as has already been described in Chapter 2.

Bulk samples having rectangular shape with surface area 3×4 mm^2 and thickness 0.5 mm have been prepared for the present measurements. The samples have been sandwiched between two SnO_2 coated conducting transparent glass plates for the measurements. The contacts have been found to be ohmic from V-I characteristic study. The sample has been illuminated by light from a Xe arc lamp. The intensity of light falling on the sample is 25 $mWcm^{-2}$ during photoconductivity and carrier lifetime measurements.

4.3 Results and discussion

4.3.1 Temperature, intensity and spectral dependence

Temperature dependence of dark conductivity for $Ge_{20}Se_{80}$, $Ge_{20}Bi_2Se_{78}$ and $Ge_{20}Bi_{10}Se_{70}$ are shown in Fig.4.1. The behaviour is almost identical to earlier reports [7-12]. Temperature dependence of a.c photoconductivity and d.c photoconductivity for the same compositions are shown in figures 4.2 and 4.3 respectively. In both these cases photoconductivity initially increases gradually with inverse temperature and then decreases. The same behaviour is exhibited by other compositions of the Ge-Bi-Se system. Photoconductivity increases by nearly two orders of magnitude with the addition of bismuth, as is clear from figures 4.2 and 4.3. The increase is reflected more or less identically in both a.c(pulsed excitation) and d.c (steady state) measurements. The enhancement in photoconductivity can be attributed to the increase in the density of charged defect states formed in the energy gap with the addition of bismuth[13]. There
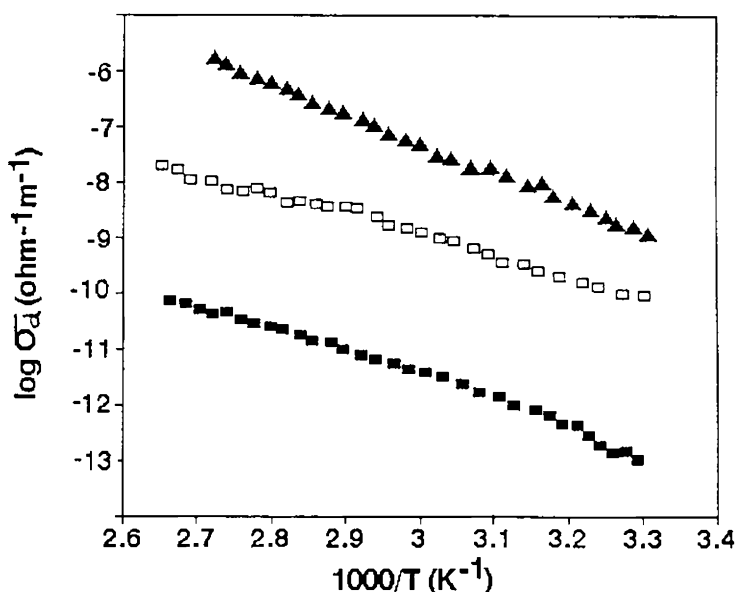
Fig.4.1 Variation of darkconductivity with temperature (plotted as 1/T). (■■■ ....$Ge_{20}Se_{80}$, □□□......$Ge_{20}Bi_2Se_{78}$, and ▲▲▲▲ ....$Ge_{20}Bi_{10}Se_{70}$)
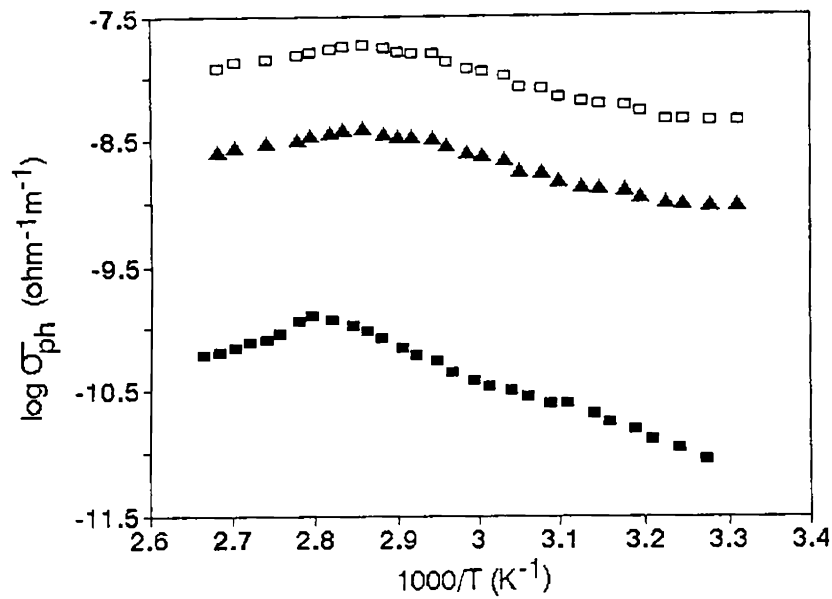
Fig.4.2 Variation of a.c photoconductivity (plotted as $\log\sigma_{ph}$) with inverse temperature for three compositions of Ge-Bi-Se system. ($Ge_{20}Se_{80}$ ....■■■ , $Ge_{20}Bi_{10}Se_{70}$......... ▲▲▲ $Ge_{20}Bi_2Se_{78}$.....□□□□). Chopping frequency is 20 Hz. Uncertainty in the values are less than 5%.
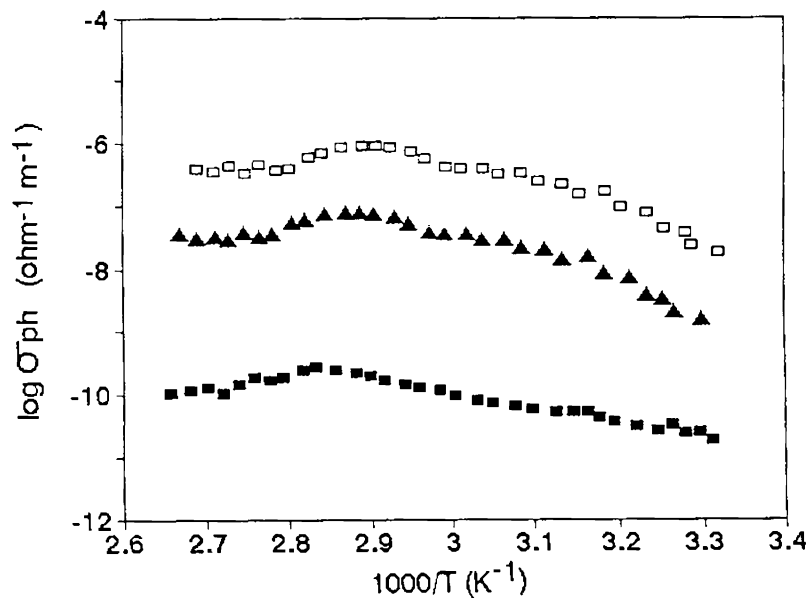
Fig.4.3 Variation of d.c photoconductivity with inverse temperature for $Ge_{20}Se_{80}$ ....■■■), $Ge_{20}Bi_{10}Se_{70}$ .... ▲▲▲) and $Ge_{20}Bi_2Se_{78}$ .... □□□)

may be hopping conduction through the defect states. Another reason may be the change in band gap with the addition of bismuth. From Fig.4.4 it can be seen that the band gap decreases appreciably by the incorporation of 2 at.% and 4 at.% of bismuth. Further addition of bismuth does not alter the band gap appreciably. Therefore it can be concluded that the observed general increase in photoconductivity of Ge-Bi-Se system compared to Ge-Se is also related to the shrinkage of the band gap[4].

The variation of optical band gap together with that of activation energy for conduction is plotted in Fig.4.4. The activation energy does not change significantly for
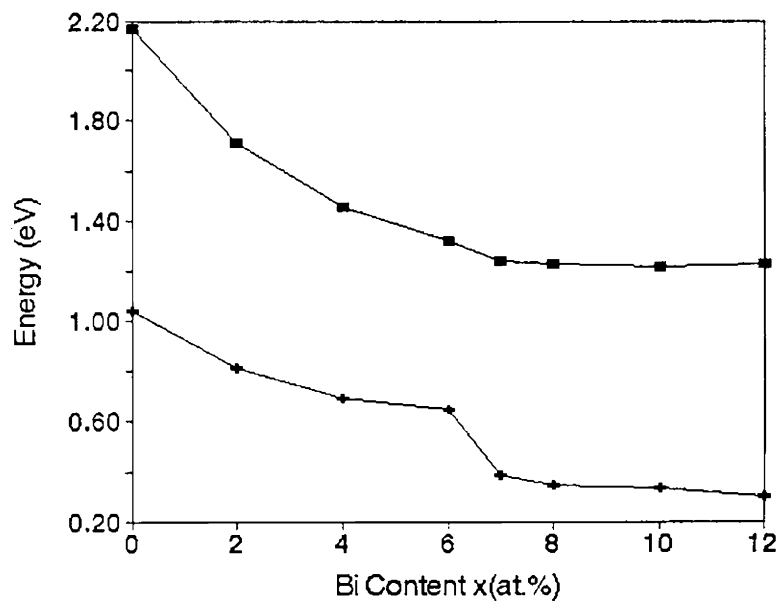
Fig.4.4 Variation of optical band gap (...........■■■) and activation energy for conduction (.................++++) with increase in Bi content.

lower concentrations of bismuth. Similar results have been obtained by Tohge et.al.[7]. At low Bi concentrations the optical band gap decreases appreciably with increase of Bi content. At higher Bi concentrations optical band gap remains unaltered whereas activation energy decreases. This occurs as a result of the shift of the Fermi level towards

the conduction band [14]. Fig.4.5 shows the variation of photoconductivity with intensity of incident light for the sample $Ge_{20}Bi_{10}Se_{70}$. Other compositions show similar variation. Photoconductivity exhibits almost a linear variation at lower intensities of illumination and become almost constant at higher intensities of illumination. The results shown in Fig.4.5 indicate that photoconductivity saturates at higher intensities of illumination.
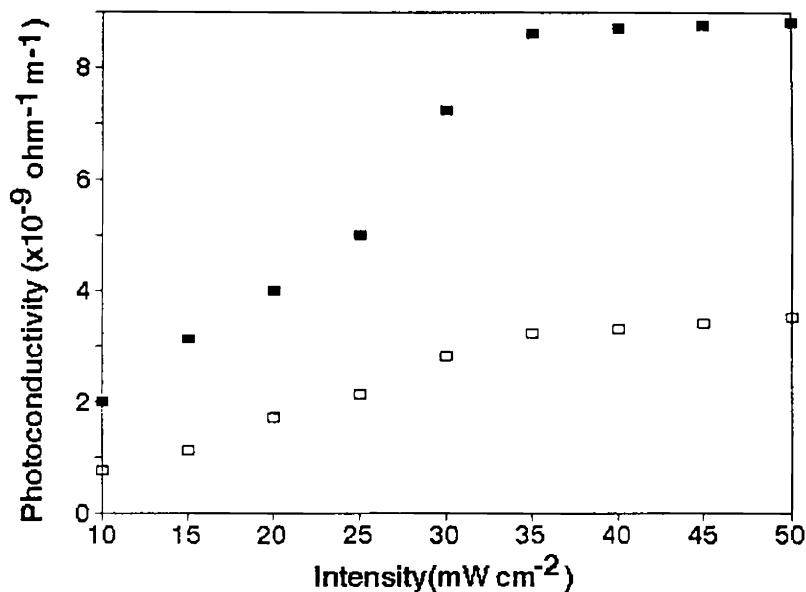
Fig.4.5 Variation of photoconductivity with intensity of illumination for $Ge_{20}Bi_{10}Se_{70}$ (□□□⊢---- ....) and $Ge_{20}Bi_2Se_{78}$(■ ■ ■ ....) glasses. Other compositions have similar variations.

The results on photoconductivity of Ge-Bi-Se system have been analysed in terms of the ABFH model and the results are shown in Fig.4.6. In the frame work of ABFH model the material exhibits characteristics of a type I photoconductor. A plot of E_g vs $T_m.ln(\sigma_{max})$ is shown in Fig.4.6. The points obtained can be fitted to a straight line. Referring to the description of the ABFH model based analysis for our photoconductivity data on these glasses fit very well with that of a type I photoconductor.
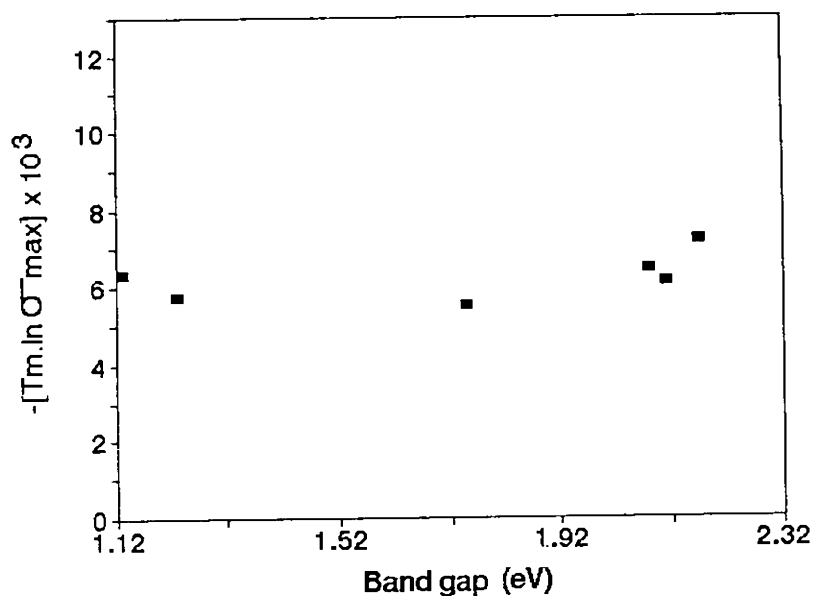
Fig.4.6 Plot of E_g against the product $T_m.\ln\sigma_{max}$ for the $Ge_{20}Bi_xSe_{80-x}$ system. The points can be fitted to a straight line.

The spectral dependence of photoconductivity for $Ge_{20}Se_{80}$ and $Ge_{20}Bi_2Se_{78}$ have been measured and are plotted in Fig.4.7. The photocurrent is normalised for the intensity
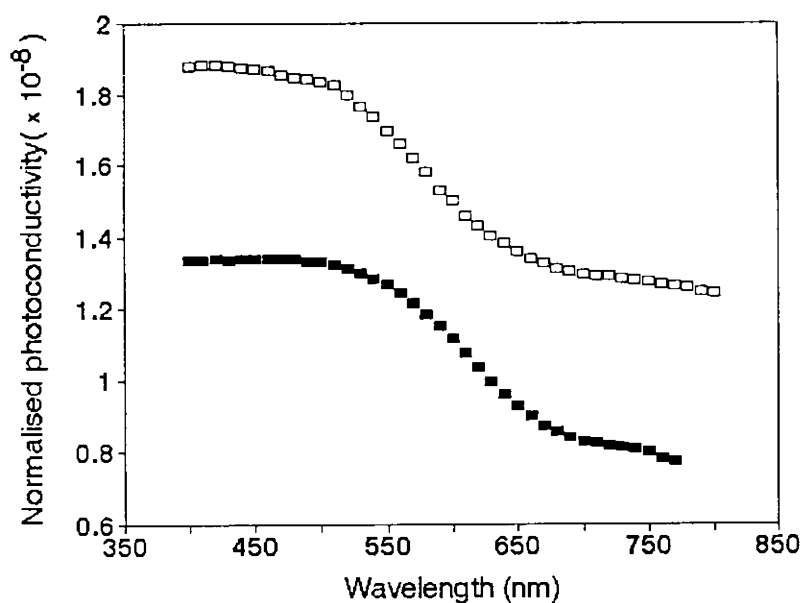
Fig.4.7 Spectral dependence of photoconductivity in $Ge_{20}Se_{80}$ ....■■■ and $Ge_{20}Bi_2Se_{78}$...............□□□

variation of the source and normalised photoconductivity gives actually quantum efficiency of the sample. Though the normalised photocurrent peaks around the absorption edge, a correct determination of the band gap is not possible from the data obtained. In general, the quantum efficiency of Ge-Bi-Se system is found to be less than that of Ge-In-Se by nearly two orders of magnitude.

4.3.2 Frequency resolved photoconductivity(FRPC) measurements.

FRPC measurements have been carried out on different compositions of $Ge_{20}Bi_xSe_{80-x}$ system and the plots for four compositions are shown in Fig.4.8. Also FRPC measurements have been carried out on various compositions at different temperatures and intensities of illumination. Each curve is normalised with respect to its maximum value. The peak position shifts to higher frequencies with increase of temperature or intensity for all the compositions. The frequency (f_{max}) corresponding to the peak in
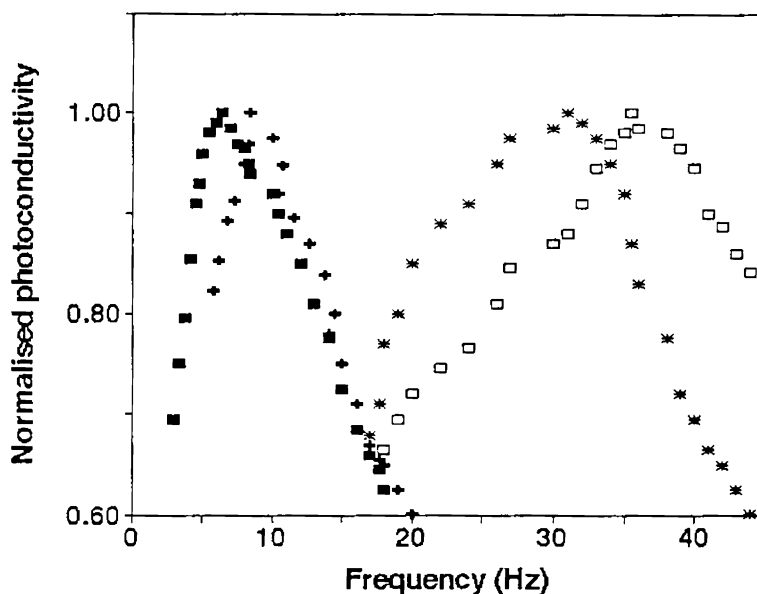
Fig.4.8 FRPC measurements in four compositions of the $Ge_{20}Bi_xSe_{80-x}$ system.(■■....x= 2, ++++........x = 6, ** **...........x = 8, □□ □□...x =12)

photoconductivity, is noted from the figures and the carrier lifetime(τ) is determined. The carrier life time is calculated from the formula $\tau=1/2\pi f_{max}$. It is found to posseses an almost linear variation with temperature as shown in Fig.4.9. Since the carrier lifetime exhibits a linear decrease with temperature we can assume that the number of traps in the band gap increases with temperature. Similar results have been reported for other chalcogenides by earlier workers[15]. The carrier lifetime measured by FRPC method is found to decrease almost exponentially with intensity. At high intensities there is no appreciable decrease and the carrier lifetime almost constant. The plot of carrier lifetime vs intensity for the composition $Ge_{20}Bi_2Se_{78}$ obtained by FRPC measurement is shown in Fig.4.10. Carrier lifetime (τ) and generation rate G are related as $\tau = AG^v$. From ln G vs
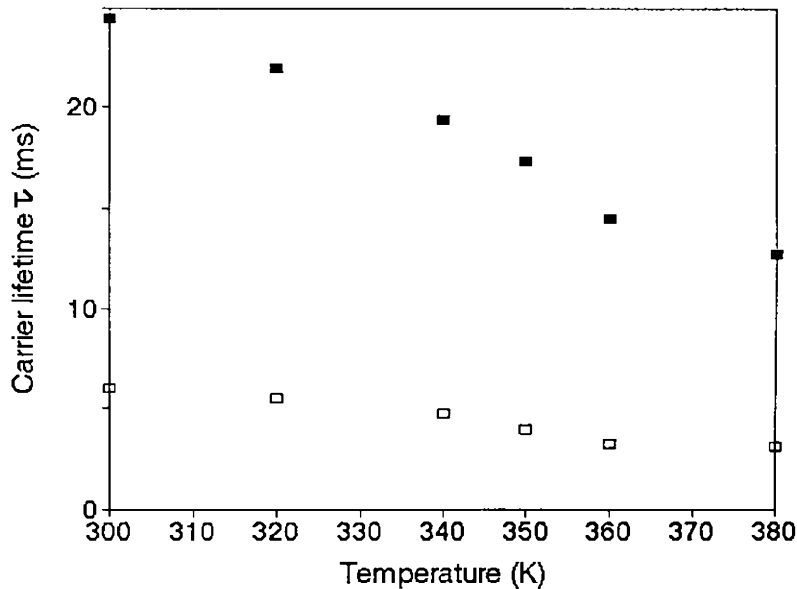
Fig.4.9 Temperature dependent variation of carrier lifetime measured by FRPC method for $Ge_{20}Bi_2Se_{78}$ (...■■■) and $Ge_{20}Bi_{10}Se_{70}$(.. □□□)samples
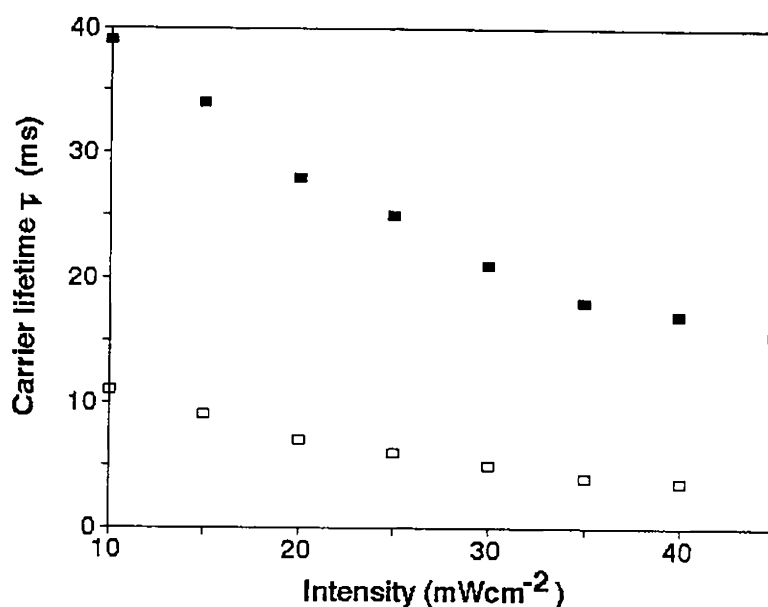
Fig.4.10 Variation of carrier lifetime with intensity for Ge$_{20}$Bi$_2$Se$_{78}$ ....■■■ and Ge$_{20}$Bi$_{10}$Se$_{70}$..........□□□.

ln τ plot the value of the exponent can be obtained. Generation rate, G is directly proportional to the intensity of illumination. From the plot shown in Fig.4.11 the value of the exponent ν have been calculated for Ge$_{20}$Bi$_2$Se$_{78}$ and Ge$_{20}$Bi$_{10}$Se$_{70}$. The value of ν for these are ≈ 0.62 and ≈ 0.867. For other compositions also similar calculations have been done and for all of them the value of the exponent ν lies between 1 and 0.5 which is an indication for the presence of localized states in the band gap of the material as explained with the results of Ge-In-Se[16-20]. Composition dependent variation of carrier lifetime is shown in Fig.4.12. In general carrier lifetime decrease with in crease in Bi content. It exhibits a clear slope change corresponding to the critical composition where p→n transition has been reported by earlier workers. A discussion of composition dependent behavoiur of Ge-Bi-Se system is given in the next section where the explanations by different workers are outlined.
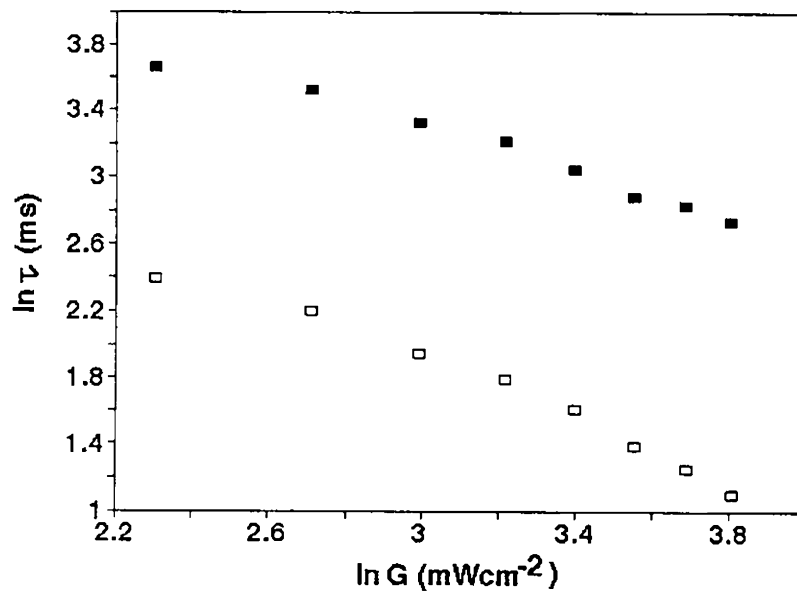
Fig.4.11 Plot of ln G vs ln τ for $Ge_{20}Bi_2Se_{78}$.......... ■■■   and $Ge_{20}Bi_{10}Se_{70}$......... ▢▢▢...
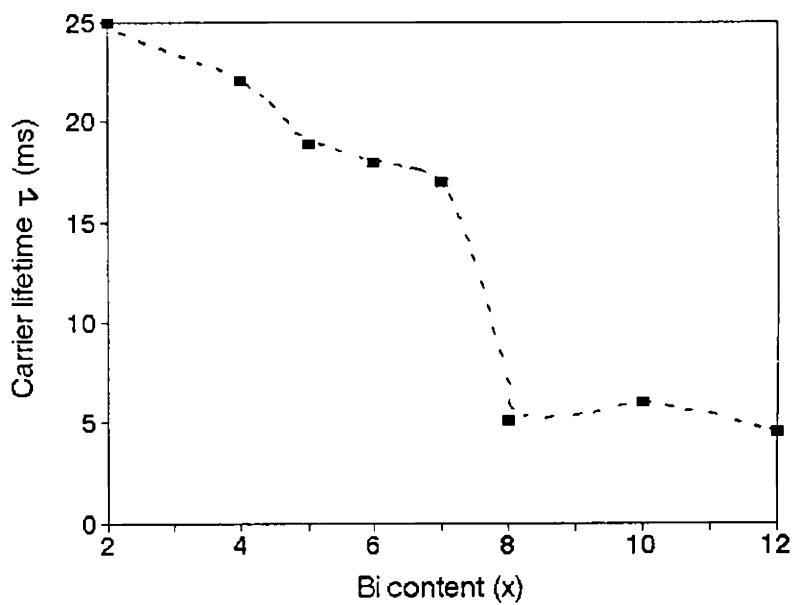

Fig.4.12 Variation of carrier lifetime with Bi content. The measurements have been carried out at 298 K . Intensity of light 25 mWcm^{-2}

4.3.3 Composition dependence of photoconductivity

The composition dependence of photoconductivity(σ_{ph}) is shown in Fig.4.13 and that of photodetectivity, the ratio of photoconductivity to dark conductivity(σ_{ph}/σ_d), is shown in Fig.4.14. Both σ_{ph} and σ_{ph}/σ_d have sharp variations around the critical composition x=7 corresponding to Z=2.47 where the p→n transition occurs. In general, photoconductivity increases upto x=6 and then decreases to a minimum and thereafter remain more or less constant. But photodetectivity, in general, decreases with increase in x and it remains almost constant beyond x=7. Photodetectivity (or photosensitivity) of the material is a factor which determines the quality of a photoconductor in using it as a photodetector.

Although p→n transition and anomalous change of many physical properties have been analysed and explained by various authors before [6-8, 20-22], the mechanism of this phenomenon is not yet fully understood. More experimentation and modeling seem to be necessary to get a clear picture of the mechanisms involved in the process. Studies of electrical, thermoelectric and optical properties as a function of composition led Tohge et.al[6] to explain the transport mechanism in Ge-Bi-Se glasses on the basis of chemical bonds. Based on EXAFs data Elliot and Steel [9] have attributed the mechanism to the formation of partially ionic Bi- chalcogen bonds and the subsequent unpinning of the Fermi level. They suggested that the p→n transition in these glasses is accompanied by a significant change in the local structural order surrounding the Bi impurity atoms. At low Bi concentrations, the Bi-Se bonds remain covalent in character and at higher Bi concentrations, it becomes partially ionic with a slight increase in bond length[9]. It has further been proposed that the process of the dissolution of the Bi impurity in the selenium rich regions at lower concentrations produce Se- centers making the Bi impurities positively charged. Further addition of Bi in larger concentrations don't produce appreciable additional defects as it enters a modified network. Consequently the absorption edges are not appreciably affected.
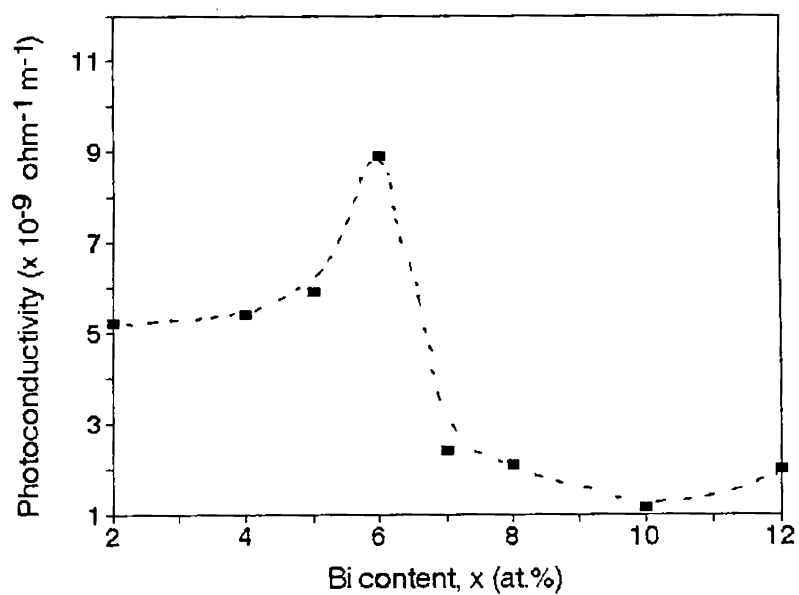
Fig.4.13 Variation of photoconductivity with increase in Bi content in the Ge-Bi-Se system.
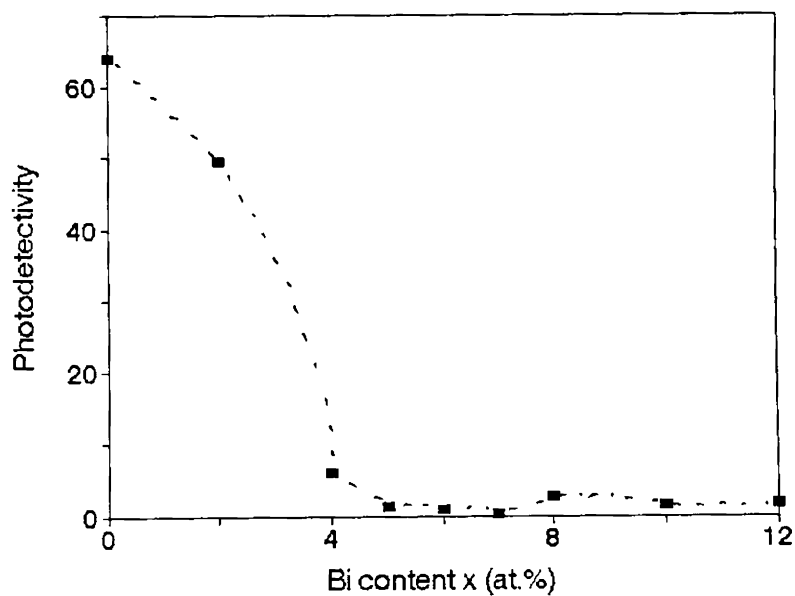

Fig.4.14 Variation of photodetectivity with increase in Bi content.

Phillips[8] and Thorpe [23] predicted the critical composition of the binary glass system of the type IV_x-VI_{100-x} to be around x= 20 at.% which corresponds to average coordination number Z= 2.4, IV and VI indicating the corresponding group of elements in the periodic table. According to this we can expect a critical composition for the $Ge_{20}Bi_xSe_{80-x}$ system to be around x=7 at.%. However, for Ge_xSe_{100-x} glasses, this value is found to be slightly higher, at x =23 at.%, which is attributed to the fact that not all bond bending constraints are effective in hindering inter cluster motions[24]. There are reports that Bi_2Se_3 is an n-type semiconductor and in Ge-Bi-Se glasses the Bi_2Se_3 clusters are embedded in the Ge-Se glass matrix[8, 25]. The $Ge_{20}Bi_xSe_{80-x}$ glasses can be represented as $Ge_{20}Se_{80-5z}$+ Bi_2Se_{3z}. According to Phillips, when Bi content is appreciably low localized unconstrained Se^- defects are present in the Bi_2Se_3 tetradymite surfaces which are dispersed uniformly in the rest of $GeSe_2$ and Se flexible chains making them p-type semiconductors. At 6 at.% of Bi, the Bi_2Se_3 clusters retain in the melt. Also x=6 corresponds to $Ge_{20}Se_{65}$-Bi_6Se_9 and $Ge_{20}Se_{65}$≈$Ge_{20}Se_{100-y}$ with y = 24, which agrees with the elastic stiffness threshold composition y_c= 23 of the binary glasses found in other experiments[24]. At x>6 at.% the Bi_2Se_3 tetradymite clusters find themselves in a matrix of increased mechanical rigidity and the mechanical misfit between the clusters become high which lead to a plastic deformation of these clusters. This gives rise to an increase in Se-defects which evolve in a percolative manner at the mechanical threshold and produce n-type conduction in these glasses.

In terms of chemical bond formation the carrier type reversal is related to the formation of fairly large number of Bi-Se bonds and the disappearance of Se-Se bonds at this critical composition. According to charge dangling bond model, the equilibrium between the positively and negatively charged dangling bonds which pin the Fermi level is affected maximum at this critical composition by charged impurities[7].

Bhatia et.al [21] have reported that, at lower Bi concentrations there is little change in the activation energy E_{av} whereas at higher concentrations a considerable decrease in E_{av}, is observed which is explained as due to the shift in the Fermi level towards the

conduction band. According to Tohge et.al[7], in $Ge_{20}Se_{80}$ glasses, only Ge-Se and Se-Se bonds are supposed to be present. When Bi is incorporated in to this glass, Bi is expected to combine freely with Se, followed by the decrease in the concentration of Se -Se bonds, because the bond energy of the Bi-Se bond is larger than that of a Bi-Ge bond(40.7 and 31 k cal/mole respectively)[26]. The concentration of Ge-Se bonds remain the same over the whole composition range whereas that of Bi-Se bond increases and that of Se-Se bond decreases monotonically with increasing Bi content up to 10 at.% after which the Se-Se bond vanishes. A further increase of the Bi content results in the formation of Bi-Bi or Bi-Ge bonds provided Bi is still six fold coordinated with Se. Coordination numbers four and two are assumed for Ge and Se respectively and the number of covalent bonds per Bi atom is reported to be six in these glasses[27]. Investigations on electrical properties on these glasses show an abrupt decrease in resistivity which may be related to the formation of fairly large number of Bi-Se bonds and the disappearance of Se-Se bonds. For six fold coordinated Bi in crystalline Bi_2Se_3, the occurrence of p^3d^3 or sp^3d^2 hybridisation have been suggested. If this is the situation with Bi in chalcogenide glasses, the Bi-Se bond becomes electron deficient and Bi atoms get negatively charged which is compensated by the positive charge on the Se atoms. Thus the equilibrium between the positively and negatively charged bonds which pins the Fermi level are affected by the charged impurities which is described in the charged dangling model. Sunil Kumar et.al [28], based on XPS measurements of Ge-Bi-Se thin films have suggested that Bi atoms are positively charged. According to their results the charged Bi atoms perturb the equilibrium between positively and negatively charged defect centers, thereby causing a shift of the Fermi level towards the conduction band.

Vaidyanathan et.al [29] have considered the Bi based glasses as a pseudobinary system with Bi acting as network modifiers to the basic $Ge_{20}Se_{80}$ network. The modification of the host network makes the Fermi level move towards the conduction band edge and alters the conduction mechanism from p-type to n-type. They have also proposed a structural model to explain the carrier type reversal in Pb incorporated

germanium chalcogenides. Spectroscopic investigations such as diffuse reflectance spectra and variation of optical energy gap obtained from peak maximum energies in diffuse reflectance spectra as a function of Pb concentration also show similar behaviour. FTIR and Raman spectra together confirm that Ge and Pb or Bi in this type of glass system are present only in tetrahedral and octahedral coordinations using the above spectroscopic features.

The Pb is assumed to be in a sp^3d^2 state of hybridisation. The Se atoms are in sp^n(n= 1,2, and 3) hybridisation. Germanium utilises its sp^3 hybridised orbitals for bond formation. The lowest energy levels result from the overlap of the bonding orbitals. The Ge-Se and Ge-Ge bonds constitute the lowest energy levels. The next higher energy level is constituted by sp^n lone pair originating from Se. The sp^3d^2 orbitals of Pb ions are likely to occupy a slightly higher level and just above Se lone pair levels. Similarly increase in Bi concentration in Ge-Bi-Se glasses leads to a rapid growth of sp^3d^2 band which results in the rapid increase of electron contribution to conductivity which exceeds contribution from holes. As consequence p→n transition occurs as a function of Bi concentration. Only Pb and Bi containing Ge-Se glasses are known to exhibit such a p→ n transition. Bi and Pb have a uniqe tendency towards octahedral coordination and more importantly the energetic disposition of their d-bands, which can overlap in energy with those of lone pair bonds of Se, in particular, may be the reasons for this p→n transition.

Based on the various explanations, we can draw the following general conclusions regarding photoconductivity of Ge-Bi-se glasses. The Ge-Bi-Se system is a pseudo binary system with Bi atoms acting as an impurity. The Bi atoms modify the structure of the host Ge-Se network and it results in the shifting of the Fermi level towards the conduction band. The decrease in photoconductivity beyond x=6 (Z=2.46) at.% can be explained as due to the formation of Bi_2Se_3 ionic bonds and the corresponding disappearance of Se-Se bonds. In the interpretation given by Vaidyanathan et.al [29], the disappearance of Se-Se bonds with increase in Bi content is outlined as due to the overlap of d-orbitals of Bi or Pb

with those of lone pair bonds in Se. The increase in defect concentration due to the addition of bismuth may be the reason for the decrease in carrier lifetime with increase in Bi content. Carrier lifetime decreases in general with increase of Bi content and exhibits a clear slope change around the critical composition with x=7 as shown in Fig.4.12. At the same time photoconductivity slightly increases with increase in Bi content and around the critical composition it exhibits a rise and a clear decrease as shown in Fig.4.13. It is interesting to note that the average coordination(Z) of this composition is 2.47 close to which the system has a mechanical threshold according to Phillips-Thorpe model.

4.4 XPS analysis of Ge-Bi-Se glasses

Two compositions from the $Ge_{20}Bi_xSe_{80-x}$ system, namely with x=2 and x=10 have been analysed by x-ray photoelectron spectroscopy. The composition with x=2 is p-type while that with x=10 is n-type. The binding energy values of the characteristic levels of pure Ge,Bi and Se as well as their values in the two compositions obtained from XPS spectra are show in Table 4.1. The corresponding spectra are given in figures 4.15, 4.16 and 4.17.

Table 4.1

Binding energy values from XPS measurements   eV

Sample	Ge $3p_{3/2}$	Bi $4f_{7/2}$	Se $3P_{3/2}$
Pure element	120.8	157.4	161.9
$Ge_{20}Bi_2Se_{78}$ (Z=2.42)	121.7 (+0.9)	158.5 (+1.1)	161.2 (-0.7)
$Ge_{20}Bi_{10}Se_{70}$ (Z=2.5)	121.3 (+0.5)	158.6 (+1.2)	160.8 (-1.1)
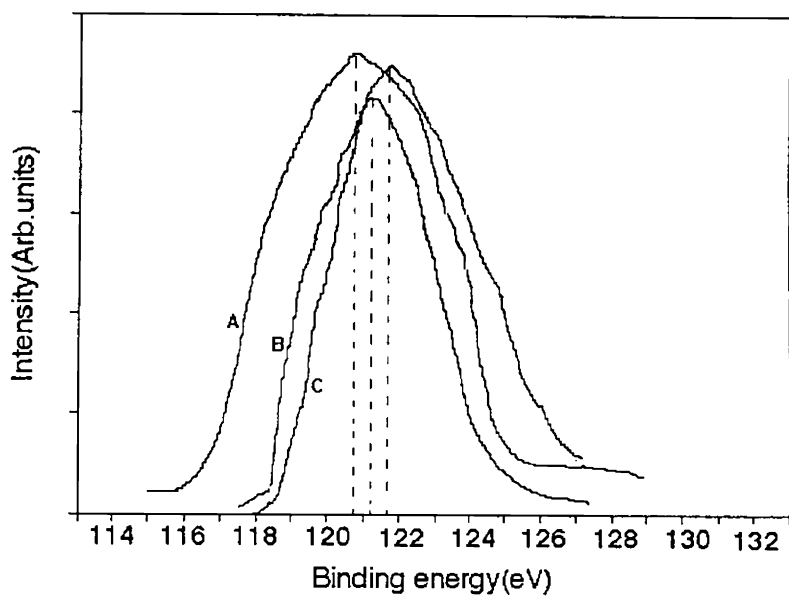
Fig.4.15 XPS of $3p_{3/2}$ levels of pure germanium(A) , germanium in $Ge_{20}Bi_2Se_{78}$ (B) and in $Ge_{20}Bi_{10}Se_{70}$. (C)
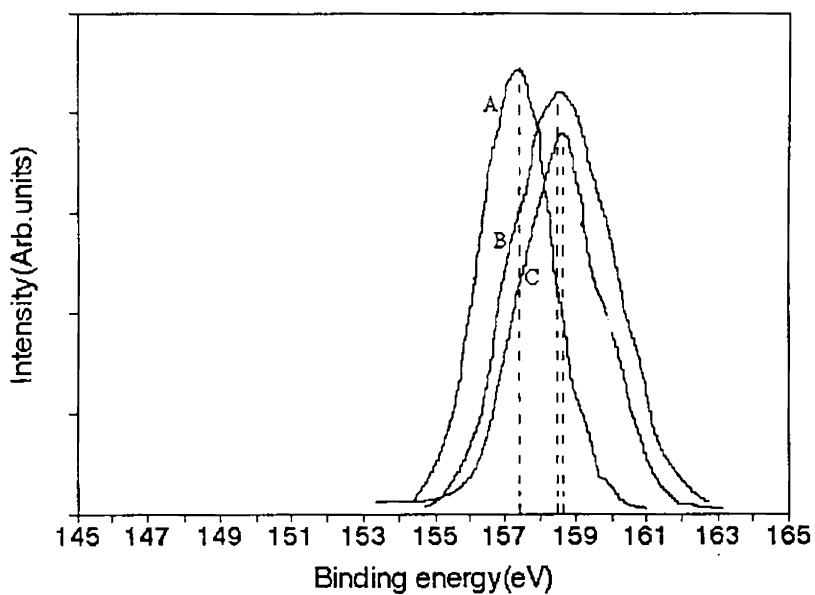
Fig.4.16 XPS of $4f_{7/2}$ levels of pure Bi (A), Bi in $Ge_{20}Bi_2Se_{78}$ (B) and in $Ge_{20}Bi_{10}Se_{70}$.(C)
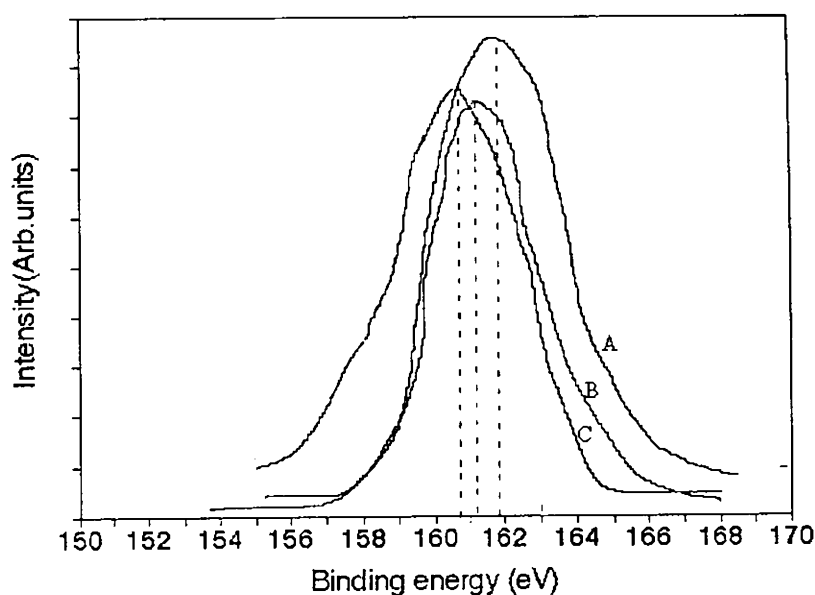
Fig.4.17 XPS of $3p_{3/2}$ levels of pure selenium.(A) selenium in $Ge_{20}Bi_2Se_{78}$ (B) and in $Ge_{20}Bi_{10}Se_{70}$.(C)

As is clear from the figures, Bi suffers a positive shift in its 4f level for the two compositions compared to that of the pure element. Germanium also undergoes positive shift when the compound is formed. But the b.e values of selenium is found to decrease in the compounds compared to that of pure selenium. The shifts can be attributed to the bonds formed and variation in number of structural units in the two compositions. The differences in electronegativity values could also be responsible for the observed shifts.

4.5 Conclusions

Our investigations indicate that photoconducting properties of Ge-Se system in general improves by the incorporation of Bi. The increase is nearly of the order of two. Photoconductivity exhibits a clear change corresponding to the critical composition of the Ge-Bi-Se system at which the material undergoes a p→n transition. At the same time

photodetectivity(σ_{ph}/σ_d), in general, decreases with the incorporation of bismuth. Photodetectivity also exhibits a clear change at the critical composition. Carrier lifetime measured by FRPC method, decreases in general with the incorporation of bismuth. Carrier lifetime has a sharp slope change around the critical composition. These results are analysed in the light of various models and explanations proposed by different research workers. Analysis of the material in terms of ABFH model reveals that the Ge-Bi-Se system is a TypeI photoconductor. One n-type and one p-type compositions have been analysed by XPS and the results are discussed.

4.6 References

1. N.F. Mott *Adv.Phys* **16** (1967) 49

2. E.A Davis and N.F Mott *Phil.Mag* **22** (1970) 903

3. B.T Kolomiets, A.Lebedev, N.A Rogachev *Fiz.Tech Poluprov.***8** (1974) 545

4. S.Okano, M.Suzuki, T.Imura, N.Fukuda and A.Hiraki *J.Non-Cryst Solids* **59-60** (1983) 969

5. R.Misra, S.Goel, A.K Agnihotri and A.Kumar *J.Mat.Sc.Lett* **11** (1992) 212

6. N.Tohge, H. Matsuo and T.Minami *J.Non-Cryst Solids* **95-96** (1987) 809

7. N.Tohge, T.Minami, Yamamoto and K.Tanaka *J.Appl.Phys.* **51** (1980) 1048

8. J.C Phillips, *Phys.Rev.***B36** (1987) 4265

9. S.R Elliot and A.T Steel *Phys.Rev.Lett* **57** (1986) 1316

10. J.Storiopoulous and W.Fuhs *J.Non-Cryst Solids* **114** (1989) 97

11. P.Nagels, L.Tichy, A.Triska and H.Ticha *J.Non-Cryst Solids* **59** (1989) 1015

12. Z.U.Borisova *"Glassy Semiconductors"* Plenum Press New York (1981)

13. A.Onozuka, O.Oda I.Isuboya *Thin solid films* **149** (1987) 9

14. K.L Bhatia and V.K Bhatnagar *J.Non-Cryst. Solids* **104** (1988) 17

15. R.Kaplan *J.Phys: Condens. Matter* **7** (1995) 6847

16. J.Bullot , P.Cordier ,M. Gauthier and G.Mawawa *Phil.mag.***B 55** (1987) 599

17. M.Bort, W.Fuhs, S.Liedtke and R.Stachowitz, *Phil.Mag.Lett* **64** (1991)227

18. T.M Searle *Phil.Mag. Lett* **61**(1990) 251

19. A.Rose *"Concepts in Photoconductivity and allied problems"* (New York: Krieger) (1978)

20. M.K Rabinal, K.S Sangunni, E.S.R Gopal and S.V Subramanyam, *Solid state commun.***88** (1993) 251

21. K.L. Bhatia, G.Parthasarathy and E.S.R Gopal *J.Non-Cryst Solids* **69** (1985) 189

22. L.Tichy, H.Ticha and A. Triska *Solid State Commun.* **53** (1985) 399

23. J.C Phillips and M.F Thorpe *Solid State Commun.* **53** (1985) 699

24. W.Bresser, P.Boolchand and P.Suranyi, *Phys.Rev.Lett* **56** (1986) 2493

25. A.Feltz *"Physical and chemical properties of semiconducting compounds"* Nauka, Moscow (1979)

26. L.Pauling " *The nature of the chemical bond*" 3 rd ed. Cornell Univ, NewYork (1960)

27. E.Mooser and W.B Pearson *J.Phys.Chem.Solids* **7** (1958) 68

28. Sunil Kumar, S.C Kashyap and K.L Chopra *J.Appl.Phys.***72** (1992) 2066

29. B.Vaidhyanathan, S.Murugavel, S.Asokan and K.J Rao *J.Phys.Chem* **B101** (1997) 9717

Chapter 5

Photoconductivity in As-Sb-Se glasses

5.1 Introduction

As_xSe_{100-x} system is probably one of the most studied ones among the binary systems of semiconducting chalcogenide glasses[1-3]. Studies on glasses based on As and Se have received much attention because of their interesting electrical and optical properties. There are a number of reports on the effect of the addition of Cu,Ag,Sn,Bi,Mg,Ga etc. on the electrical properties of the stoichiometric As_2Se_3[4-7]. Recently there has been considerable interest in the study of the effect of replacing As in the As-Se system by other elements. Nandakumar et.al have reported the composition dependence of optical energy gap[8], glass transition temperature and thermal diffusivity[9] of As-Sb-Se glasses. Actually the As-Sb-Se glasses are formed not by the incorporation of Sb as an impurity but by the replacement of As by Sb, since As and Sb are isovalent elements. Low temperature elastic behaviour in these glasses have been reported by Gopal et.al[10] and thermal analysis using differential scanning calorimetry have been reported by Mahadevan et.al[11]. Also Giridhar et.al[12] have investigated the composition dependence of electrical conductivity, glass transition temperature and density in different families of the As-Sb-Se system.

Since As and Sb are isovalent the replacement of As by Sb does not alter the basic structure of the glass drastically. The bond energies of As-Se and Sb-Se are respectively 52 kcal/mol and 51 kcal/mol[13]. It is clear that the replacement of As by Sb can not affect the bond energy or coordination number significantly. Even then variations are observable from the basic As_xSe_{100-x} system. Addition of Sb to the As-Se system could form good ternary glasses to certain extent. The maximum Sb content that forms glass is 20 at.%. We

have carried out investigations on As-Sb-Se systems with the general formula As_xSb_{15} Se_{85-x} and $As_xSb_{10}Se_{90-x}$ where Sb content is fixed at 15 at.% and 10 at.% respectively with variation in As and Se contents. In each of these systems the composition which can be represented by $(As,Sb)_{40}Se_{60}$ is the stoichiometric composition for the system. In $As_xSb_{15}Se_{85-x}$, the stoichiometric composition is $As_{25}Sb_{15}Se_{60}$ and in $As_xSb_{10}Se_{90-x}$ the stoichiometric composition is $As_{30}Sb_{10}Se_{60}$. These two compositions belong to the As_2Se_3-Sb_2Se_3 pseudobinary group. Considering this composition as reference glasses with Se content more than 60 at.% can be called Se rich glasses and those with Se content less than 60 at.% can be called As rich glasses of the As-Sb-Se families.

Our investigations are centred around the composition dependence of photoconductivity and carrier lifetime in these systems. The temperature dependence of photoconductivity is also analysed. The ratio (σ_{ph}/σ_d) which represents the photodetectivity is calculated for each composition. Two compositions of the $As_xSb_{15}Se_{85-x}$ system have been analysed by XPS and the results are analysed.

5.2 Experimental details

Samples with the general formulae $As_xSb_{15}Se_{85-x}$ (x=15-35) and $As_xSb_{10}Se_{90-x}$ (x=20-40) are prepared in bulk form by the conventional melt quenching technique as described in Chapter 2. Amorphous nature of the samples have been confirmed by XRD. Samples having 4 x 3 mm^2 surface area and 0.5 mm thickness have been used for the present measurements. Electrical contacts are taken using sandwich contacts by SnO_2 coated transparent conducting glass. Intensity of light used for photoconductivity measurements is 25 mW/cm^2 The contacts have been studied to analyse their resistance behaviour and are found to be ohmic. Pulsed excitation(a.c) and steady state (d.c) photoconductivity and carrier lifetime are measured by the experimental procedures already outlined in Chapter 2.

5.3 Results and discussion

5.3.1 Photoconductivity measurements by a.c and d.c methods

Photoconductivity measurements have been carried out by both pulsed excitation(a.c) and steady state(d.c) methods. Fig.5.1 shows the plot of $1/T$ vs $\sigma_{ph(a.c)}$ for three samples of the $As_xSb_{15}Se_{85-x}$ system. In fig.5.2 the $1/T$ vs $\sigma_{ph(a.c)}$ variation is plotted for different compositions of $As_xSb_{10}Se_{90-x}$ system. Photoconductivity increases with temperature initially and attain a maximum at a particular temperature(T_m) and then decreases in all the samples. T_m values are different for different samples. The same type of behaviour has been exhibited by the samples in d.c measurements also. Plot of $\sigma_{ph(d.c)}$ vs $1/T$ for three compositions of the $As_xSb_{15}Se_{85-x}$ system is shown in Fig.5.3. The photodetectvity(σ_{ph}/σ_{dc}) vs $1/T$ variation for representative samples are shown in Fig.5.4. Also photoconductivity has been measured with varying intensity of illumination. Photoconductivity varies linearly with intensity at low intensities and almost seem to be saturated at higher intensities. Fig.5.5 shows the variation for two compositions.
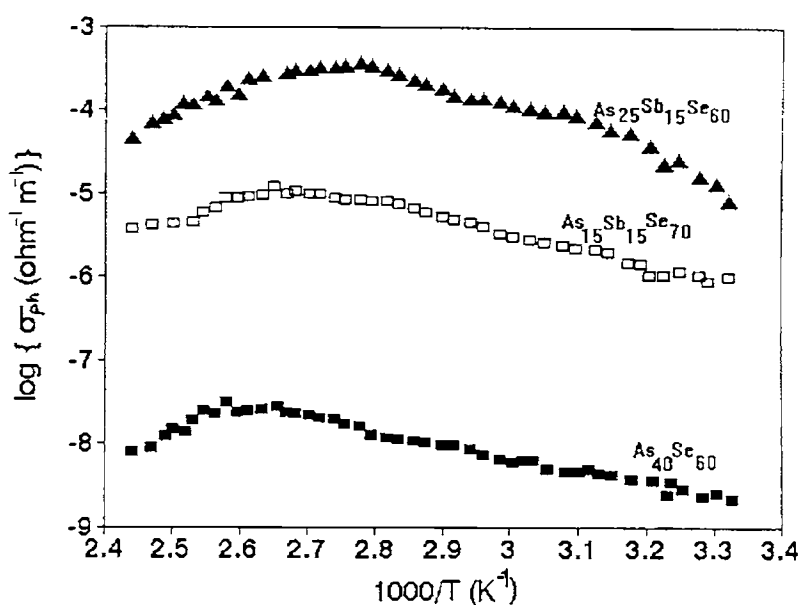
Fig.5.1 Temperature dependent variation of photoconductivity measured by a.c method for two compositions. of $As_xSb_{15}Se_{85-x}$ Results for $As_{40}Se_{60}$ is also presented. Chopping frequency is 10 Hz. Uncerainty in values are less than 4 %.
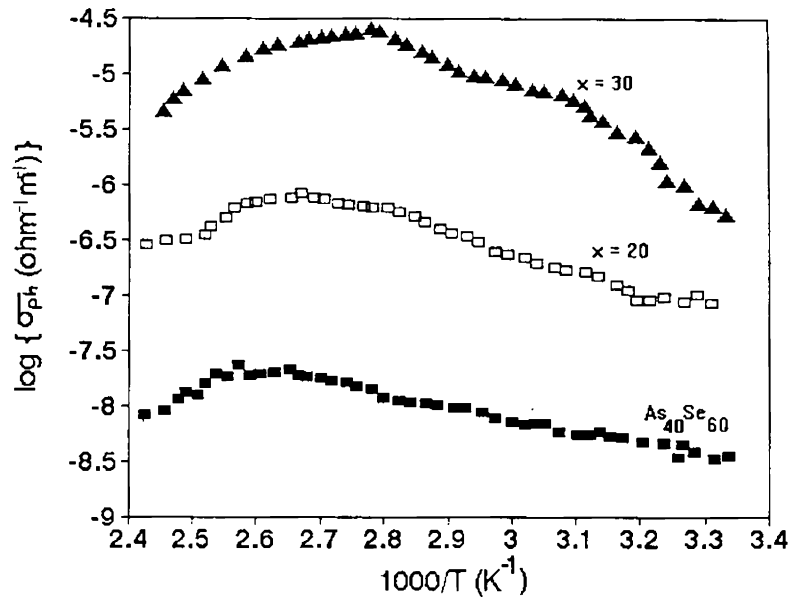
Fig.5.2 Temperature dependent variation of photoconductivty measured by a.c method for two compositions of $As_xSb_{10}Se_{90-x}$ and $As_{40}Se_{60}$.
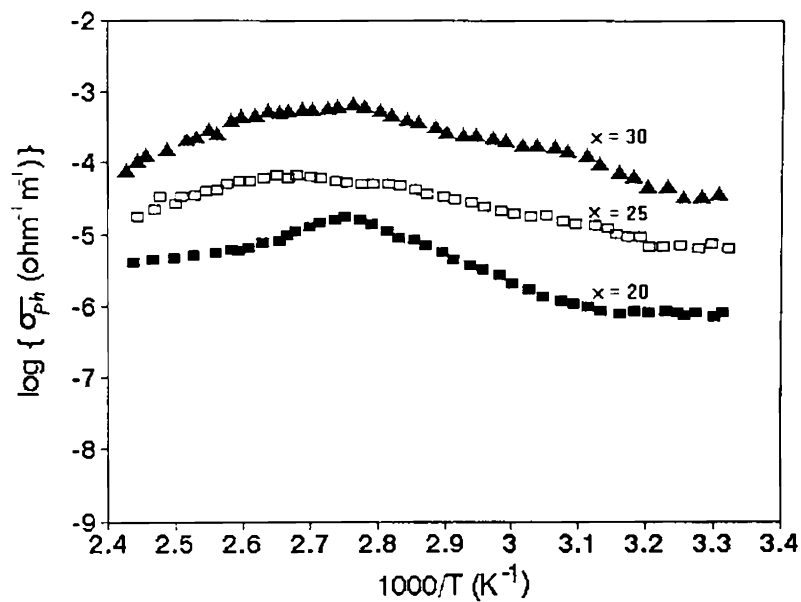

Fig.5.3 Variation of d.c photoconductivity with temperature for three samples of the $As_xSb_{15}Se_{85-x}$ system.

From the temperature dependent study of photoconductivity in the two As-Sb-Se systems, it is found that they are type I photoconductors as outlined by the ABFH model[14-16]. Photoconductivity exhibits clear activation above and below a particular temperature(T_m) where the photoconductivity is maximum. Also photoconductivity is grater than dark conductivity for a range of temperatures which is clear from Fig.5.4 where photodetectivity(σ_{ph}/σ_d) is plotted with temperature. A plot of E_g vs $T_m.\ln(\sigma_{max})$ is shown in Fig.5.6. The points obtained can be fitted to a straight line[17]. Referring the description
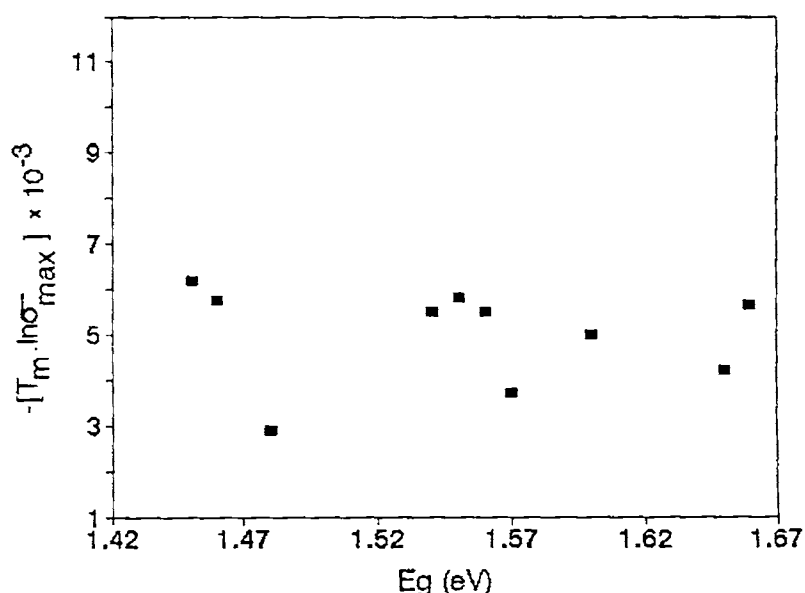
Fig.5.6 Plot between E_g and $T_m.\ln\sigma_{max}$ for the two As-Sb-Se systems. The points can be fitted to a straight line which is a characteristic feature of the type I photoconductivity

of the ABFH model for photoconductivity analysis the behaviour is shown in Fig.5.6 is that of a type I photoconductor.

Spectral variation of phtoconductivity has been studied in the As-Sb-Se systems and the results for two compositions are presented in Fig.5.7. Photoconductivity peaks around 700-750 nm which corresponds to the absorption edge of these samples.
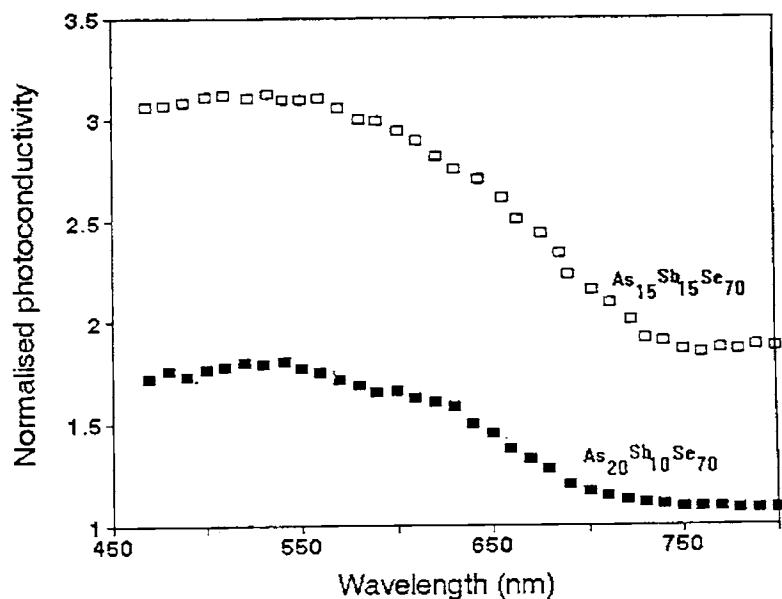
Fig.5.7. Spectral variation of photoconductivity in two compositions of the As-Sb-Se systems.

5.3.2 Composition dependence of photoconductivity

Temperature dependent variation of photoconductivity of $As_{40}Se_{60}$, which is the stoichiometric composition of As_xSe_{100-x} and that of $As_{30}Sb_{10}Se_{60}$ and $As_{25}Sb_{15}Se_{60}$,which are stoichiometric compositions of the two systems under our consideration, are shown in figures 5.1 and 5.2. It is clear that photoconductivity increases by nearly three orders of magnitude due to the incorporation of Sb into As-Se system. The enhancement may arise from the defect states formed in the energy gap[18]

In Fig.5.8 the composition dependence of photoconductivity for the $As_xSb_{10}Se_{90-x}$ and $As_xSb_{15}Se_{85-x}$ systems are plotted. It can be seen that in both these systems photoconductivity increases with increase in As content and for the stoichiometric composition, the variation exhibits a clear slope change and thereafter increases slightly for all compositions with still higher As content. The composition dependence of photodetectivity (σ_{ph}/σ_d) also exhibits a clear slope change corresponding to the stoichimetric composition as shown in Fig.5.9. The observed composition dependence of

photoconductivity in the As-Sb-Se family of glasses can be explained on the basis of chemical ordering between the constituent atoms[1]. According to the concepts of chemically ordered covalent network model(COCN), the As-Sb-Se glasess can be considered as made up of completely cross linked three dimensional structural units of As_2Se_3-Sb_2Se_3 with either As or Se in excess.
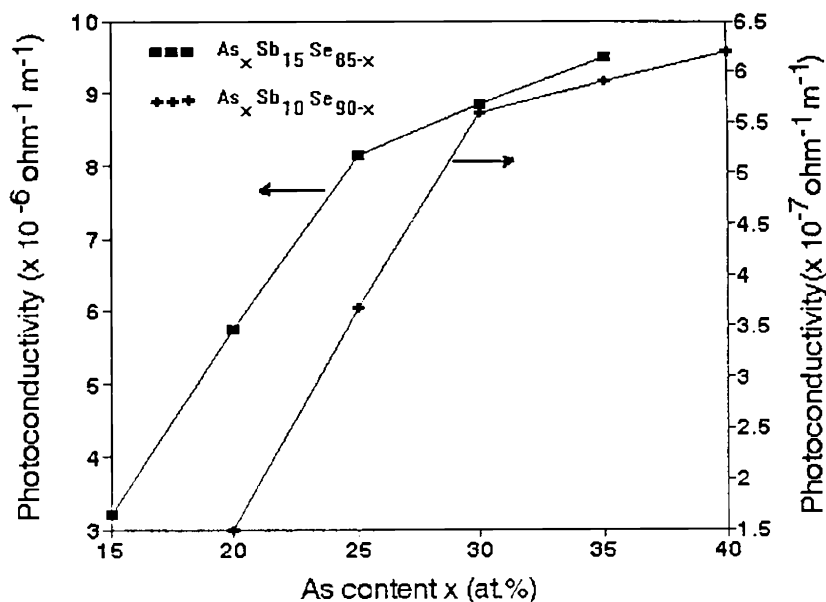

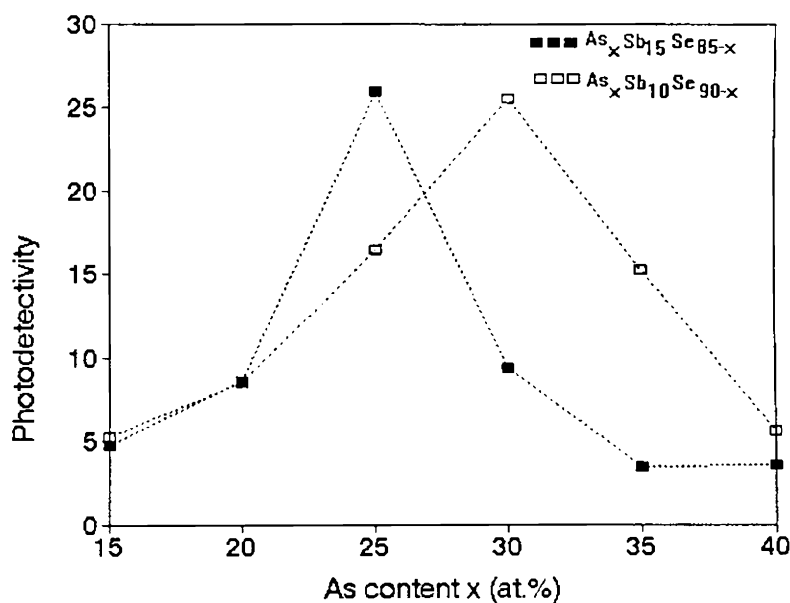**Fig.5.8** Composition dependence of photoconductivity in the two As-Sb-Se systems

Fig.5.9 Composition dependence of photodetectivty in the two As-Sb-Se systems

In the Se rich glasses some of the original As structural units are replaced by Se and the two fold coordinated Se atoms form $(Se)_n$ chains or $(Se)_8$ rings. In the As rich glasses three fold coordinated As atoms break these $(Se)_8$ rings or $(Se)_n$ chains to satisfy coordination number requirement and form very complex network structure. The chemical order is maintained for As atoms as As_2Se_3 structural units. With the introduction of Sb atoms, the Se atom chains get interconnected with both As and Sb atoms and the composition dependence is brought about by the occupation of Se atoms in favourable positions in the network[11-12].

Apart from As-Se, Sb-Se and Se-Se bonds, As-As and Sb-Sb bonds will also be involved in the formation of the network. The bond energies of As-Se, Sb-Se, Se-Se, As-As and Sb-Sb bonds are 52.51,49,56 and 42 kcal/mol respectively[13]. With the decrease in Se content in As rich glasses the Sb_2Se_3/As_2Se_3 ratio progressively increases resulting in a decrease in average bond energy of the system. But for the Se rich glasses with increase in Se content more As_2Se_3 structural units are present in the network than the Sb_2Se_3 structural units and results in an increase of average bond energy. Considering the two aspects we can infer that, in general, with increase in As concentration (or decrease in Se concentration) the average bond energy decreases. There is a slope change in the increase corresponding to the stoichiometric composition. This explains the observed composition dependent behaviour of the system.

The results on the composition dependence of optical band gap in the two systems are presented in Fig.5.10. The optical band gap decreases rapidly with increase of arsenic content and at the stoichiometric composition the decrease exhibits a slope change. Thereafter the rate of decrease is low.

According to Kastner's model [19], in the band structure of chalcogenide glasses the decrease in average bond energy of the system tends to decrease the energy of the conduction band edge. This effectively decreases the optical band gap. The shrinkage of optical band gap with variation in composition may also be a reason for the observed
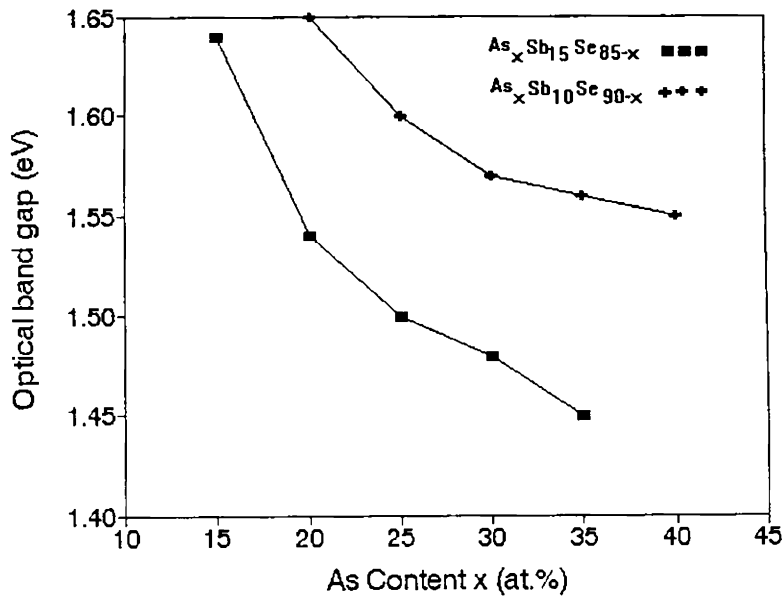
Fig.5.10   Variation of optical band gap with composition for $As_xSb_{10}Se_{90-x}$ and $As_xSb_{15}Se_{85-x}$ systems.

increase in photoconductivity. Another observation is that the stoichiometric composition of this system corresponds to an average coordination number (Z) =2.41.

One can not expect drastic changes of properties in As-Sb-Se system compared to that of As-Se, because the basic structure of the glass network is not much affected by the replacement of As by Sb, since As and Sb are isovalent. But the Sb-Se bonds formed by the inclusion of Sb causes a reduction in the average bond energy which affect the properties of the As-Se system.

5.3.3 Frequency resolved photoconductivity(FRPC) and carrier lifetime measurements

Modulation frequency vs photoconductivity plots for four compositions of the As-Sb-Se system are shown in Fig.5.11. Photoconductivity in each plot is normalised with respect to its maximum value. Carrier lifetime is calculated using the formula[20]

$\tau = 1/2\pi f_{max}$ where f_{max} is the frequency at which photoconductivity shows a peak in its value. From FRPC data at different intensities of illumination and at different temperatures it has been found that position of f_{max} shifts to higher frequencies with increasing temperature or intensity. The variation of carrier lifetime with intensity and temperature are shown in figures 5.12 and 5.13 for the compositions $As_{25}Sb_{15}Se_{60}$ and $As_{30}Sb_{10}Se_{60}$. Other compositions also exhibit similar variations. For all the compositions the carrier lifetime decreases with increase in intensity or temperature. Similar results have been obtained with Ge-In-Se and Ge-Bi-Se glasses. Since the intensity of excitation light is directly proportional to the carrier generation rate G, the carrier lifetime (τ) and G can be related by the expression[21-22]

$$\tau = AG^{\upsilon}.$$

The slope of the plot of ln τ vs ln G shown in Fig.5.14 gives the value of υ. The value of υ for various compositions lie between 1 and 0.5. For the two compositions presented here the values are ≈ 0.61 and ≈ 0.778. This behaviour is an indication of a continuous distribution of traps in the energy gap.
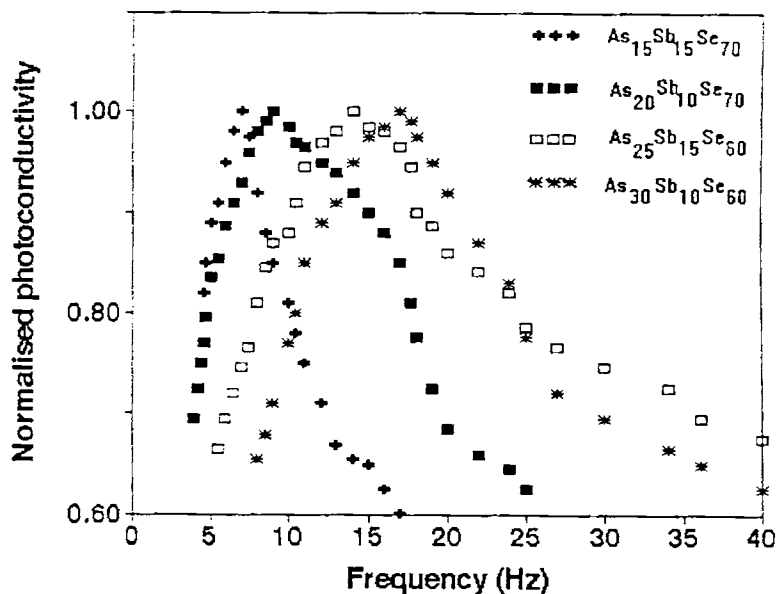

Fig.5.11 Plot of FRPC measurements for various compositions of the As-Sb-Se system.
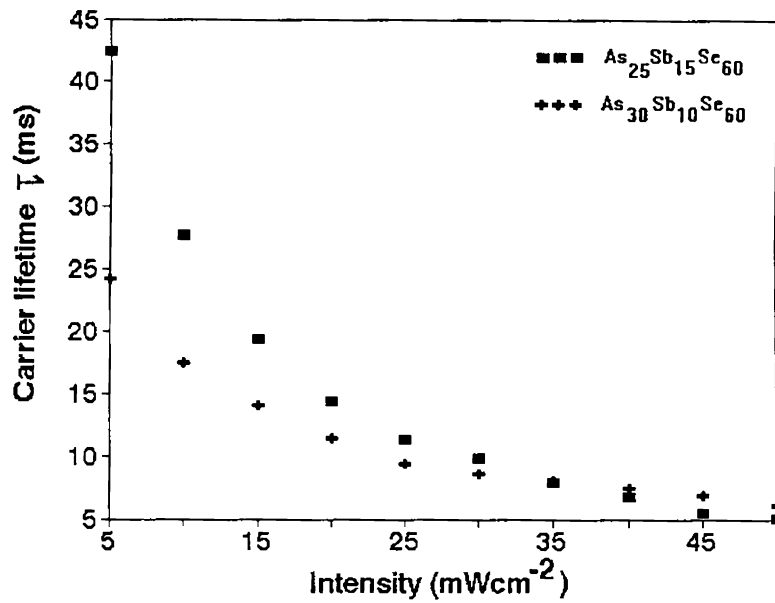
Fig.5.12 Variation of carrier lifetime with intensity for two compositions of the As-Sb-Se system.
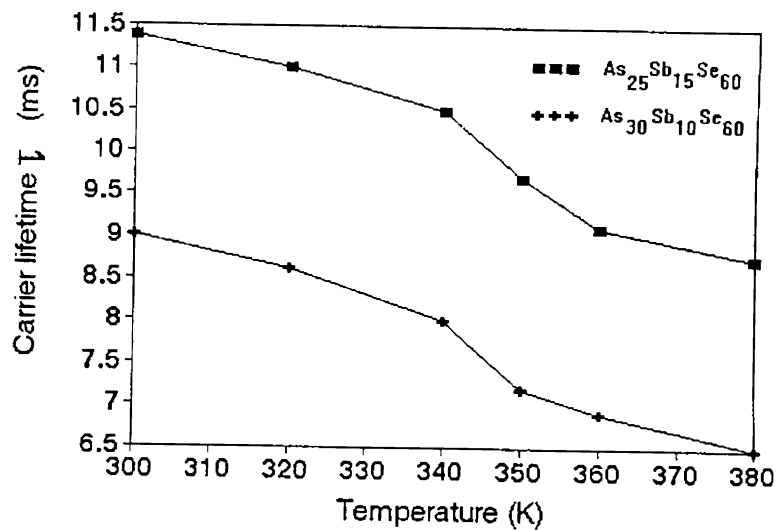
Fig.5.13 Variation of carrier lifetime with temperature for two compositions of the As-Sb-Se system.
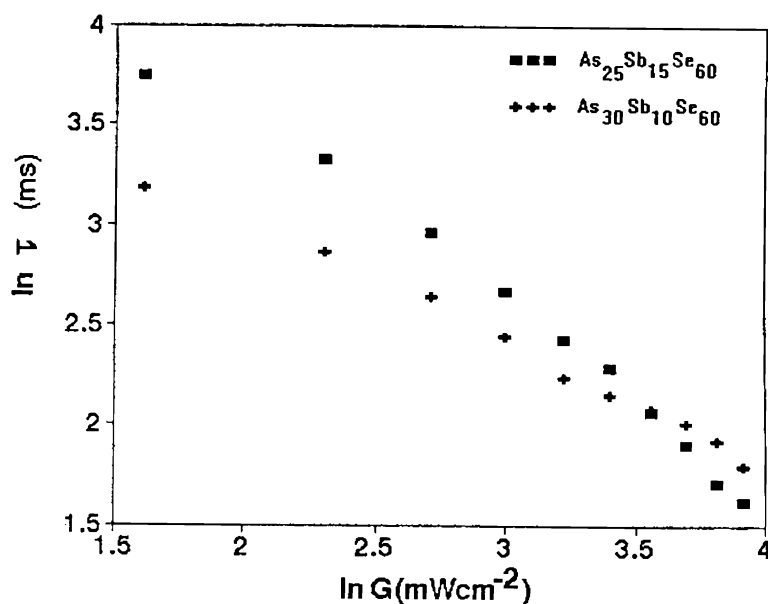
Fig.5.14 Logarithm of intensity of illumination plotted aginst logarithm of carrier lifetime for two compositions. Other compositions also have similar variations.

Composition dependence of carrier lifetime in both of the As-Sb-Se systems are shown in Fig.5.15. Carrier lifetime decreases sharply up to the stoichiometric composition and it exhibits a clear slope change at the stoichiometric compositions. Thereafter it decreases only slightly.

Photoconductivity can be represented by the equation

$$\Delta\sigma_{ph} = e(\Delta n.\mu_n + \Delta p.\mu_p)$$

$$= e.g(\tau_n.\mu_n + \tau_p\mu_p)$$

where g is the generation rate, μ is the carrier mobility and τ is the carrier lifetime. For the stoichiometric compositions of As-Sb-Se system photoconductivity is high while carrier lifetime is low. Increase in mobility of the carrier and /or generation rate with change in compositions may be the reason for this behaviour. The most probable reason is increase in the generation rate of carriers with change in composition, since the average bond energy decreases sharply up to the stoichiometric composition.
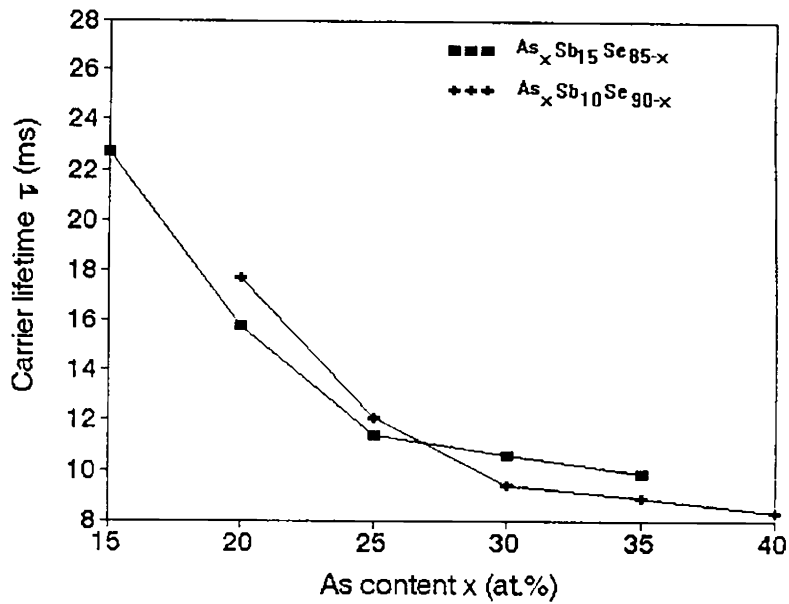
130

Fig.5.15 Composition dependent variation of carrier lifetime in the two systems of As-Sb-Se glasses.

5.4 XPS analysis

Two compositions of the $As_xSb_{15}Se_{85-x}$ system have been analysed by XPS. The compositions studied are those with x=15 and 25. Figures 5.16, 5.17 and 5.18 show the XPS of As, Sb and Se in the three compositions with the spectra of the elements in pure form. The binding energy values of the characteristic levels of the elements in compound and in pure form are given table 5.1. The observed b.e shifts from pure form are shown in brackets with appropriate signs. Selenium suffers a negative shift in b.e while As and Sb exibit positive shifts in their b.e values. The results are consistent with those obtained for Ge-In-Se and Ge-Bi-Se glassses.

Table 5.1

Binding energies obtained from XPS measurements in units of eV

Sample	As $3p_{3/2}$	Sb $3d_{5/2}$	Se $3p_{3/2}$
Pure element	143	530	161.9
$As_{15}Sb_{15}Se_{70}$	144 (+1)	532 (+2)	161.1 (-0.8)
$As_{25}Sb_{15}Se_{60}$	144.5 (+1.5)	531.8 (+1.8)	160.5 (-1.4)
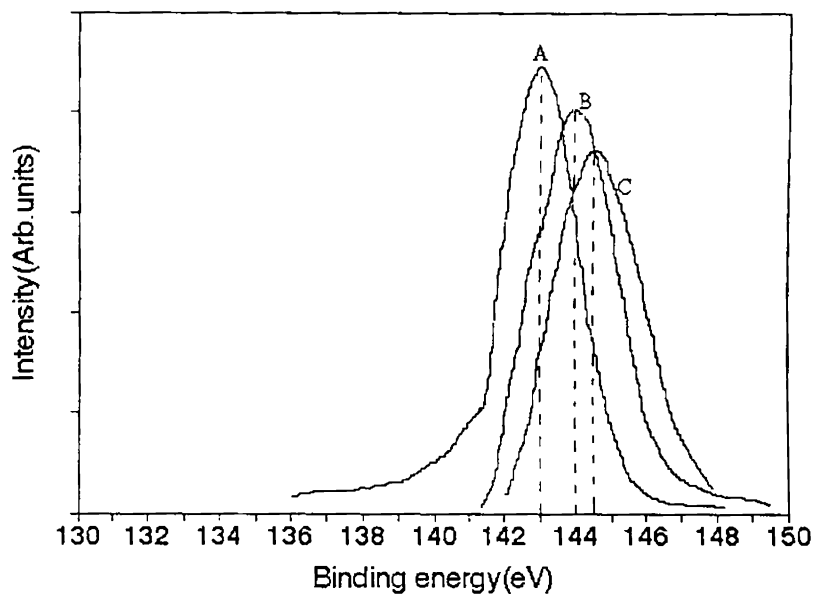
Fig.5.16 XPS spectra of $3p_{3/2}$ levels of pure arsenic(A)   arsenic in $As_{15}Sb_{15}Se_{70}$(B) and in $As_{25}Sb_{15}Se_{60}$(C)
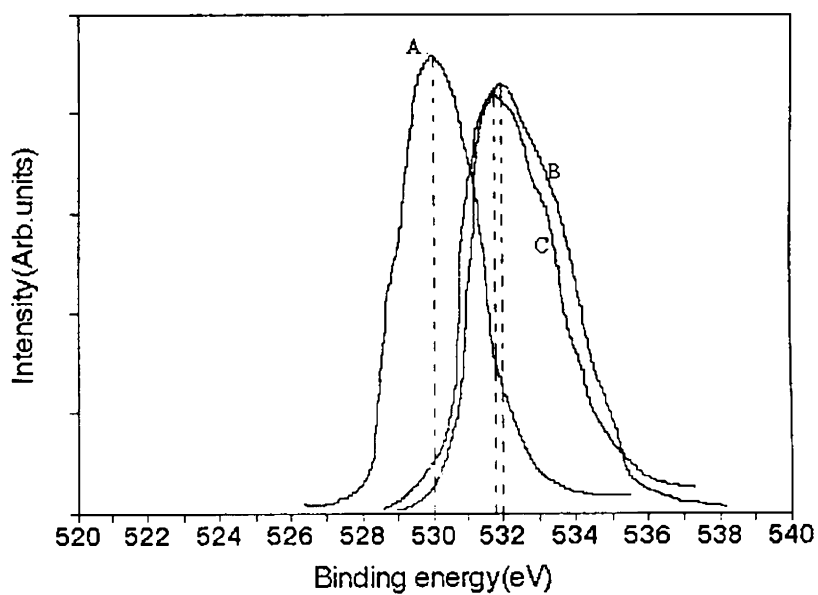
Fig.5.17 XPS spectra of $3d_{5/2}$ level of pure antimony(A) antimony in $As_{15}Sb_{15}Se_{70}$(B) and in $As_{25}Sb_{15}Se_{60}$(C).
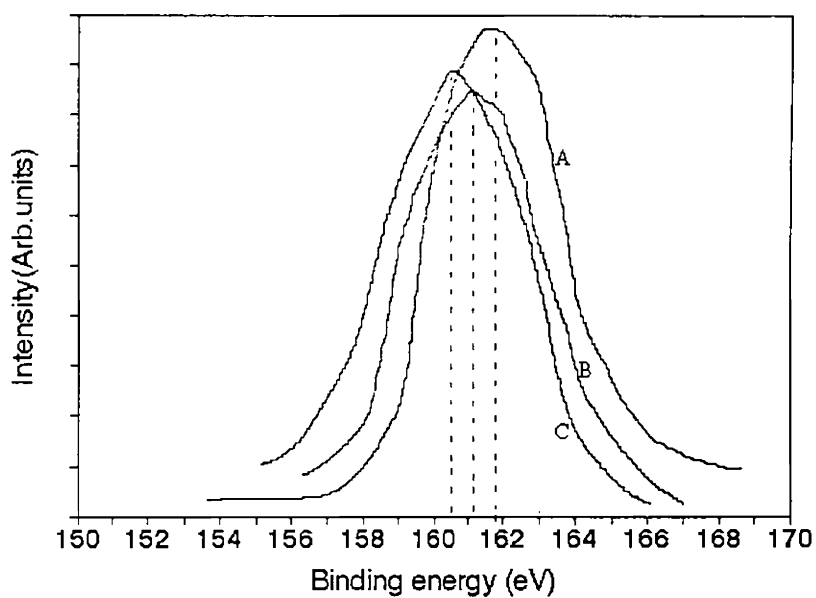

Fig.5.18 XPS spectra of $3p_{3/2}$ levels of pure Se(A), selenium in $As_{15}Sb_{15}Se_{70}$ (B)and in $As_{25}Sb_{15}Se_{60}$(C).

133

5.5 Conclusions

Photoconductivity and carrier lifetime in two As-Sb-Se systems, $As_xSb_{15}Se_{85-x}$ and $As_xSb_{10}Se_{90-x}$ have been studied. From the temperature dependent behaviour of photoconductivity the samples of these systems are found to be Type I photoconductors. The photoconductivity data fit well with ABFH model. Photoconductivity increases with increase in As content and it exhibits a slope change in the variation corresponding to the stoichiometric composition. Photodetectvity(σ_{ph}/σ_d) also have been calculated for all the compositions. Frequency resolved photoconductivity measurements have been carried out for obtaining the carrier lifetime. The variation of carrier lifetime with temperature, intensity and composition have been analysed. Carrier lifetime decreases with increase in As content. The variation exhibits a slope change corresponding to the stoichiometric composition and thereafter the rate of decrease is found to be low.

It has been found that in general the photoconductivity in As-Sb-Se systems is higher by nearly three orders of magnitude compared to the As-Se system. From the composition dependent analysis of photoconductivity it has been noted that the change of slope in the variation occurs corresponding to the stoichiometric composition whose average coordination number is 2.4.

5.6 References

1. G.Lucovsky and T.M Haynes in *Amorphous semiconductors* ed: M.H Brodsky, Oxford, Clarendon(1979)

2. R.J Nemanich, G.A.N Connel, T.M Hayes and R.A Street *Phys.Rev.*B18 (1978) 6900

3. R.A street, R.J.Nemanich and G.A.N Connel *Phys.Rev.*B18 (1978) 6915

4. R.L. Myuller in *Solid state chemistry*" ed: Z.U Borisova , Consultants Bureau. New York (1966)

5. Y.Sawan, F.G .Wakim, M.El. Gabaly and M.El.Rayess *J.Non-Cryst.Solids* 41(1980) 319.

6. Y.Sawan, F.G Wakim, M.El Gabaly and R.Prasad *J.Non-Cryst.Solids* 30(1979) 293.

7. B.T Kolomiets. Yu.V. Rukhlyadev and V.P Shilo *J.Non-Cryst Solids* 5 (1971) 389

8. K.Nandakumar and J.Philip *Bull.Mat.Science* 11 (1988) 297

9. K.Nandakumar and J.Philip *Phil.Mag* B63 (1991)493

10. E.S.R Gopal, T.S. Mukundan J.Philip and S.Sathish *Pramana J.Phys.* 28 (1987) 471

11. S.Mahadevan, A.Giridhar and A.K Singh *J.Non-Cryst Solids* 88 (1986) 11

12. A.Giridhar and S.Mahadevan *J.Non-Cryst Solids* 51(1982) 305

13. G.C Das, N.S platakis and M.B.Bever *J.Non-Cryst Solids* 15 (1974) 30

14. T.C Arnoldussen. R.H Bube, E.A Fagen and S.Holmberg *J.Appl.Phys.*43(1972) 1798

15. T.C Arnoldussen, R.H Bube E.A Fagen and S.Holmberg *J.Non-Cryst Solids* 8-10 (1972) 933

16. R.T.S Shiah and R.H Bube *J.Appl.Phys.*47 (1976) 2005

17. R.H Bube *"Photoelectronic properties of semiconductors"* Cambridge Univ. (1992)

18. A.Onozuka, O.Oda, I. Isuboya *Thin Solid Films* 149(1987) 9

19. M.Kastner *Phys.Rev.Lett* 28 (1972) 355

20. R.Kaplan *J.Phys:Cond..Matter* 7(1995) 6847

21. J.Bullot, P.Cordier, M.Gauthier and G.Mawawa. *Phil.Mag* B55 (1987) 599

22. T.M.Searle, *Phil.Mag Lett.*61(1990) 251

23. R.H Bube *"Photoconductivity of solids"* Krieger, New York (1978)

Photoconductivity in amorphous Ge-Sb-Se thin films

6.1 Introduction

The Ge-Se glasses become very good transmitters of IR radiation in 2-16μm region by the incorporation of antimony in them[1]. These glasses have found various applications where a high degree of IR transmittance is necessary. Also it has been found that the presence of antimony affects the optical and electrical properties of Ge-Se appreciably. The change in properties may be due to the formation of defect states or localized states created in the energy gap by the incorporation of antimony. These observations have attracted the interest of many research workers to study the properties of Sb doped Ge-Se further. Giridhar et.al[2] investigated the d.c and a.c electrical properties of bulk $Ge_xSb_{10}Se_{90-x}$ glasses. They observed a maximum in glass transition temperature and minimum in conductivity corresponding to the stoichiometric composition of the system. The electrical properties of two systems of Ge-Sb-Se, namely $Ge_xSb_{15}Se_{85-x}$ and $Ge_xSb_5Se_{95-x}$, bulk glasses have been studied by Narasimham et.al[3]. They confirmed the composition dependence of the properties of these systems and the remarkable variations at the stoichiometric composition. In the above two systems also, the stoichiometric composition exhibits a minimum in conductivity, maximum in activation energy and a maximum in glass transition temperature. Srinivasan et.al[4] observed a threshold behaviour in optical band gap and thermal diffusivity for critical compositions of the Ge-Sb-Se system. They explained the observations on the basis of changes in the network topology due to the formation and development of layered structure in the glasses. The effect of incorporation of metallic antimony in amorphous thin films of $Ge_{20}Se_{80}$ has been

studied by Mehra et.al[5]. They observed that by increasing the antimony content, the d.c conductivity of the system decreases, whereas the optical band gap of the system increases. Density and microhardness of Ge-Sb-Se glasses have been studied by Giridhar te.al[6]. According to their results microhardness shows a monotonic increase with Ge content for all families of Ge-Sb-Se system. The stoichiometric composition in each family exhibits a minimum in density and a maximum in molar volume as compared with the Se rich or Ge rich glasses of the corresponding family.

In this chapter we present the results of our investigations on dark conductivity and steady state photoconductivity in $Ge_xSb_{10}Se_{90-x}$ amorphous thin films($10<x<32.5$). Photoconductivity studies are informative in the case of amorphous semiconductors which are known to have a high density of states in the band gap associated with defects. The information obtained can be used to test the validity of various models proposed for the nature and distribution of localized states in the gap[7-9].

Steady state photoconducivity has been investigated in a number of amorphous chalcogenide semiconductors[8]. Based on the results of various measurements like thermoelectric power, field effect measurements etc., it has been suggested that in many of the amorphous semiconductors, there exists sharp discontinuities in the density of localized states in the forbidden gap and that the transitions between localized states play an important role in carrier recombination[9-12]. Such measurements have also established a strong dependence of photoconductivity on light intensity, temperature and photon energy in amorphous chalcogenides. The most striking conclusion that can be drawn from these studies is that the temperature and intensity dependence of photoconductivity show some common features suggesting that similarity exists in the distribution of localized states in the forbidden gap and in the recombination mechanism for a wide variety of materials. As described in Chapter 1 photoconductivity in amorphous chalcogenides can broadly be divided into two types, namely type I and type II [13-15]. Most amorphous chalcogenides exhibit type I photoconductivity which has the following characteristics; (i) photoconductivity shows a maximum at a temperature T_m, and it has defined activation energies above(E^+) and below(E^-) the maximum, (ii) it shows a linear

variation with light intensity and an exponential increase with $1/T$ at temperatures above T_m,(iii) a square root variation with light intensity at high intensities, a linear variation at low intensities and an exponential decrease with $1/T$ at low temperatures and (iv) dark conductivity higher than photoconductivity for $T>T_m$, and lower for $T<T_m$. In the case of type II photoconductors the maximum is not present and photoconductivity is much smaller than dark conductivity at all temperatures. Moreover, photoconductivity increases exponentially with temperature for them.

The general features found in photoconductivity of amorphous chalcogenides can be explained by the model proposed by Arnoldussen et.al.(Arnoldussen-Bube-Fagen-Holmberg or ABFH model)[13-15]. The results we obtained on amorphous $Ge_xSb_{10}Se_{90-x}$ thin films can also be analysed on the basis of this model.

The present work is aimed at studying the composition dependence of photoconductivity in Ge-Se chalcogenide glasses containing antimony and to establish the features of steady state photoconductivity in different compositions of this system in the light of the general features of photoconductivity reported in amorphous chalcogenides as outlined earlier.

6.2 Experimental method

$Ge_xSb_{10}Se_{90-x}$ glasses have been prepared in the bulk form from their constituent elements of 5N purity by the conventional melt quenching technique. The glassy nature of the bulk glasses thus prepared are confirmed by x-ray diffraction. The glasses are then used as the source material for the preparation of thin films. Samples are deposited onto ultrasonically cleaned glass substrates by sputtering in an argon atmosphere. The film thickness is determined by the interference method and is found to be in the range 2000 to 5000 A^0. The films are confirmed to be amorphous by x-ray diffraction method again. From electron probe micro analysis it has been found that the composition of the film is within 2% of the corresponding bulk value.

Two probe technique with coplanar configuration of electrodes is used for d.c conductivity measurements. The ohmic nature of the contacts is confirmed by linear

current-voltage characteristics. The sample is mounted on a copper plate which can be uniformly heated. The sample holder is enclosed in a chamber which can be evacuated. The temperature of the sample is measured and controlled within ± 0.1 K using a temperature controller. A 1000W tungsten halogen lamp is used as the light source for photoconductivity measurements. The photoconductivity is measured with a picoammeter as has already been described in Chapter 2.

6.3 Results and discussion

6.3.1 Temperature and intensity dependence of photoconductivity

The temperature dependence of dark d.c conductivity for three representative samples of Ge-Sb-Se thin films are shown in the $\ln\sigma_T$ vs $1/T$ plots exhibited in Fig.6.1. The d.c conductivity exhibits Arrhenius type behaviour with an activated conduction above certain temperature which varies with sample and following the relation

$$\sigma_T = \sigma_0 \exp(-\Delta E/kT) \tag{6.1}$$

where ΔE is the activation energy. The electrical activation energy is determined from the straight fit to the $\ln \sigma_T$ vs $1/T$ plot for each sample. The variation of the activation energy with composition for the Ge-Sb-Se thin films is shown in Fig.6.2 along with the corresponding variation of the optical energy gap determined from optical absorption and Photoacoustic measurements[4]. The electrical activation energy is found to approximately 45% of the optical band gap.

The temperature dependence of photoconductivity for the thin film samples are shown in figures 6.3 and 6.4. The measurements have been performed with an intensity of 200 mWcm^{-2} falling uniformly on the samples. All the samples exhibit similar features in the temperature variation of photoconductivity. Photoconductivity shows a maximum
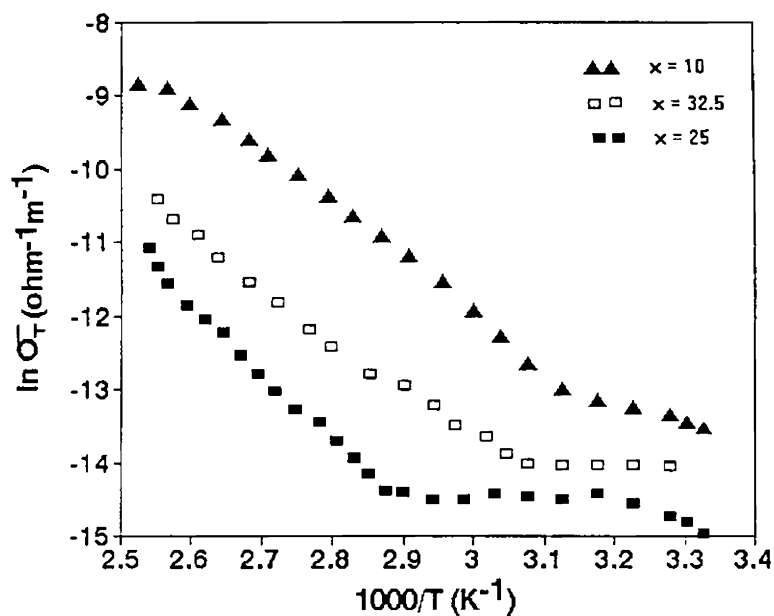
Fig.6.1. Temperature dependence of dark conductivity of three compositions of $Ge_xSb_{10}Se_{90-x}$ thin films. Other compositions show similar variations.

E_g (■) ΔE (I) $E^- + E^-$ (II)
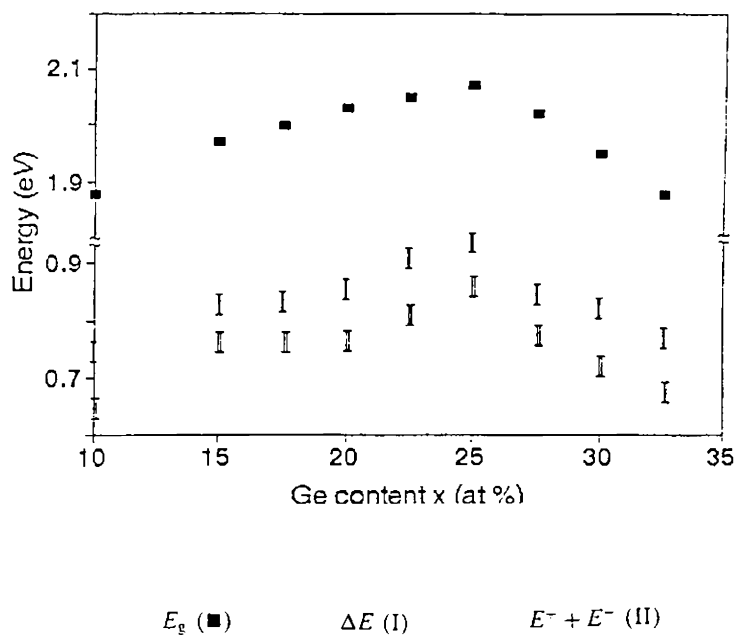
Fig.6.2. Variation of optical band gap E_g, activation energy ΔE and the sum of activation energies for photoconductivity $E^+ + E^-$ with composition in $Ge_xSb_{10}Se_{90-x}$ thin films.
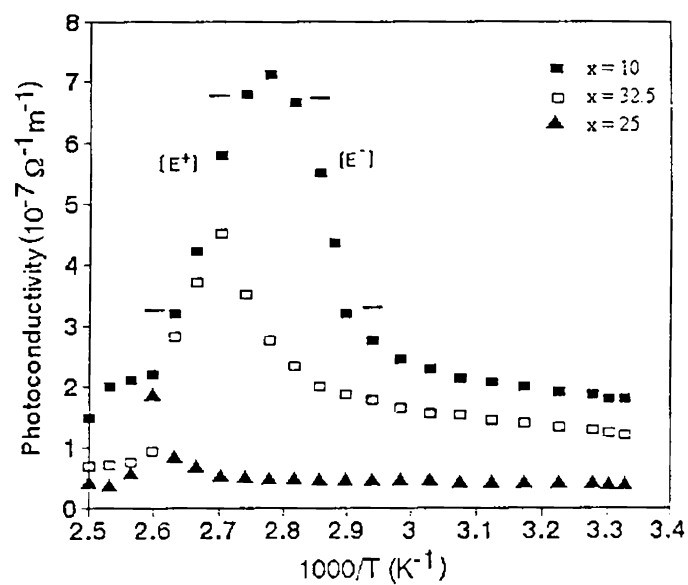
Fig.6.3 Temperature dependence of photoconductivity in three compositions of $Ge_xSb_{10}Se_{90-x}$ thin films. Other compositions show similar variations. The values of E^+ and E^- are calculated from these plots.

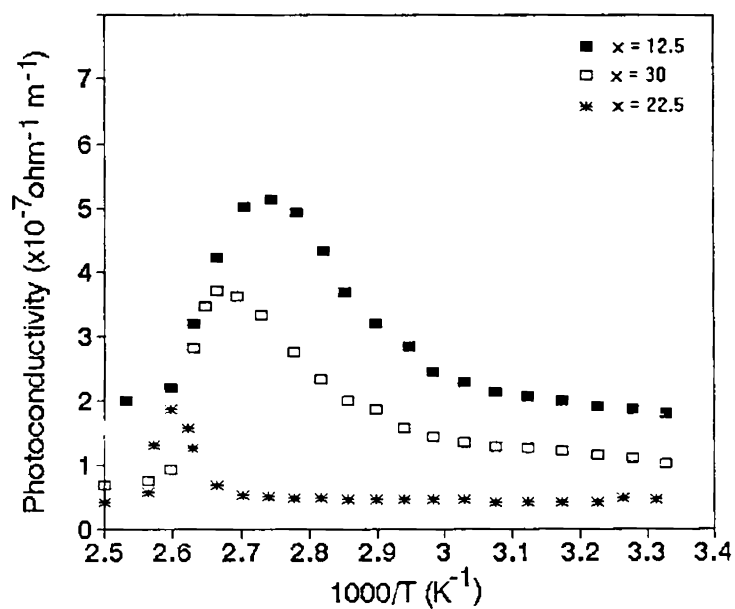**Fig.6.4** Temperature dependence of photoconductivity in three compositions of $Ge_xSb_{10}Se_{90-x}$ thin films.

141

which has different magnitudes for different compositions. Moreover, the temperature at which maximum in photoconductivity occurs (T_m) varies with composition. The photoconductivity decreases with increasing temperature for temperatures above T_m, while it increases with temperature for temperatures below T_m in the vicinity of the maximum. When the temperature is low, the variation in photoconductivity is very small and approaches a constant value for all compositions. Photoconductivity is found to be smaller than dark conductivity in the entire range of temperatures.

The variation of photoconductivity with light intensity at room temperature for three compositions is shown in Fig.6.5. At lower intensities photoconductivity increases linearly with intensity while at higher intensities photoconductivity tends to saturate.

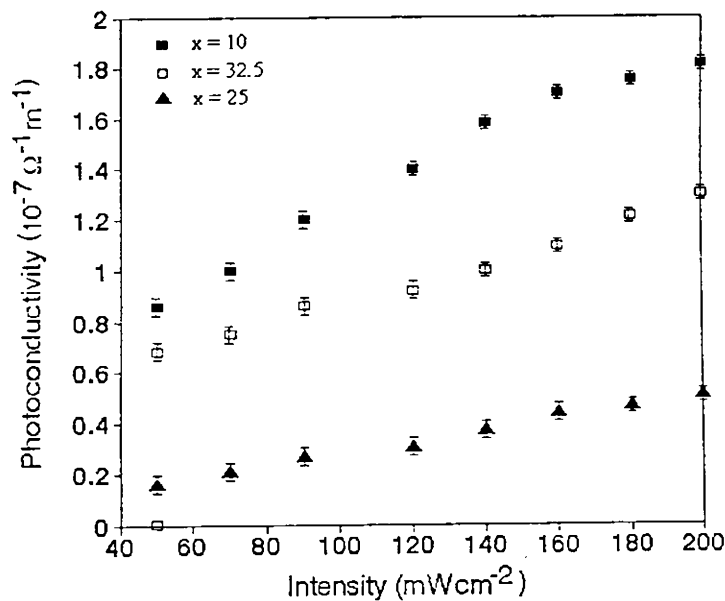Photoconductivity measurements carried out on amorphous Ge-Sb-Se thin films

Fig.6.5 Dependence of photoconductivity on light intensity for three compositions of $Ge_xSb_{10}Se_{90-x}$ thin films.

show that their photoconductivity behaviour is close to type I photoconductivity showing a maximum at a particular temperature T_m. The measurements have been carried out in the intensity regime where a linear dependence on intensity is observed for photoconductivity. However, the behaviour observed is different from typical type I behaviour in one aspect:

photoconductivity in the present case is found to be less than dark conductivity in the entire temperature range. The results are consistent with the ABFH model which takes into account, apart from the valence and conduction band states, localized states near the valence and conduction band edges and localized states in the middle of the gap near the Fermi level[16]. As explained earlier, type I photoconductivity can be explained on the basis of recombination from (i) localized to extended states(high temperature region ie T >T_m), (ii) localized to localized states (for T<T_m near T_m) and (iii) localized states at the conduction band edge to conduction band extended states. There are two possibilities for localized to localized transitions, namely transitions involving (i) localized states at the valence band or conduction band edge and (ii) localized states at the valence or conduction band edge and localized states near the Fermi level. The latter one, which gives a linear dependence for photoconductivity on intensity is predominant in the present case. In glassy samples the localized states near the band edges arise due to disorder associated with variations in the bond angle. bond length and dihedral angle whereas the localized states near the Fermi level are associated with bonding defects such as C^0, C^+ and C^-[16]. Since photoconductivity is always less than dark conductivity it can be concluded that the carrier generation and recombination mechanisms in these materials are such that the concentration of photogenerated carriers is less than that of the thermal equilibrium carriers in the entire range of temperatures investigated.

In type I materials, for temperatures above T_m, the photoconductivity increases with 1/T with a variation that can be characterized by a single activation energy E^+ given by

$$\Delta\sigma \propto \exp[E^+/kT] \tag{6.2}$$

For temperatures just below T_m photoconductivity decreases with 1/T and the corresponding activation energy E^- is given by

$$\Delta\sigma \propto \exp[-E^-/kT] \tag{6.3}$$

Values of E^+ and E^- have been calculated for all compositions of the Ge-Sb-Se system and are found to be 0.32 and 0.33 respectively for $Ge_{10}Sb_{10}Se_{80}$. The E^+ and E^- values scale with the optical band gap with a factor ≈ 0.2. The sum ($E^+ + E^-$) is also plotted in Fig.6.2 for a direct comparison with the optical band gap and activation energy. E+ and E^- are also found to possess a composition dependence, with maxima for the composition x=25. The sum ($E^+ + E^-$)is found to differ from ΔE, the conductivity activation energy, on an average by 10%. These characteristics are followed by several other type I materials like Ge-Te-Sb-S, Sb_2Te_3, GeAS etc.[15].

Fig.6.6 shows the exponential curve fit to the photoconductivity data for temperatures below T_m. The exponential variation of photoconductivity, which is less than
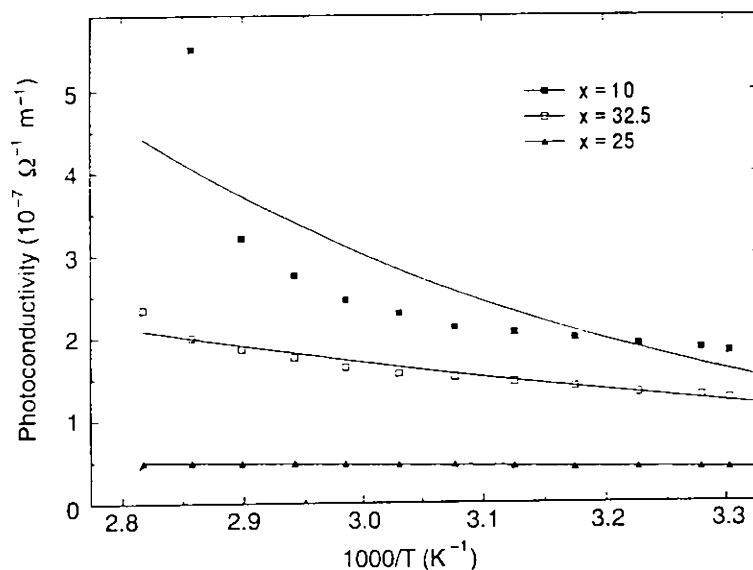

Fig.6.6. Exponential curve fit (continuous lines) for photoconductivity data(points) at temperatures below T_m for three different compositions

dark conductivity in this temperature range, is characteristic of a type II photoconductor[9]. Moreover, the photoconductivity increases slowly and monotonically with increasing temperature which is again found in type II materials like $Ge_{41}Sb_{59}$,

$Ge_{57}Sb_{43}$, $Ge_{38}As_{62}$ and $Sn_{55}As_{45}$[9,15]. It can be assumed that at temperatures below T_m, the presence of exponentially varying density of localized states does not give rise to a rapid variation of carrier density with temperature.

Since the Ge-Sb-Se system has a photoconductivity maximum as in type I photoconductors, it is possible to analyse this system in the same way as done in type I photoconductors[9,12]. In the frame work of ABFH model for type I photoconductors the relation between maximum photoconductivity σ_{max} and E_g can be expressed as

$$\sigma_{max} \propto \exp[-(E_v^* + E_\mu)/kT_m] \tag{6.4}$$

Generally, E_v^*, the valence band edge activation energy, and E_μ, the mobility activation energy, scale with the optical band gap E_g. Therefore

$$\sigma_{max} \propto \exp[-aE_g/kT_m] \tag{6.5}$$

or

$$T_m.\ln(\sigma_{max}) \propto -a.E_g \tag{6.6}$$

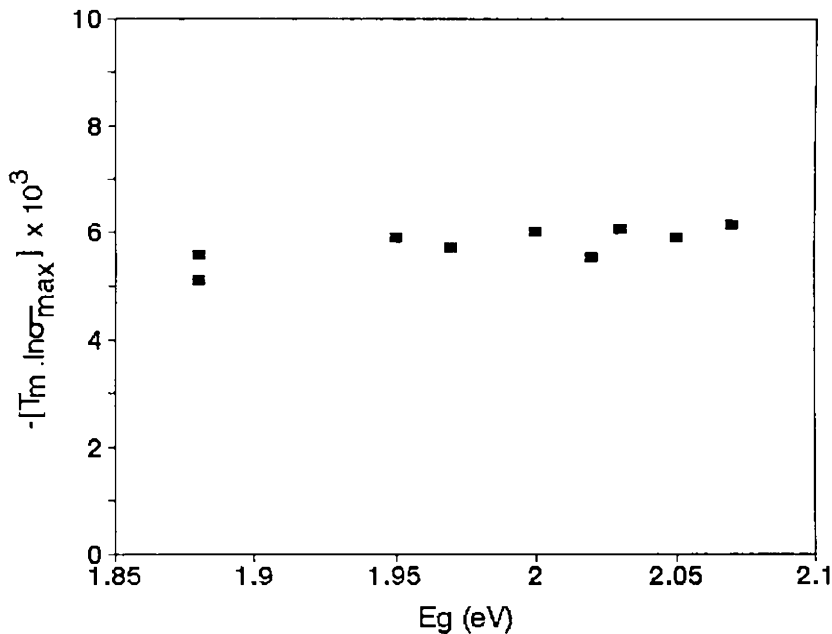The linear scaling of $\ln\sigma_{max}$ with E_g obtained from ABFH model is illustrated in Fig.6.7 for

Fig.6.7 Plot between E_g and $T_m.\ln\sigma_{max}$ for the Ge-Sb-Se system investigated. The points can be fitted to a straight line.

the Ge-Sb-Se system under discussion. For all the compositions the value of the proportionality constant a is found to be approximately 0.3 which is close to that of type I photoconductors [9]. This also indicates the similarity of the photoconductivity behaviour of this system with that of type I photoconductors.

6.3.2 Composition dependence of photoconductivity

The composition dependence of photoconductivity is illustrated in Fig.6.8 where the room temperature values of photoconductivity for different samples is plotted as a function of Ge content x. Photoconductivity is found to decrease with increase in x and shows a minimum at x=25. For all compositions with x>25 the photoconductivity again increases. Photoconductivity maximum and dark conductivity at 400 K are plotted with x and is shown in Fig.6.9. There also a minimum is observed corresponding to the stoichiometric composition with x =25. The composition dependent variation of photoconductivity and dark conductivity is complementary to the variation of activation energy with composition. which is shown in Fig.6.2. The $Ge_xSb_{10}Se_{90-x}$ system is dominated by flexible two fold coordinated Se chains with Se-Se bonds. The addition of Ge and Sb increases the cross linking between these chains with the formation of Ge-Se and Sb-Se bonds. Among the various possible bonds in the system, Ge-Sb, Sb-Sb, Se-Se, Ge-Sb and Sb-Se, the heteropolar Ge-Se and Sb-Se bonds have higher energies[17-20]. The variation of photo and dark conductivities with temperature for different compositions reveal the influence of composition dependent structural effects on the performance of the material. The composition dependence of photo and dark conductivities illustrated in figures 6.8 and 6.9 can be explained with the help of the chemically ordered covalent network model[17,19]. The Ge-Sb-Se system can be considered as made up of structural units of tetrahedral $GeSe_2$ and trigonal Sb_2Se_3 dispersed among other constituents. The maximum number of heteropolar bonds are formed first and the remaining valencies are satisfied by homopolar
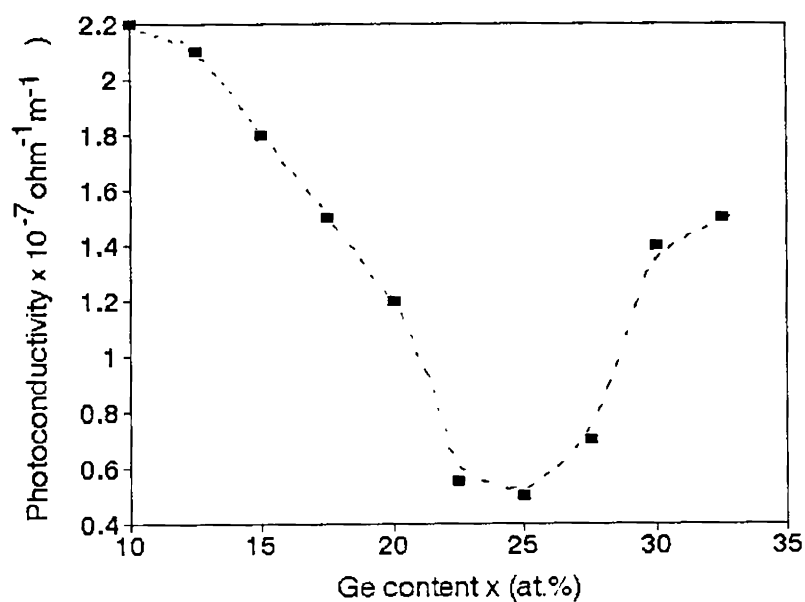
Fig.6.8 Composition dependence of photoconductivity for the $Ge_xSb_{10}Se_{90-x}$ system measured at 298 K.

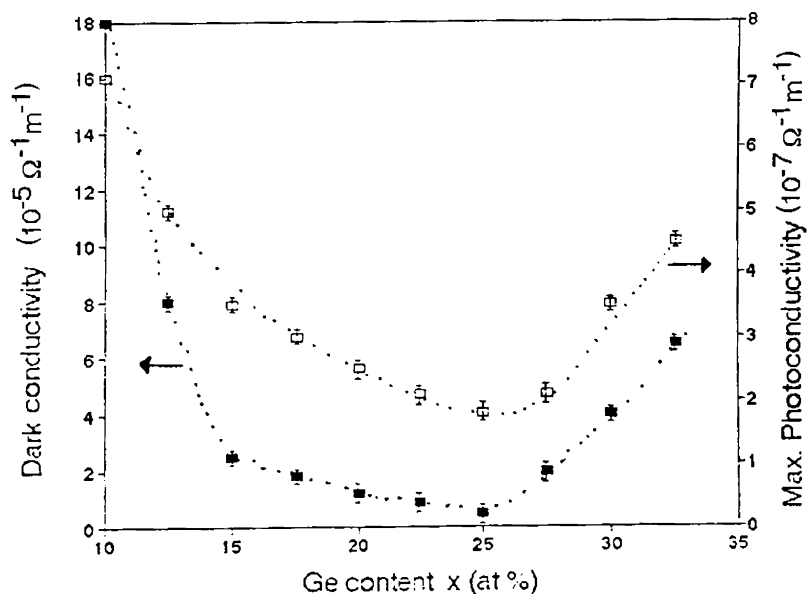**Fig.6.9** Composition dependence of dark conductivity at 400 K and photoconductivity maxima for $Ge_xSb_{10}Se_{90-x}$ thin films. Note that maxima in photoconductivity occur at different temperatures for different samples as illustrated in figures 6.3 and 6.4

bonds[2,5,21-22]. From the analysis of the various compositions it can be seen that the glass with 25 at.% Ge consists of structural units of the type $GeSe_2$ and Sb_2Se_3 only with neither Ge or Se present in excess. Thus for the composition $Ge_{25}Sb_{10}Se_{65}$, a completely cross linked 3D network consisting of $GeSe_2$ and Sb_2Se_3 units is attained and hence this structure exhibits a minimum in photoconductivity and dark conductivity.

As the composition is varied from $Ge_{25}Sb_{10}Se_{65}$, some of the $GeSe_2$ or Sb_2Se_3 units are replaced by weaker Ge-Ge or Se-Se bonds. The bond energies of Se-Se and Ge-Ge are ≈ 205 kJmole^{-1} and 188 kJmol^{-1} respectively. The Ge rich glasses (x>25) show a steeper increase of conductivity compared to Se rich glasses (x<25). The smaller bond energy of the Ge-Ge bond may be the reason for this behaviour.

6.4 Conclusions

The results on the $Ge_xSb_{10}Se_{90-x}$ system presented in this chapter are in good agreement with the general features reported for chalcogenides, showing maximum photoconductivity σ_{max} at a particular temperature. Localized electronic states in the band gap play an important role in the transport properties of these materials. The photoconductivity beheviour can be analysed on the basis of ABFH model which is found to be the most suitable one for chalcogenide semiconducting glasses. Photoconductivity behaviour of Ge-Sb-Se system is found to be close to that of type I photoconductors. At the same time this system exhibits some of the feature of type II photoconductors. The composition dependence of dark conductivity, activation energy, optical band gap and photoconductivity make clear that in the $Ge_xSb_{10}Se_{90-x}$ system a stable structure is formed for the composition with x=25 which corresponds to the stoichiometric composition of this system.

6.5 References

1. A.R Hilton, D.J Hayes and M.D Rechlin, *J.Non-Cryst Solids* **17** (1995) 319

2. A.Giridhar, P.S.L Narasimham and S.Mahadevan *J.Non-Cryst Solids* **37** (1980) 165

3. P.S.L Narasimham. A.Giridhar and S.Mahadevan *J.Non-Cryst .Solids* **43**(1981) 365

4. A.Srinivasan, K.N Madhusoodanan and E.S.R Gopal and J.Philip *Phys.Rev.*B**45** (1992) 8112

5. R.M. Mehra, R.Kumar and P.C .Mathur *Thin Solid Films* **170** (1989) 15

6. A.Giridhar, P.S.L Narasimham and S.Mahadevan *J.Non-Cryst.Solids* **43** (1981) 29

7. R.H.Bube *"Photoconductivity of solids"* Krieger Publ.Co, New York (1978)

8. J.Mort and D.M .Pai *"Photoconductivity and related phenomena"* Elsevier Sci.Publ.Co New York (1976)

9. R.H Bube *"Photoelectronic properties of semiconductors"* Cambridge University Press (1992).

10. N.F. Mott and E.A. Davis *"Electronic Processes in Non-Crystalline Materials"* Clarendon Press, Oxford(1971)

11. T.C. Arnoldussen, C.A. Menezes,Y. Nakagawa and R.H. Bube *Phys. Rev.* **B9** (1974) 3377

12. R.H. Bube *RCA Rev.* **36** (1975) 467

13. T.C. Arnoldussen, R.H. Bube, E.A. Fagen and S. Holmberg *J. Appl. Phys.* **43** (1972) 1798

14. T.C. Arnoldussen, R.H. Bube, E.A. Fagen and S. Holmberg *J. Non- Cryst. Solids* **8-10** (1972) 933

15. R.T.S. Shiah and R.H. Bube *J. Appl. Phys.* **47** (1976) 2005

16. E.A. Davis and N.F. Mott *Phil. Mag.* **22** (1970) 903

17. R.T. Sanderson " *Chemical bonds and bond energy*" Vol. 21 Academic Press New York (1971)

18. J.C. Phillips *J. Non-Cryst. Solids* **43** (1981) 37

19. A. Feltz, M. Phole, H. Steil and G. Herms *J. Non-Cryst. Solids* **69** (1984) 271

20. M. Mooser and W.B. Pearson *Prog. in Semicond.* **5** (1960) 103

21. H. Fritsche " *Amorphous and Liquid Semiconductors*" Ed. J.Tauc, Plenum Press, London (1974)

22. M. Kastner *Phys. Rev. Lett.* **28** (1972) 365

Chapter 7

Electrical switching in In-Te glasses

7.1 Introduction

Electrical switching is the rapid and reversible transition between a highly resistive OFF state and a conductive ON state driven by an external electric field and characterised by a threshold voltage. Depending on the material, switching can be of threshold type or of memory type. In threshold type switching the ON state persists only while a current flows, down to a certain holding voltage whereas in memory type switching the ON state is permanent until a suitable reset pulse is applied. A detailed description of the features of switching phenomenon has already been presented in chapter 1.

A great deal of effort has been expended to understand the switching process in chalcogenide glasses[1-6]. The conduction during switching is via a crystalline filamentary path through the material between the electrodes. A highly conducting crystalline filament is expected within the material as the cause of memory switching[2,7-8]. Network connectivity, rigidity and nature of bonding have important roles to play in the process of electrical switching.

The nature of glass forming tendency is an important factor for a chalcogenide glass to exhibit electrical switching. If the switching process occur by glass to crystalline transition, it should be observed in glasses which exhibit crystallization upon heating. Though elemental selenium which melts at 217^0 C undergoes a glass to crystalline transition near 100^0 C upon heating, it does not exhibit switching. Selenium is a very good glass former also. Many of the selenium based glasses, like Ge-Se, Ge-Bi-Se, Ge-In-Se, Ge-Se-Te, Ge-Sb-Se etc. are easy

glass formers. These glasses do not exhibit switching. Hence it is likely that the systems which can readily form glasses may not exhibit switching phenomenon.

In comparison with selenium based systems, Te based systems are not good in glass forming. Faster cooling is essential for Te based systems to form glasses compared to Se based systems. Memory type switching has been reported in Al-Te and As-Te glasses[9], whereas in Al-As-Te glasses, the switching observed is of threshold type. The addition of Al to As-Te system improves the glass formation and slow cooling is sufficient for the Al-As-Te system to form glass[10]. So it can be inferred that glasses which can be formed by moderate cooling may exhibit threshold type switching. Stable crystalline phases formed by melting is essential for memory switching. The heat produced during electrical conduction, which is not conducted away from the sample due to the poor thermal conductivity of the material, causes the formation of the crystalline path.

In this chapter we present the results of our investigations on the switching behaviour of bulk indium telluride glasses prepared by melt quenching technique. Though there are reports on switching in glasses like Al-Te, Al-As-Te, Ge-Te-Cu, Ge-Te-Ag in the bulk form[11], in general, bulk glasses are not much investigated compared to samples prepared in the thin film form.

7.2 Experimental details

Indium Telluride glasses with the general formula In_xTe_{100-x} were prepared in the bulk form by melt quenching technique with x varying from 20 to 40. Five different compositions of the material with x = 20, 25, 30, 35 and 40 were prepared from 5N purity constituents. The glasses obtained were annealed at 100°C for half an hour. The samples were analysed by XRD to confirm their amorphous nature. The XRD patterns of two representative samples are shown in Fig 7.1
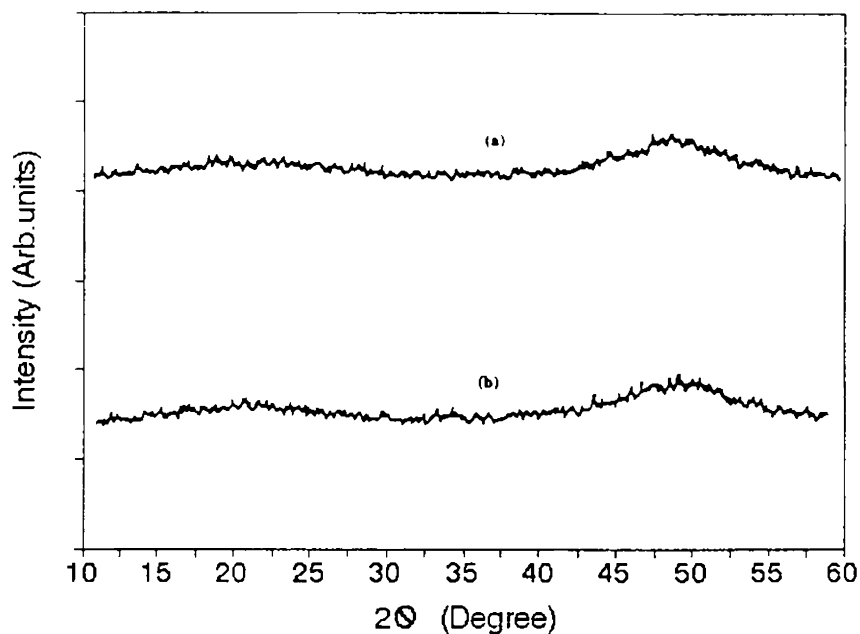
Fig.7.1 XRD patterns of two compositions of In_xTe_{100-x} system. (a) $In_{40}Te_{60}$ (b) $In_{20}Te_{80}$

Two compositions of the In_xTe_{100-x} system, namely $In_{40}Te_{60}$ and $In_{30}Te_{70}$, have been analysed by XPS also. The X-ray photoelectron spectrum of In and Te in both of these compositions are shown in figures 7.2 and 7.3.

For electrical measurements the samples were cut and polished to appropriate sizes and kept in a holder which was mounted in an evacuated chamber. Electrical switching measurements were carried out on samples of different thicknesses by varying the temperature of the sample from room temperature (298 K) to 375 K. During temperature dependence measurements, the samples were kept at the desired temperature with the help of a temperature controller. The sample was illuminated uniformly with polychromatic light from a 1kW tungsten halogen lamp while investigating the influence of radiation on switching properties. The experimental set up has already been shown in Fig 2.6 of chapter 2.
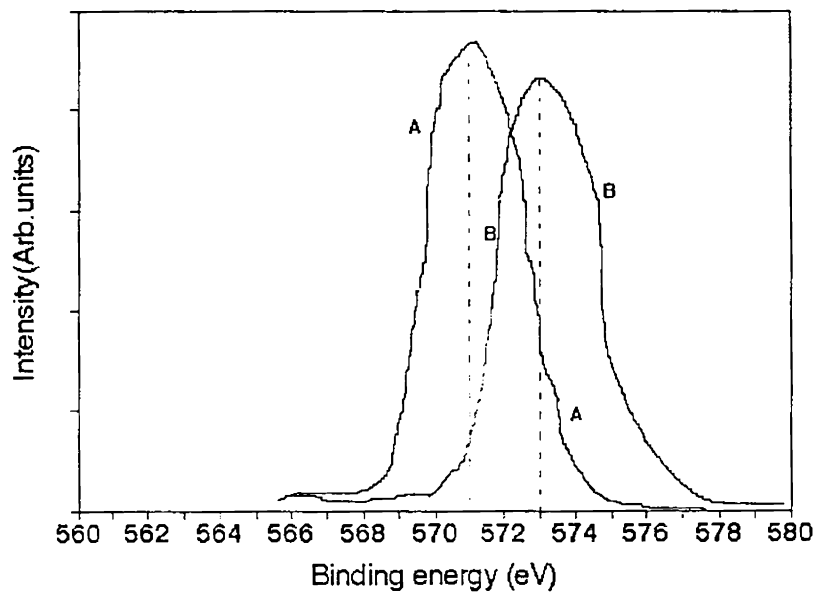
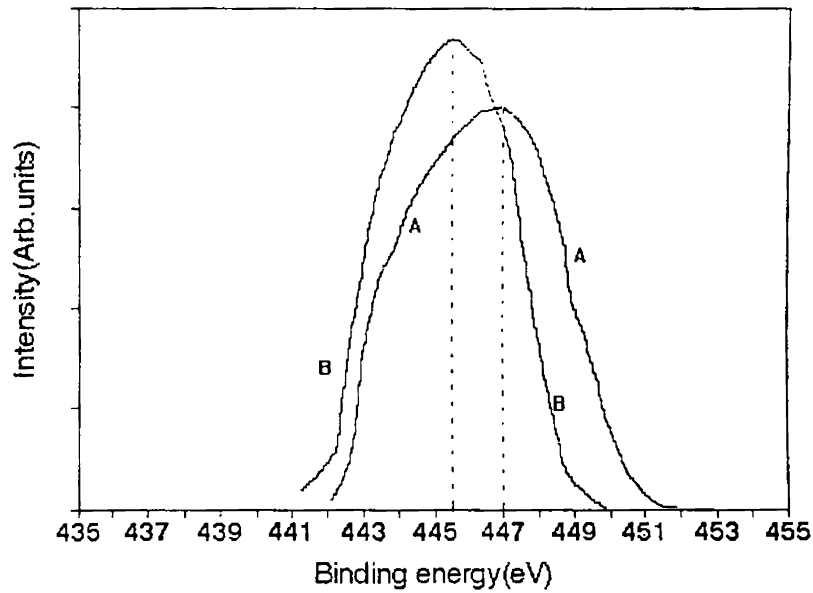**Fig.7.2** XPS of $3d_{5/2}$ levels of tellurium in (A) $In_{40}Te_{60}$ (B) $In_{30}Te_{70}$

Fig.7.3 XPS of 3d5/2 levels of indium in (A) $In_{40}Te_{60}$ (B) $In_{30}Te_{70}$

7.3 Results and discussion

7.3.1 OFF state behaviour and switching

The V-I characteristics corresponding to the OFF state and switching for In_2Te_3 glass are shown in Fig. 7.4. The region OA is normally the OFF state. It has three subsidiary regions as is evident from the OFF state V-I characteristics shown separately in Fig. 7.5. In the second y-axis of Fig. 7.5 logarithm of current is plotted against applied electric field. In the first region marked 1 in figure, the current increases linearly with voltage. In the second sub region, marked 2 in figure, the current increases exponentially with square root of the voltage following the relation

$$I = I_0 \exp (V/V_0)^{1/2}, \tag{7.1}$$

and in the third sub region marked three in figure, current increases exponentially with voltage following the relation

$$I = I_0 \exp (V/V_0) \tag{7.2}$$

On analysis of the three regions it can be seen that region 1 corresponds to the ohmic behaviour of the material. But in region 2 current has an exponential dependence on the square root of the applied voltage. This behaviour may be a result of the change in quasi-equilibrium within the semiconductor due to the applied electric field [12]. This region follows Poole- Frenkal law [13]. As applied field increases further, the generation of carriers due to change in equilibrium reaches a saturation exponentially which corresponds to region 3.

When the applied field is increased further the OFF-ON transition occurs at a high conduction region where $I \propto V^n$ (n>2) which is followed by a negative resistance region just before breakdown. In Fig. 7.5 the region AS corresponds to electrical switching in the material with a differential resistance. It requires the operation of a positive feed back
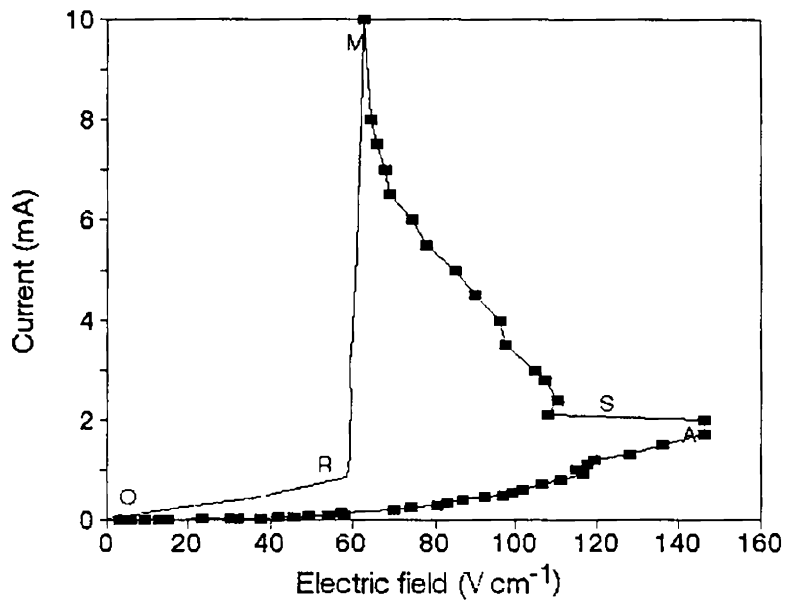
Fig.7.4 Switching behaviour of In₂Te₃ bulk stoichiometric glass at room temperature(298 K). Threshold electric field is 146 Vcm⁻¹. The region OA corresponds to the OFF state.
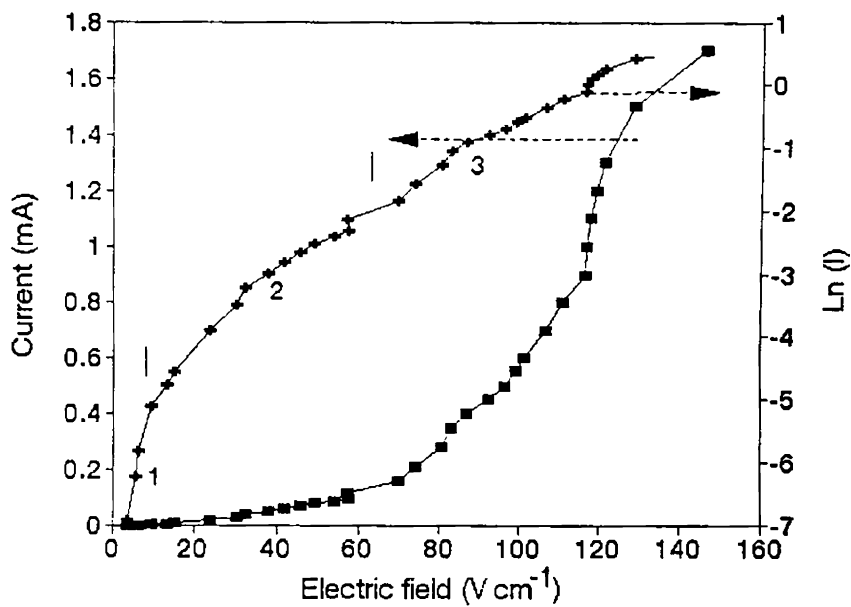

Fig.7.5 The OFF state V-I characteristics of In₂Te₃ glass at room temperature. The OFF state has three subregions as shown in the figure and discussed in the text.

156

mechanism during the occurrence of this instability condition. It is provided by the field induced carrier generation which occur with a decrease of activation energy. The region MS represents the state of the material with practically zero differential resistance. After the point M, the current gradually decreases in steps and the corresponding voltages are plotted in the region MR. This region, as is evident from the figure, possesses memory.

The OFF state behaviour is almost consistent with van Roosbroeck's model [14-15] for amorphous alloys. According to this model, the ohmic conduction at low fields results from the small number density of carriers in the extended band state. The exponential increase in current at high fields may be attributed to an increase in mobile carrier concentration, specifically to a field assisted thermal activation of electrons and holes, initially localized at the deep acceptor and donor levels, into extended states. Switching occurs when this activation process has been completed. Also it has been found that the effect of illuminating these samples with polychromatic light on their switching properties is negligibly small.

7.3.2 Composition, temperature and thickness dependence of switching behaviour

The V-I characteristics for different compositions of In-Te glass samples are shown in Fig.7.6. The observed threshold electric field (E_{th}) values have been plotted as a function of composition in Fig.7.7. As can be noted from this figure, the threshold field increases with increase in indium content. The stoichiometric composition $In_{40}Te_{60}$ or In_2Te_3 shows maximum value for threshold field among the compositions investigated. Samples with x>40 have not been investigated as they do not form uniform glasses. In_xTe_{100-x} glasses can be considered as consisting of In-Te stoichiometric structures dispersed in excess Te-Te bonds. The number of Te-Te bonds decreases with increase of x. The stoichiometric composition, $In_{40}Te_{60}$, consists of heteropolar In-Te bonds only. Since the bond energy of heteropolar bonds is higher than that of homopolar bonds, the composition $In_{40}Te_{60}$ is the most stable one
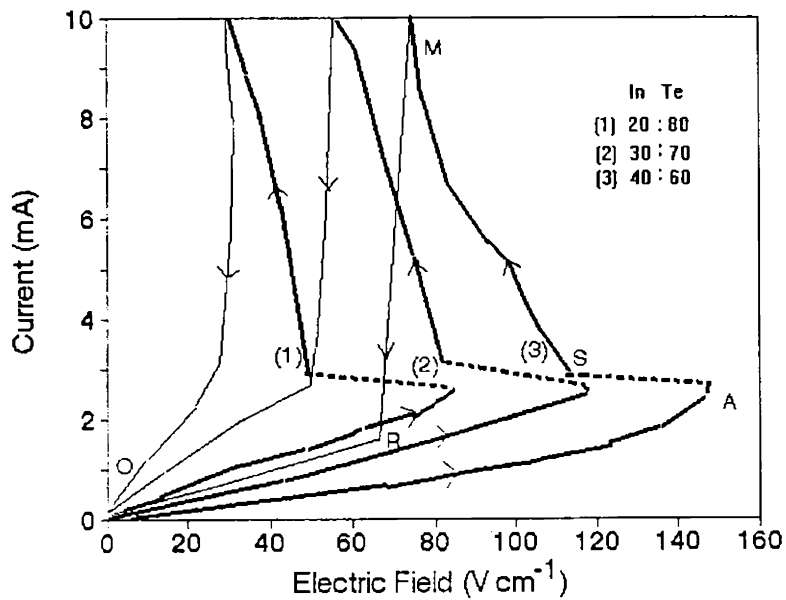
Fig.7.6 Switching observed in three different compositions of In-Te bulk glasses at room temperature
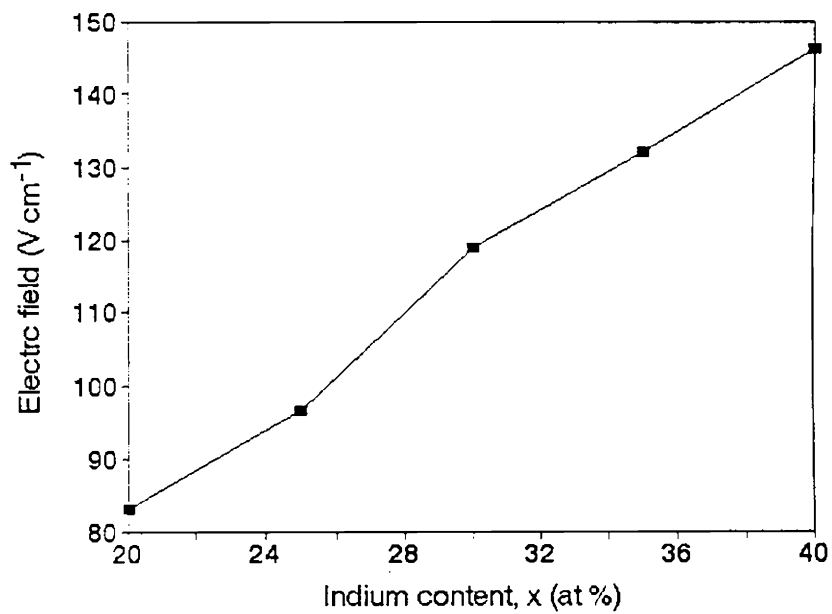

Fig.7.7 Variation of threshold electric field(E_{th}) with composition   of the material at room temperature.

among the different compositions[16-18]. Field induced carrier generation occurs at lower fields in other compositions compared to the stoichiometric $In_{40}Te_{60}$. The temperature dependence of the switching characteristics of three In-Te glasses are shown in Fig.7.8. The threshold field (E_{th}) decreases with increase of temperature. A plot of the variation of E_{th} with temperature for three samples is illustrated in Fig.7.9. Other compositions exhibit similar temperature dependence in their behaviour.

When the temperature is raised under a steady electric field, the thermally generated carriers also contribute to the neutralisation of the C_1^- and C_3^+ sites. Correspondingly the switching current increases and 'E_{th}' decreases. Temperature is a critical parameter that affects the ON state of the switching material. From the temperature dependence of the OFF state conductivity the activation energy(E_σ) is obtained as 0.5eV for $In_{40}Te_{60}$. The ratio E_s/E_σ, where E_s is the switching activation energy is obtained as 0.485. Similar results were reported on In-Te thin film[19].

Boer and Ovshinsky [20] analysed electrothermal initiation for electronic switching mechanism in semiconducting glasses. They have showed that one kind of initiation of the switching transition in layers of semiconducting glasses between two highly conducting electrodes can be caused by Joule heating of a current channel resulting in a conducting path. Switching and its dependence on temperature can be analysed best based on electrothermal model. According to this model the time dependent heat transport is given by the following equations [21]

$$C.\rho.dT/dt = K. \nabla^2 T + \sigma E_A^2 \qquad\qquad (7.3)$$

where C is the heat capacity, ρ is the density, E_A is the applied electric field, K is the thermal conductivity and σ is the electrical conductivity. When the heat generated by Joule heating cannot be removed fast enough by thermal conduction, break down of the steady state occurs.
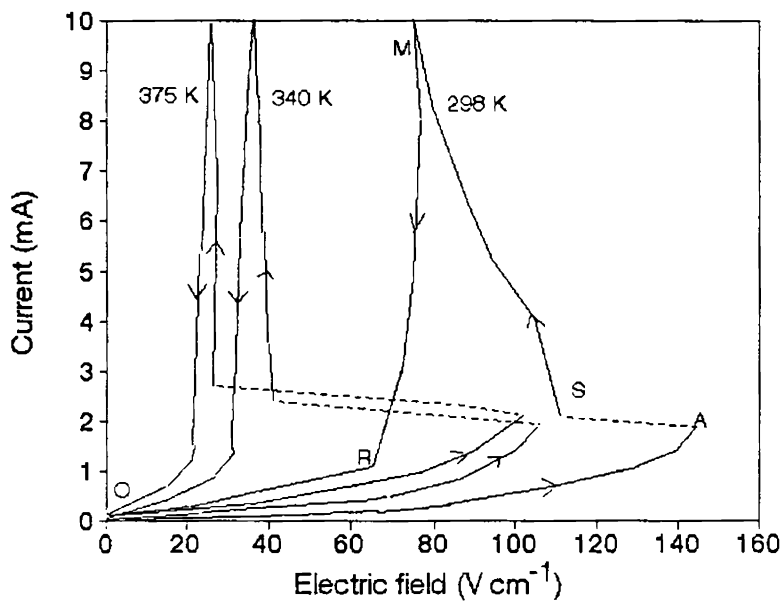
Fig.7.8 Switching behaviour of In_2Te_3 glass at three different temperature. Other compositions show similar temperature dependent variations.
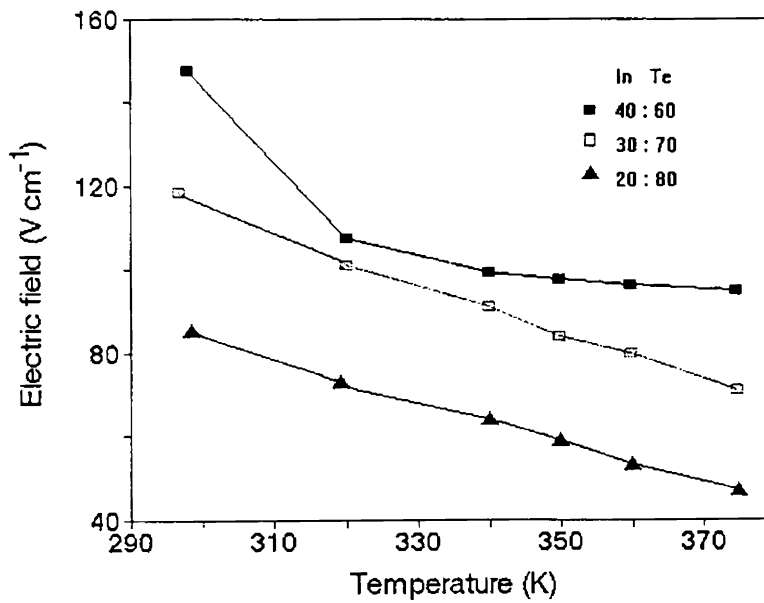
Fig.7.9 Variation of E_{th} with temperature for three different compositions of In-Te glasses.........

160

The electrical conductivity σ in eqn.7.3 is given by

$$\sigma = \sigma_0 \exp(-E_\sigma / k_B T) \qquad (7.4)$$

where σ_0 is the pre-exponential factor. The applied electric field E_A is given by $E_A = V_{th}/d$, where d is the thickness of the sample. In the steady state, time derivative of temperature, dT/dt becomes zero and then the eqn 7.3 can be rewritten as

$$8.K.\Delta T/d^2 + \sigma.E_A^2 = 0 \qquad (7.5)$$

In such a situation there will be a temperature difference between the surface and the interior of the sample, which can be obtained from the expression

$$\Delta T = T^2/(E_\sigma/k_B) \qquad (7.6)$$

The ΔT values at temperatures 298K, 340K, 360K and 375K are obtained for $In_{40}Te_{60}$ and are 15.3K, 19.94K, 22.35K and 24.25K respectively. These values are in agreement with the corresponding values obtained for thin films reported in literature[19].

It has been found that, in general, the threshold voltage increases with thickness of the sample for all compositions. The variation of threshold voltage with sample thickness for $In_{40}Te_{60}$, $In_{30}Te_{70}$ and $In_{20}Te_{80}$ are shown in Fig.10. Similar behaviour has been observed in thin films also. Fig.7.11 shows the thickness dependence of threshold voltage for In_2Te_3 thin film, reported in ref.[19]. Both in thin film and bulk sample threshold voltage has linear dependence on thickness. But by extrapolating one of them to the range of the other, we cannot obtain the observed behaviour. If the linear relation between thickness and threshold voltage in thin films is extrapolated to the thickness range of bulk samples, the threshold voltage is found to be high, which is not observed experimentally. The origin of this behaviour may be the difference in the nature of defects in the materials. Since the dimensionality of the two types of samples are different, possibility exists for the influence of structural defects in the two types to be different.
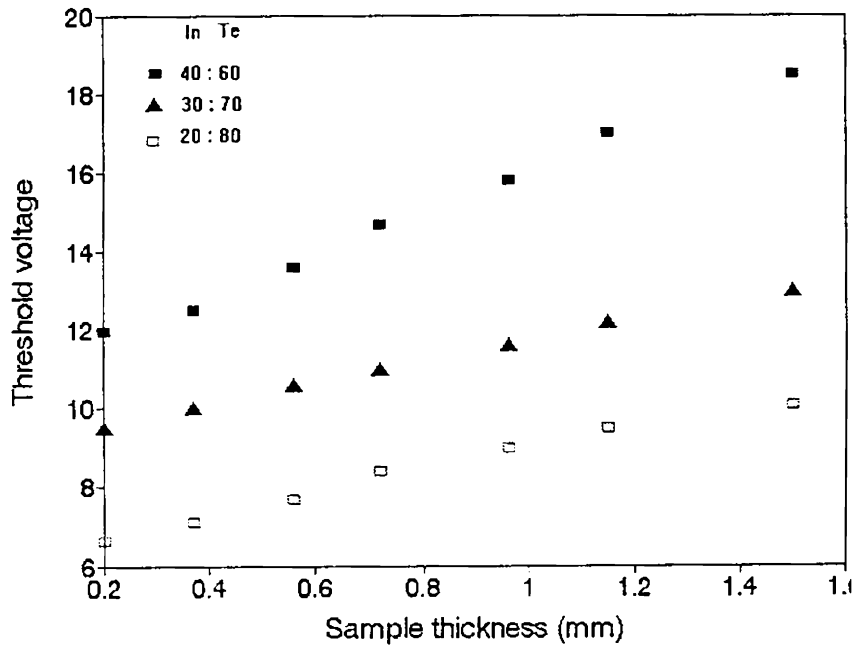
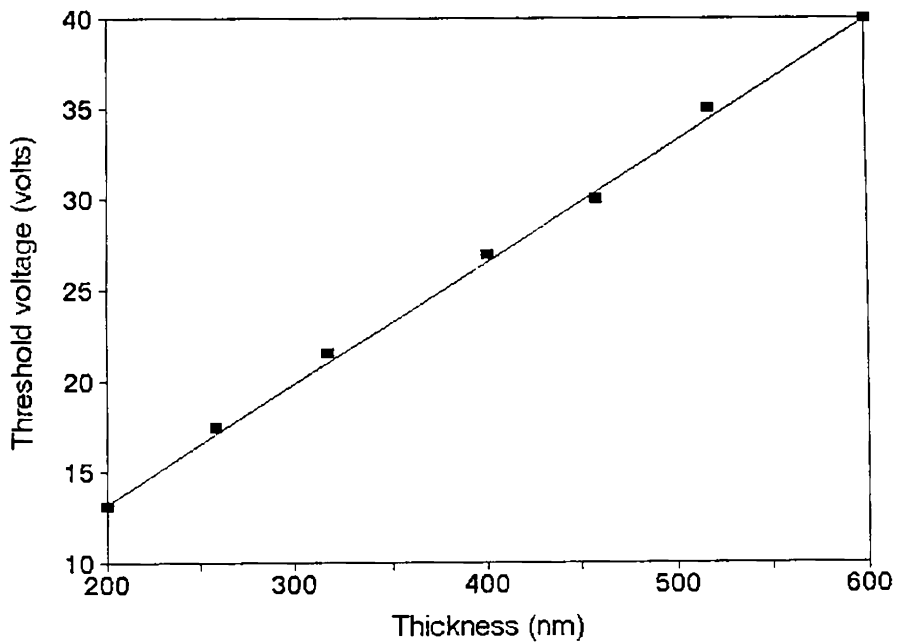**Fig.7.10** The variation of threshold voltage with thickness for three samples.

Fig.7.11 Thickness dependence of threshold voltage for In_2Te_3 thin film, reported in ref.[19].

7.4 Conclusions

Characteristics of memory type electrical switching in indium telluride glasses have been studied and reported. The dependence of threshold voltage on composition, temperature and thickness of the material have been investigated. The OFF-state behaviour has also been analysed. In comparison with the reported work on In_2Te_3 thin films, it is found that eventhough the variation of threshold voltage with thickness of the sample is linear both in thin films and bulk samples, one cannot be extrapolated to the range of the other. With increasing temperature the threshold field is found to decrease. The stoichiometric composition In_2Te_3 has the maximum threshold field among the compositions investigated. The switching behaviour of the material has been analysed in terms of electrothermal model.

7.5 References

1.   S.R.Ovshinsky and H.Fritzche, *Met. Trans.* **2**(1971) 641.

2.   A.E.Owen and J.M.Robertson, *IEEE Trans. on Electron Devices* **20** (1973) 105.

3.   D.Adler and S.C.Moss, *J.Vac.Sci.Technol.* **9** (1972) 1182.

4.   D.Adler, H.K.Henisch and N.F.Mott, *Rev.Mod.Phys.* **50** (1978) 209.

5.   K.Nakashima and K.C.Rao, *J. Non-Cryst. Solids* **33** (1979) 189.

6.   A.G.Stevenson, *J. Non-Cryst. Solids* **21** (1976) 319.

7.   H.Fritzche *"Amorphous and Liquid semiconductors"* ed: J.Tauc Plenum, London, (1974).

8.   D.Adler, *Sci. Am.* **236** (1976) 36.

9.   S.Prakash, S.Asokan and D.B.Ghare, *Semicond. Sci. Technol.* **9** (1994) 1484.

10.   J. A. Savage, *J.Non-Cryst. Solids* **11** (1972) 121.

11.   K. Ramesh, *Ph.D Thesis Indian Institute of Science*, Bangalore (1997).

12.   N. F. Mott and E. A. Davis " *Electronic Processes in Non-Crystalline materials* Clarendon, Oxford (1979).

13.   R. L. Hargraves, P. R. Mason and J. C. Anderson , *J. Phys D: Appl. Phys.* **7** (1974) 85.

14.   G. A. Denton, G. M. Friedman and J. F. Schetzina, *J. Appl. Phys.* **46** (1975) 3044.

15.   W.van Roosbroek, *J. Non-Cryst. Solids* **12** (1973) 232.

16.   R.T. Sanderson, " *Chemical Bonds and Bond Energy*" vol. 21, Academic Press, New York (1971).

17.   J.C. Phillips, *J. Non-Cryst. Solids* **43** (1981) 37.

18.   A.Feltz, M. Phole, H. Steil and G. Hesms, *J. Non-Cryst. Solids* **69** (1984) 271.

19.   M.A. Afifi, N. A. Hegab, A. E. Bekheet, *Vacuum* **47** (1996) 265.

20.   K. W. Boer and S. R. Ovshinsky, *J. Appl. Phys.* **41** (1970) 2675.

21.   K. Subhani, M. S. Shur, M. P. Shan and D. Alder, *Proc. Int. Conf. on Amorphous Semiconductors*, Ed: Spear W. E., Univ. of Edinburgh (1977)

Chapter 8

Summary and conclusions

Photoconductivity and electrical switching are two interesting and important phenomena exhibited by many of the chalcogenide compound semiconductors and selected conducting polymers. Study of these phenomena are useful both from the basic and application points of view. Our aim in this thesis has been to investigate photoconducting as well as electrical switching properties of selected chalcogenide semiconducting glasses.

The work presented in this thesis is centered around the photoconducting properties of selected selenium based ternary systems and electrical switching properties of one tellurium based binary system. Photoconductivity has been studied in bulk glasses of Ge-In-Se, Ge-Bi-Se and As-Sb-Se and in thin films of Ge-Sb-Se systems. In-Te bulk glasses have been investigated for their electrical switching property.

The bulk glasses have been prepared by the conventional melt quenching technique and thin films by argon sputtering of the corresponding bulk glasses. The amorphous nature of the samples have been confirmed by XRD. Also, selected compositions have been analysed by XPS. Details of experimental techniques and results obtained are presented in earlier chapters.

Both photoconductivity and electrical switching have been analysed mainly with their dependence on composition of the material as well as temperature. The results on composition dependence have been explained on the basis of COCN model and temperature dependence of photoconductivity has been analysed on the basis of Arnoldussen - Bube - Fagen and

Holmberg (ABFH) model. The electrical switching exhibited by In-Te system has been explained on the basis of electrothermal model.

While considering the composition dependence of properties, it has been noted that for all the systems a remarkable change in the variation of properties occurs at the composition corresponding to stoichiometry. It may be a minimum or maximum of the property, or a clear slope change in the variation. The stoichiometric compositions generally consist of heteropolar bonds only and average bond energy will be high compared to other compositions. This composition can be considered as the "most crystalline" one in an amorphous system as it is better ordered than other compositions.

For the Ge-In-Se bulk glasses and Ge-Sb-Se thin films photoconductivity exhibits a minimum at the composition corresponding to the stoichiometric composition. For the As-Sb-Se bulk glasses photoconductivity exhibits a clear slope change corresponding to stoichiometric composition. In comparison with Ge-In-Se and Ge-Sb-Se, the behaviour of the stoichiometric composition of As-Sb-Se is different. For Ge-In-Se and Ge-Sb-Se photoconductivity decreases with decrease in Se content, (or increase in Ge content) and exhibits a minimum at the stoichiometric composition and then increases. In the case of As-Sb-Se photoconductivity increases with decrease in Se content (or increase in As content), and corresponding to the stoichiometric composition the variation suffers a clear change of slope. The behaviour of As-Sb-Se can be explained on the basis of COCN model and variation of Sb_2Se_3/As_2Se_3 ratio. In As-Sb-Se it has been found that the average bond energy is minimum at the stoichiometric composition. As-Sb-Se has a special feature compared to Ge-In-Se and Ge-Sb-Se that As and Sb are isovalent. So the replacement of As by Sb may not influence the material like In or Sb in Ge-Se networks.

The Ge-Bi-Se system under our investigation does not cover the stoichiometric composition. The general formula of this system is given by $Ge_{20}Bi_xSe_{80-x}$ ($x = 0 - 12$). When

x =7 at.% (or average coordination number Z = 2.47) it has been reported by various workers that the system undergoes a p- type to n-type transition. Results of photoconductivity and carrier life time measurements in this system carry interesting signatures corresponding to the critical composition where p→ n transition occurs. Photoconductivity exhibits a maximum to minimum transition and carrier life time has a slope change corresponding to this critical composition. The results have been analysed in the light of various models. More experimentation and modeling are needed to understand this phenomenon in depth. Systems like Ge-Pb-Se and As-Bi-Se are also reported to exhibit p→ n transition. So there is scope for the study of p→ n transition and change in photoconducting properties around their critical compositions.

In the framework of ABFH model, Ge-In-Se, Ge-Bi-Se and As-Sb-Se bulk glasses are found to be type I photoconductors. Ge-Sb-Se thin films also exhibit characteristics of a type I photoconductor, but it exhibits some features of characteristic type II photoconductors at the same time.

Our results on Ge-Bi-Se and Ge-In-Se systems can be compared with that of the basic binary Ge-Se networks. The incorporation of In brings about increase in photoconductivity by nearly four orders of magnitude while the incorporation of Bi causes an increase of nearly two orders. The enhancement in photoconductivity with the incorporation of In or Bi as impurities can be attributed, in general, to the formation of defect states in the band gap of the material. In As-Sb-Se also an increase by nearly three orders of magnitude has been observed for photoconductivity in comparison with As-Se glasses. Properties of Ge-In-Se, Ge-Bi-Se and As-Sb-Se systems investigated have been compared with $Ge_{20}Se_{80}$ and $As_{40}Se_{60}$ respectively. These two compositions are more closer to the structure of the corresponding ternary glasses Though the incorporation of impurities enhances photoconductivity, it has been observed that it causes a decrease in the photodetectivity, which is given by $(\sigma_{ph}/\sigma_d.)$ The reason is clear

from the expression for the determination of photodetectivity. The incorporation of impurities generally causes an increase of dark conductivity also, the rate of which is higher than that of photoconductivity.

Frequency resolved photoconductivity measurements (FRPC) have been carried out on the bulk systems Ge-In-Se, Ge-Bi-Se and As-Sb-Se. From the frequency resolved photoconductivity measurements trap limited carrier generation time or carrier lifetime has been calculated using the formula, $\tau = 1/2\pi f_{max}$ where f_{max} is the frequency at which photoconductivity is maximum.

The variation of the carrier life time with composition of the material, temperature and intensity of light have been studied. Carrier life time also exhibits clear variations corresponding to the stoichiometric compositions. Carrier life time is found to decrease with increase in intensity and temperature. Intensity of illumination is directly proportional to generation rate (G). The carrier life time (τ) and G can be related as $\tau = AG^{v}$. From ln τ vs ln G plots, the values of the exponent 'v' have been calculated and found to be in between 1 and 0.5 for all the samples studied. $v = 1$ corresponds to monomolecular recombination and $v = 0.5$ corresponds to bimolecular recombination of carriers. Since the values of v are between 1 and 0.5 one can infer that localized states or traps are present in the energy gap of the materials.

In addition to the above measurements, the spectral dependence of photoconductivity has been analysed for Ge-In-Se. From the data obtained, spectral sensitivity and quantum efficiency are calculated. The quantum efficiency is found to be low ($= 10^{-6}$). Selected compositions of Ge-Bi-Se and As-Sb-Se also have been studied for spectral characteristics. Because of the low band gap (near IR) values, the absorption region could not be obtained clearly in some compositions from these measurements.

The electrical switching observed in In-Te glasses is of memory type. The OFF-state behaviour of the material is analysed and found to be consistent with explanations put forward by earlier workers on other materials. The stoichiometric composition exhibits a maximum for the threshold field among the samples investigated. With increasing temperature the threshold field decreases. Also the threshold voltage increases linearly with thickness. The results are compared with the reported results on In_2Te_3 thin films. Threshold field is found to be low for the bulk glasses. The thickness dependence cannot be extrapolated from the region of thin films to the bulk. The difference may be due to the difference in dimensionality of the material. The general switching behaviour has been analysed in the light of the electrothermal model.

We have carried out X-ray photoelectron spectral analysis (XPS) of selected compositions and the results are presented in respective chapters. The b.e of characteristic levels of an element in pure form and in the compositions studied are given. Chemical shifts in b.e have been observed in the compositions studied. The application of XPS is to identify the constituents of a compound and to estimate b.e of characteristic levels. Moreover this analysis give information about the electronic structure of the material.

Scope for further work

For throwing more light into the photoconductivity properties of amorphous semiconductors, transient photocurrent measurements and study of characteristics of rise and decay of photocurrent would be useful. Photocurrent modulation spectroscopy is a powerful and new technique. Photocrystallisation and photodissolution are two fields in which intensive research are going on. Corona discharge studies can lead to the optimisation of xerographic quality of the material. Electrical switching properties of 'Te' based systems can be done with determination of switching delay time, which will help to understand the phenomenon in more

depth. Incorporation impurities may be done with the aim to move towards almost an ideal switch which can have practical applications. ✦   ➤

On the dynamics and structure of the material, neutron scattering, electron microscopies, EXAF studies etc. can provide more information. Eventhough there are many limitations to perform these studies on network glasses, it is worthwhile to make attempts since such investigations could improve our present understanding of the glassy state.